Carbon Dioxide Hydrogenation over Nickel-, Ruthenium- and Copper-based Catalysts: Review of Kinetics and Mechanism

Kalala Jalama

Department of Chemical Engineering, Faculty of Engineering and the Built Environment, University of Johannesburg, Doornfontein 2028, SOUTH AFRICA, kjalama@uj.ac.za

Abstract

This study critically reviews the mechanism of CO_2 hydrogenation over Ni, Ru and Cu, and the effect of catalyst properties and operating conditions on reaction kinetics. Most studies have reported the presence of CO and formate species on Ni-, Ru- and Cu-based catalysts, where subsequent conversion of these species depends on the type of catalyst and the physicochemical properties of the catalyst support. Methane is the major product that forms during CO_2 hydrogenation over Ni and Ru catalysts, while methanol and CO are mainly produced on Cu catalysts. A different approach for catalyst formulations and/or process development is required where long chain hydrocarbons are desired.

Keywords: CO_2 hydrogenation; Nickel; Ruthenium; Copper.

1 Introduction

Hydrogenation of CO_2 to fuel has received greater attention, especially over the last decade. This is due primarily to increased global energy demand and the need for mitigating carbon emissions to the environment by targeting a possible closed carbon cycle through CO_2 utilization. The number of investigations on the development of new catalysts formulations and optimization of operating conditions for CO_2 hydrogenation has increased rapidly, requiring a compilation to distill the major findings in this research area. A number of reviews on catalytic

CO_2 hydrogenation to methane (1 - 5), long chain hydrocarbons (3, 6), methanol (3, 6 - 9), dimethyl-ether (3) and higher alcohols (3) have been compiled over the past few years.

The catalytic hydrogenation of CO_2 to methane is an old process that was mainly used for the purification of hydrogen by removing small amounts of CO_2 prior to ammonia synthesis (10, 11), and for the production of substitute natural gas (SNG) (12 - 14). The desire to produce long chain hydrocarbons from CO_2-containing feedstock has emerged in recent years, with mostly transition and noble metals being evaluated for this process. Unlike Fischer-Tropsch synthesis where predominantly longer chain hydrocarbons are produced in presence of CO and H_2, CO_2 hydrogenation over conventional Fischer-Tropsch synthesis catalysts yields significantly higher amounts of methane. There is a strong need to develop fundamental understanding for this reaction. Among transition metals, Ni constitutes a relatively simple system, as it is one of the most methane-selective catalysts. Fundamental understanding of this system can shed light on more complex systems that involve the formation of a broad range of products. Many excellent reviews on CO_2 hydrogenation have suggested a general reaction route based on data obtained from a number of different catalytic systems. Reviews that specifically examined CO_2 hydrogenation over metal-based catalysts such as Ni, Ru or Cu separately, are scarce. The review by Vlasenko and Yuzefovich (1) in 1969 focused on the mechanism of CO and CO_2 hydrogenation over iron-group metals. Their study discussed two major routes for CO_2 hydrogenation, namely i) the scheme involving CO as an intermediate and ii) an independent route that does not involve CO. At the time of their review, most existing experimental data to deeply analyze the mechanism on the Ni surface were not available. For example, experimental studies on the behavior of adsorbed CO_2 on Ni in the presence of H_2 were nonexistent. The interpretation of the mechanism was largely based on kinetic data generated on supported Ni, such as Ni on kieselguhr and binary systems such as Ni-Cr. Possible

contributions from the support or a second metal can complicate any investigation of the intrinsic behavior of a catalyst.

Darensbourg *et al.* (2) categorized the mechanistic aspects of CO_2 methanation into two types: i) early mechanisms that suggest CO_2 methanation without CO formation and ii) recent mechanisms suggested by studies published from 1977 to 1982 which point to a mechanism for CO_2 methanation that occurs through the formation of adsorbed CO. Studies involving Ni catalysts were limited, as the review involved many other catalysts such as Rh, Ru, Cu, and Pd. Studies on Ni catalysts were mainly based on the analysis of methanation reaction products and/or reactant adsorption-desorption techniques. Wang *et al.* (3) reported on general advances in CO_2 hydrogenation covering the period from 1997 to 2010. For CO_2 hydrogenation using Ni as a catalyst, the review mainly gave an overview on the effects of catalyst supports such as MCM-41, rice husk ash (RHA) silica-alumina composite, ZrO_2, La_2O_3 and Ce-Zr binary oxides.

The most recent review by Aziz *et al*. (5) looked at kinetics and the mechanism of CO_2 methanation over a number of catalysts including Ni, Ru, Rh, Pd, Au, Co and Mg. They extensively reviewed the effect of support, metal loading, second metal and preparation method on the physicochemical and catalytic properties of Ni catalysts based on studies published from 2011 to 2015. In reviewing mechanistic aspects, which essentially involved supported catalysts, the support was suggested to play a role.

Recent studies employing in-situ spectroscopic techniques (15, 16) have shown that the nature of the support influences the CO_2 hydrogenation mechanism on Ni-based catalysts. One possibility is that different active intermediate species form on the catalyst surface depending on the support used. This can, at least in part, account for differences that have been reported on this topic.

By scrutinizing recent and earlier studies on CO_2 methanation, this review aims to establish the most likely active intermediate in the *intrinsic* mechanism of CO_2 methanation occurring on the Ni surface in comparison to Ru- and Cu-based catalysts. In addition, the kinetics of this reaction will be reviewed with a greater focus on aspects that have not yet been extensively reviewed such as kinetic models and the influence of reaction conditions.

2 Reaction Mechanism

The early literature that was summarized by Vlasenko and Yuzefovich (1) on CO_2 hydrogenation suggested two major reaction routes: i) the scheme proposed by Bahr, as cited in (1) involving the formation of CO as an intermediate and ii) the direct hydrogenation of CO_2 by activated hydrogen to formic acid, structural rearrangement, and stepwise hydrogenation of intermediates. Bahr's scheme was mostly supported by studies using Fe-Cu, Cu-Cr_2O_3, Co-Cu-ZnO, Ru and a number of catalysts based on metals of the iron group and on various binary systems. On the other hand, the direct scheme was supported by studies involving Ni-Cr catalysts. A number of findings were highlighted to be unfavorable to the Bahr scheme (1), for example: i) the hydrogenation of CO_2 on Fe- and Ru-based catalysts, mainly produces CH_4 unlike CO hydrogenation; ii) CO_2 is not hydrogenated in the presence of CO and does not influence its transformation; and iii) CO_2 is hydrogenated at a lower temperature than CO.

Based on their analysis of the literature, Vlasenko and Yuzefovich (1) were in favor of a direct CO_2 conversion route, without formation of CO as intermediate. This scheme suggests that hydrogen is activated on the catalyst surface, after which the reaction takes place in the gas phase. The hydrogenation of adsorbed CO_2 at the start of the process is dismissed.

Several subsequent studies from different research groups have been conducted with the aim of determining the active intermediate species on the catalyst surface. The findings are still controversial as the major question is now to determine whether the active intermediate is CO,

formate species or both. The various routes on Ni, Ru and Cu catalysts are discussed in the following sections.

2.1 Reaction via CO

Various techniques have been used to confirm that CO is formed as an intermediate species in CO_2 hydrogenation over nickel-based catalysts. They include i) spectroscopic (11) , desorption (13) or adsorption (17) analyses of species formed on the catalyst surface upon CO_2 adsorption in the absence of H_2; ii) analysis of the product formed during hydrogenation of pre-adsorbed CO_2 species on the catalyst (12, 13); iii) product analysis of a typical CO_2 hydrogenation reaction where H_2 and CO_2 were fed simultaneously to the system (18 - 21); iv) transient response analysis (22 - 26) and v) diffuse reflectance infrared Fourier transform spectroscopy (DRIFTS) analysis during CO_2 hydrogenation (25, 27).

Martin *et al*. (11) used infrared spectroscopy and magnetic techniques to study reactions of CO and CO_2 on a Ni/SiO_2 catalyst. CO_2 chemisorption on nickel surface at 300 and 580 K showed two bands at 2020 and 1835 cm^{-1} assigned to CO species bonded to four Ni atoms. No carboxylate, nor carbonate bands were detected. The reactivity of these species towards hydrogen was studied (12) by first adsorbing CO_2 on the catalyst at 300 K and subsequently introducing hydrogen. Methane was detected at temperatures above 355 K. The authors also tested the hydrogenation of a superficial carbide prepared by ethane cracking and found that it formed methane. They then proposed that CO_2 hydrogenation is likely to proceed via CO_2 dissociative adsorption and the formation of superficial carbide which is subsequently hydrogenated to form methane as shown in Fig. 1.

Figure 1: CO_2 hydrogenation via CO and superficial carbide.

Falconer and Zagli (13) used temperature programmed desorption (TPD) and temperature programmed reaction (TPR) to study the adsorption and methanation of CO_2 over a Ni/SiO_2 catalyst. They found that CO_2 adsorption on the catalyst surface was activated and increased significantly with temperature with a maximum value obtained around 473 K. The adsorbed CO_2 desorbed as CO and CO_2 during TPD. They found similarities between CO and CO_2 adsorption indicating that CO_2 dissociates to CO and oxygen upon adsorption at higher temperatures. The TPR was performed by first adsorbing CO_2 at high temperature, cooling and then switching to H_2 before heating. They observed the formation of water, comparable to the amount of CO_2 adsorbed, upon catalyst contact with H_2 at room temperature and confirmed the presence of oxygen atoms on the catalyst surface. They also found the same TPR results for CO and CO_2 methanation and suggested that once adsorbed, CO and CO_2 follow the same mechanism to yield methane.

CO_2 pulses were used on Al_2O_3-, SiO_2- and TiO_2-supported Ni by Osaki and Mori (17) to study the kinetics of CO_2 dissociation. They observed CO formation but could not detect O_2. The exponential decay of the amount of CO formed with the number of CO_2 pulses suggested an irreversible adsorption of O_{ads} on the Ni active sites through CO_2 dissociation.

Using Ni/SiO_2 catalyst, Weatherbee and Bartholomew (19) observed CO in the product of CO_2 hydrogenation at 500 – 600 K and 140 kPa. They suggested that the amount of CO measured in the product was determined by equilibrium between surface and gas phase CO species. Based on their kinetic results, they proposed a complex Langmuir-Hinshelwood mechanism involving dissociative adsorption of CO_2 to CO and atomic oxygen followed by the hydrogenation of CO via a carbon intermediate to methane as shown in Fig. 2. The rate-limiting step was assumed to be CO dissociation.

Figure 2: Proposed sequence of elementary steps in CO_2 methanation (S refers to a surface site)

Large amounts of CO were also measured during CO_2 methanation on Ni (100) catalyst by Peebles *et al*. (20). Based on higher initial specific rates for CO production compared to CH_4 and lower activation energy, they proposed that a balance between the formation of adsorbed carbon and its removal by reaction with surface hydrogen are the controlling factors for CO_2 methanation.

Fujita *et al*. (22, 24) used transient response and TPR (24) methods to study the mechanism of both CO and CO_2 methanation over unsupported Ni. They found that CH_4 was produced from adsorbed surface carbon species resulting from strongly adsorbed CO on the catalyst surface. They also found that CO_2 dissociation to adsorbed CO and O was enhanced in the presence of H_2. The amount of surface carbon was much less compared to adsorbed CO and the amount of reversibly adsorbed CO was negligible. The kinetics were different in the case of CO hydrogenation, where more surface carbon was present along with strongly adsorbed CO. They suggested that reversibly adsorbed CO inhibits the hydrogenation of adsorbed carbon species. When they used DRIFTS, TPR and the transient response method (TRM) techniques over an Al_2O_3-supported Ni catalyst (25), they found that the following species were present on the catalyst surface during CO_2 methanation at 453 K: i) unidentate formate on the Ni surface, ii) bidentate formate on the support, iii) linear CO on Ni, iv) bridged CO on Ni and v) carbonates on the support. After steady-state methanation and flushing the reactor with He, they found that strongly adsorbed bridged CO and bidentate formate were the most predominant species on the catalyst surface. Using temperature programmed hydrogenation, they found that both species formed CH_4 and H_2O at 433 and 533 K respectively. Bridged CO species were believed to dissociate into surface oxygen species and carbon which were rapidly hydrogenated to water

and methane respectively. Like in their earlier studies on unsupported Ni (22, 24), they also found differences in the species formed on the catalyst surface during CO_2 and CO methanation, respectively. In contrast to CO_2 methanation, considerable amounts of carbidic carbon species and linear CO in addition to bridged CO, formate, methoxide and surface hydrocarbon species were present during CO methanation. Linearly adsorbed CO markedly retarded the hydrogenation of carbidic carbon to methane during CO hydrogenation.

Using the transient response method, Spinicci and Tofanari (23) observed a rapid increase in CO formation with an overshoot within the initial few minutes of CO_2 hydrogenation over SiO_2- and TiO_2-supported Ni catalysts while the methane formation was progressive. They attributed the overshoot response for CO formation to the slow regeneration of vacant active sites as a consequence of slow surface reactions or desorption of other products, and the progressive increasing response for CH_4 to a combination of slow surface reaction and desorption of the ensuing product. Thus, they suggested that the rate-limiting step of CO formation might be the regeneration of the active site or its intermediate and assumed that CO can be formed on the same active site as CH_4.

A study by Lapidus *et al*. (26) who used isotopes, non-steady-state and steady-state methods, found that significant amounts of CO and CH_4 were produced after switching a H_2-containing feed to a CO_2-containing feed over a carbon felt-supported Ni catalyst and suggested that a significant amount of H_2 was adsorbed on the catalyst surface. CO was considered as a possible main intermediate, as it appeared faster in the gas product than CH_4. CO_2 and H_2 adsorption was faster on the catalyst surface having preadsorbed hydrogen. The study suggests that CO and CH_4 are produced from CO_2 and H_2 in their adsorbed states. The fast and slow steps were suggested to be the hydrogenation of carbon fragments and CO formation, respectively.

Most of these studies, that suggest CO as the active intermediate, did not report the formation of other species such carbonates or formates on the catalyst surface. This does not completely

dismiss their formation. Appropriate techniques such as infrared (IR) spectroscopy that can detect such compounds were not used in most of these studies. In some case (11), IR spectroscopy was used on a catalyst surface with preadsorbed CO_2 in the absence of H_2. It has been reported (28 - 31) that in the absence of H_2, only CO and O_2 are formed by CO_2 dissociation above 200 K. Ren *et al*. (27) who recently used DRIFTS analysis, detected peaks for adsorbed CO_2, CO, hydrogen carbonates, monodentate carbonates and bicarbonate species during CO_2 methanation over unpromoted and Fe-promoted Ni/ZrO_2 catalysts. They, however, indicated that some of the species (monodentate, bicarbonate or hydrogen-carbonates) convert to CO_2 when the concentration of CO_2 is below a certain threshold value. As they observed a significant decrease in the peak intensities for adsorbed CO_2 and CO after exposure to H_2, they suggested that CO may be the active surface species in CO_2 methanation where CO_2 dissociates to CO by interaction with oxygen vacancies formed by reduction of the ZrO_2 surface.

Mainly Gupta *et al*. (32 - 34) have proposed a mechanism for CO_2 hydrogenation that involves CO as the main intermediate, without any significant role of formate species, on Ru catalysts. In their early study (32), they used experiments which essentially consisted in injecting CO_2 into a He feed stream followed by H_2 injections at different time intervals and analyzing the eluted products over a 1.8%Ru/molecular-sieve catalyst. The measurements were performed at different temperatures (400 – 600 K). Using electron spin resonance (ESR) technique, they observed no signal when CO_2 was introduced on the catalyst in the absence of H_2; however, a signal suggesting the formation of carbon on the catalyst surface was observed when the injection of CO_2 was followed by that of H_2 below 500 K. They suggested that CO_2 chemisorbs on the catalyst and is subsequently reduced by H_2 to yield methane through the formation of CO and active carbon as intermediates. In their subsequent study (33), they observed CO formation along CH_4 using a H_2:CO_2 ratio of 6:1 and temperatures above 523 K. They also observed some CO_2 adsorption and even some small extent of CO_2 reduction to CO at high

temperatures, in presence of H_2 on Ru-free supports. However, they indicated that the hydrogenation of the CO that formed, only occurred on Ru sites. No CO was observed in the absence of H_2. Using FTIR spectroscopy (34), they detected adsorbed CO (CO_a) on a Ru/TiO_2 catalyst after H_2 treatment at 475 and 575 K and subsequent exposure to CO_2. They detected these CO_a species even on a sample which was not H_2-pretreated. They suggested that possible sites for CO_2 reduction could include both Ru^0 and the $Ti_{2-\delta}$ moieties at the Ru/TiO_2 interface. As they observed that CH_4 formation was accompanied by simultaneous decrease of CO_a species on the surface when exposed to H_2, they proposed that the adsorbed CO is the precursor to CH_4 via active carbon formation. They found that the stability of CO_a species is considerably affected by coadsorbed or gaseous H_2. In the absence of H_2, the CO_a that formed upon exposure to CO_2 is strongly bonded to the surface and is not easily removed upon evacuation at elevated temperatures. However, in the presence of CO_2/H_2, the formed species were easily removed at room temperature. They concluded that the CO_a, which formed following the reactions proposed in Fig. 3, is very reactive to H_2 in preadsorbed or gaseous form.

Figure 3: Reactions occurring at catalyst surface during CO_2 or CO_2/H2 interaction with Ru/TiO_2 catalyst.

CO also forms on Cu-based catalysts during CO_2 hydrogenation and is not generally reported as an intermediate for methanol formation. It is rather a product of a parallel reverse water-gas-shift (RWGS) reaction (35, 36). Only few studies have reported CO as intermediate in methanol formation from CO_2 and H_2 over Cu-based catalysts. For example, Inui *et al*. (37) found that CO_2 was exclusively converted to CO at short contact times at 563 K over a $Cu/ZnO/Cr_2O_3$

catalyst promoted by Pd and Na. As the selectivity to methanol increased at prolonged contact times, they concluded that CO is an intermediate in CO_2 hydrogenation on this catalyst.

2.2 Reaction via formates

CO_2 methanation through the formation of formate species as active intermediates on Ni catalysts has mainly been proposed by studies that used in-situ spectroscopic techniques. Schild *et al*. (38) used in-situ diffuse reflectance spectroscopy in the hydrogenation of CO_2 over Ni/ZrO_2 catalysts. Under static conditions, they found that surface carbonate and formate species formed at 363 K, water and methane above 383 K and no gaseous CO was observed. In their dynamic experiment using a continuous flow of H_2 and CO (H_2:CO_2 ratio of 4:1), they found that carbonates and formates were detected from the beginning of the reaction. Adsorbed CO was only observed later in the reaction suggesting that it originated from the formate species that were steadily accumulating on the surface. Upon replacing the CO_2 and H_2 mixture with pure H_2 (under static conditions at 383 K) they found that methane was formed while the formate signals were decreasing and suggested that the formate species on the surface acted as the CH_4 precursor. The adsorbed CO did not desorb from the surface but was found to dissociate. They suggested the mechanism shown in Fig. 4 that combines CO and CO_2 hydrogenation and takes into account the RWGS that they observed to take place at elevated temperatures. The high methane selectivity observed for CO_2 compared to CO hydrogenation was explained by a non-dissociative path via formate hydrogenation.

Figure 4: Proposed reaction scheme for the hydrogenation of CO and CO_2 over nickel/zirconia catalysts.

The distribution of intermediate species on the surface of Ni/CeO_2-ZrO_2 and Ni/SiO_2 surface was found to be influenced by the catalyst support. Aldana *et al*. (15) used IR operando spectroscopy during CO_2 methanation, and found that significant surface concentrations of carbonates, of mainly the mono and bidentate types, were present on the Ni/CeO_2-ZrO_2 catalyst at 423 K and formate species were detected after 30 min of reaction. As their amount increased with temperature until 523 K before decreasing drastically while a significant amount of methane was formed, the authors suggested that formates are either intermediates or inhibiters involved in CO_2 methanation. CO formation on the surface also occurred from 423 K but the amount did not change with the increases in temperature. On the other hand, they found that formates species were already present on Ni/SiO_2 at 423 K with a lower surface coverage of carbonates being formed. Combining these findings with those of transient reaction techniques over the Ni/CeO_2-ZrO_2 catalyst, they proposed a mechanism where CO does not appear in the main pathway of methane formation (Fig. 5). Rather, the CeO_2-ZrO_2 support contributes to the formation of carbonates and formates as intermediates.

Figure 5: Reaction mechanism proposed on Ni-CZsol-gel sample for CO_2 methanation.

Similarly, Pan *et al*. (16) also proposed a mechanism (Fig. 6) that does not include CO as an active intermediate. Using in-situ FTIR spectroscopy, they found that carbonates and formates are intermediates for CO_2 methanation over Ni/$Ce_{0.5}Zr_{0.5}O_2$ and Ni/γ-Al_2O_3 catalysts. They suggested that the reaction over Ni//γ-Al_2O_3 proceeds through the hydrogenation of bidentate formates while that on Ni/$Ce_{0.5}Zr_{0.5}O_2$ proceeds through both bidentate and monodentate formates. They indicated that the hydrogenation of monodentate formates, derived from

monodentate carbonates (formed on medium basic sites such as ceria), is faster than that of the bidentate formates derived from hydrogen carbonates.

Figure 6: Proposed pathways for CO_2 activation and methanation, a) on $Ni/Ce_{0.5}Zr_{0.5}O_2$, b) on $Ni/\gamma\text{-}Al_2O_3$.

Most studies (26, 35, 39 - 51), that investigated the mechanism of CO_2 hydrogenation on Cu-based catalysts have reported formate species as the main reaction intermediate. However, controversial reports on the nature of the active site and the limiting steps of the reaction still exist. As Chinchen *et al*. (43) found similar specific activity for unsupported polycrystalline copper and supported Cu/Al_2O_3 catalysts exposed to a mixture of CO_2 and H_2 at 1 bar during TPR, they proposed that the critical step is the hydrogenolysis of formate on the copper surface. In a similar study where $60\%Cu/30\%ZnO/Al_2O_3$ and polycrystalline copper catalysts were involved, Bowket *et al.* (44) used TPR, TPD and microreactor kinetic measurements, and found that during methanol synthesis, from CO_2/H_2 at 500 K, the Cu surface was covered by oxygen (70-78% saturation) and formate species, while ZnO contained interstitial hydrogen. They also proposed that the limiting step was the hydrogenation of formate intermediates formed on the Cu surface by H_2 and CO_2 coadsorption. Hadden *et al.* (35) used ^{14}C-labelled CO_2 to study the adsorption and decomposition of CO_2 on polycrystalline copper at ambient temperature and low pressure (< 0.013 bar), and TPD after CO_2 adsorption on Cu surface at low temperatures (213– 498 K). They found that CO_2 was first weakly adsorbed at the clean Cu surface and that upon activation, it dissociated to produce adsorbed CO and surface oxygen that partially oxidized the Cu surface. Thereafter, CO_2 strongly adsorbed on this oxidized Cu surface in a state that can be hydrogenated to methanol via formate formation. When a $Cu/ZnO/Al_2O_3$ catalyst was used (45), an increased amount of CO_2 was measured on the partially oxidized

surface of Cu compared to a freshly reduced catalyst. The authors proposed that surface hydroxyl groups form on the oxidized catalyst as part of the H_2 reacts with the surface oxygen while some is dissociated on the metallic Cu. They also indicated that the formation of formate species through CO_2 interaction with surface hydroxyl species enhances CO_2 adsorption in the presence of H_2. In contrast, Rasmussen *et al*. (48) found no evidence of copper oxidation after the reaction of CO_2 and H_2 on Cu (100) surface and concluded that methanol can be formed on metallic copper with reaction rates comparable to commercial catalysts. They proposed that methanol is formed following the elementary steps reported in Fig. 7, where the hydrogenation of dioxomethylene (step 8) or the hydrogenation of formaldehyde (reaction 13) are the rate-limiting steps.

Figure 7: The elementary reaction steps relevant for methanol synthesis.

As Yoshihara and Campbell (50) used TPD technique and detected formates that were adsorbed on a Cu (110) surface after CO_2 hydrogenation, they also suggested that the active site for methanol synthesis on Cu/ZnO is metallic Cu. They believed that the role of ZnO may be to maintain a large proportion of the metallic Cu in ultrathin islands that behave like a Cu (110) surface.

Using XPS analyses, Nakamura *et al.* (49) detected formate species on a Zn-deposited polycrystalline Cu surface, which increased with increasing Zn coverage up to a coverage of 0.2 and decreased after this value. They proposed that formate species formed on the active sites that are located in the vicinity of ZnO_x species and that the rate-determining step for methanol formation is the hydrogenation of formate to methoxy species. Similar findings were reported when Zn with different coverages was deposited on Cu (111) surface by vapor deposition (51). Using XPS, the authors detected formates on the surface, after reaction, in an

amount that increased linearly with an increase in Zn coverage below 0.15 and suggested that Zn species stabilize formates. They indicated that the active sites for methanol synthesis are not only metallic Cu but also special sites such as Cu-Zn sites that work in synergy with Cu. They proposed a mechanism on a Zn/Cu(111) surface with Zn coverage below 0.2, where the formate species forms on the Cu atoms of the Cu (111) surface and subsequently migrates to the Cu-Zn site where it is hydrogenated to methanol through a methoxy species.

2.3 Reaction via formate and CO

Vesselli *et al*. (21) investigated CO_2 coadsorption with H_2 on Ni (110). They combined TPR in ultra-high vacuum (UHV), X-ray photoelectron spectroscopy (XPS) and high resolution electron energy loss spectroscopy (HREELS) techniques and observed the formation of formates on the catalyst surface. With the aid of density functional theory (DFT) calculations, they found that at 90 K, CO_2 is chemisorbed and activated on the surface via the carbon atom as $CO_2^{\delta-}$. This geometrical configuration changes when the temperature is increased in the presence of hydrogen as the H-CO_2 complex flips and binds to the surface through the two oxygen atoms while H binds to the carbon atom to yield formate. Further hydrogenation of formate by coadsorbed hydrogen was not observed to occur but instead, formate dehydrogenation took place when the temperature was increased to around 305 K (52) . CO formation from formate decomposition was not observed, and they found that the energy barrier for this decomposition was very high (> 3 eV) suggesting that formate is very stable, precluding further hydrogenation. After exposing preadsorbed CO_2 on Ni (110) to atomic hydrogen gas at 90 K and using TPD, XPS and HREELS analyses, they detected the formation of H_2O, formate and CO, the latter of which was shown to form by hydrogen-assisted CO_2 dissociation following the Eley-Rideal (ER) mechanism at 90 K. Combining with DFT calculations, they contended that the favourable reaction path is through a parallel ER mechanism involving CO as an intermediate (52). In their subsequent study (53) on an

unsupported model Ni catalyst using chemical transient kinetics at 1 bar, they found that CO_2 adsorption is strongly affected by hydrogen coadsorption and coverage. They suggested two parallel reaction mechanisms: i) fast direct hydrogenation of CO_2 at the beginning of the reaction where a complex obtained is suddenly dissociated and further reacts to produce gaseous methane and ii) a mechanism involving formate-derived species at steady state conditions. The rate-limiting step was believed to be the removal of these oxygen-containing intermediates that are slow to react and accumulate on the catalyst surface.

Recently, Westermann *et al*. (54) used operando IR spectroscopy for both CO_2 adsorption and methanation conditions over Ni/USY zeolite catalysts (5 – 14% Ni). Based on the evolution of the relative concentration of methane in the gas phase, adsorbed CO and formates, and the CO_2 conversion during TPSR (Fig. 8) they observed that the intensity of carbonyl bands was increasing with a corresponding decrease in formate band intensity between 150 and 250 ^oC. They suggested that CO arises from formate decomposition and was subsequently dissociated and /or was hydrogenated within a temperature range of 200 - 300 ^oC as the system gained more energy. They also considered a direct hydrogenation of formates at higher temperatures where they were observed to suddenly decrease. Their proposed mechanism in Fig. 10 involves hydrogen dissociation on the Ni surface and reaction with weakly adsorbed CO_2 or carbonates to form monodentate formates, and then carbonyls, which are hydrogenated to methane.

Figure 8. Evolution of the relative concentrations of $CH_{4(g)}$, adsorbed CO (2100‑1740 cm $^{-1}$) and formates (1573 cm^{-1}) and CO_2 conversion (%) during TPSR Ar/H_2/CO_2 (75/20/5) over 14% NiUSY zeolite.

Figure 9: Proposed mechanism for CO_2 hydrogenation on NiUSY zeolites.

In contrast, Fan *et al.* (55) have proposed that carbonates are spectator species on Ni/$MgAlO_4$ catalysts, as CO_2 adsorption analysis at 523 K suggested that they form in the absence of H_2 and Ni^0 and arise from the surface reaction of CO_2 with O^{2-} from the support. Using DRIFTS analysis, they found that surface carbonyls were produced above 473 K and were believed to be the true intermediate for CO_2 methanation. They suggested that the reaction proceeds via the dissociation of formates to adsorbed CO, which is subsequently hydrogenated to methane. From the studies reviewed in the above sections, it can be generally accepted that CO and formate species form on the catalyst surface during CO_2 methanation on Ni-based catalysts. However, the role of CO and formate still needs to be clearly understood. This task becomes more complex on supported catalysts where the support may play a role in the mechanism. Indeed, the role of the catalyst support cannot be underestimated as it can significantly modify catalyst surface properties and its adsorptive features. For example, in addition to adsorptive properties toward CO_2 observed on some supports (15, 16, 55, 56), some degree of interaction between Ni species and the support such as alumina has been reported (57 - 65) and can produce some surface spinel/Ni aluminate species with modified properties. Therefore, the analysis of intermediates species on supported Ni catalysts requires more caution. More insight on the mechanism can be obtained from unsupported (20, 22, 24, 25, 53), model (21, 52) and supported Ni catalysts (11 – 13, 19, 23) with support materials that possess low or virtually no basicity and which do not strongly interact with Ni, such as SiO_2. Almost all these studies suggest a mechanism of CO_2 methanation via CO as the main route. In parallel to CO_2 dissociation, formate species are also formed on the Ni surface. As mentioned earlier, these species were not detected in other studies mostly because appropriate techniques suitable for their detection were not used.

Since it has been reported that before CO_2 dissociation on a Ni surface, the adsorbed CO_2 is negatively charged and most likely possess a C_{2v} symmetry where it is coordinated to the metal

surface through oxygen (28 – 30, 66), it is possible that the hydrogenation of this species leads to bidentate formate as also found by Vesselli *et al*. (21). These species are slow to react and accumulate on the catalyst surface (53). A different mechanism is possible on a catalyst where the support promotes the formation of monodentate formate that can, in turn, be hydrogenated faster than bidentate formate (16).

The absence of heavier hydrocarbons during CO_2 hydrogenation as compared to CO hydrogenation is usually explained by reasons that include the following: i) a lower surface concentration of carbon in the case of CO_2 hydrogenation (12); ii) geometric dilution by adsorbed oxygen atoms which are relatively more abundant in the case of CO_2 adsorption and which contribute to decreased probability for C-C bond formation (12); iii) the slow activated adsorption of CO_2 which may create a higher H_2:CO surface ratio during steady-state hydrogenation (13) and iv) a limited amount of reversibly adsorbed CO which is reported to inhibit the hydrogenation of surface carbon (22, 24, 25).

Solymosi *et al.* (67) used a microscale, IR spectroscopy, thermal desorption, mass spectroscopy, a micro reactor, and micro catalytic pulse system to study the hydrogenation of CO_2 on supported Ru catalysts. They found that CO_2 was adsorbed on a Ru/Al_2O_3 catalyst at 298 – 373 K and its coverage decreased with increasing temperature. The adsorption was mainly observed on the Al_2O_3 support and was enhanced in the presence of H_2. They observed the formation of CO_a and formate in presence of CO_2 and H_2 at 373 K and also during CO_2 hydrogenation at high temperatures. No formate was detected on any Ru-free support at 298-573 K. They considered formates as inactive species in the methanation of CO_2 as they proposed that they form on the Ru surface but migrate rapidly to the support. They based their findings on the following observations: i) the adsorption of formic acid on the support, or on supported Ru, gave identical formate bands as recorded during the surface reaction of H_2 and CO_2; ii) the stability of the formate ion was the same; iii) the accumulation of the formate ion

on the Ru/Al_2O_3 sample during the reaction did not influence the rate of methanation and iv) the preadsorption of formic acid had no influence on the band areas for the adsorbed CO. They proposed a mechanism (Fig. 10) where Ru activates H_2 molecules by producing adsorbed hydrogen atoms that react with CO_2 to produce formate. Part of the formate species decomposes on the Ru surface, yielding CO_a and the remainder quickly migrates to the support. Since they also identified surface carbon during the reaction, they proposed that this surface carbon is most probably produced by the dissociation of chemisorbed CO, promoted by the adsorbed H.

Figure 10: Mechanism for CO_2 methanation on Ru catalyst.

Prairy *et al.* used DRIFTS, transient and steady-state experiments to study CO_2 hydrogenation mechanism over Ru/TiO_2 (68 - 70), and Ru/Al_2O_3 (70) catalysts. They observed that CO was adsorbed in the on-top position on Ru^0 and formate formed under steady conditions in presence of CO_2 and H_2 at 393 K on the Ru/TiO_2 catalyst. They proposed that CO_a is formed via the RWGS reaction in which formate ion is implicated. They studied the role of CO_a in producing CH_4 using transient experiments. They did not find any rate dependence on CO_a coverage but suggested that CO is the primary intermediate in CO_2 methanation (68). Some carbonates, bicarbonates and/or formates also formed on the catalyst support. As these species disappeared with time while the surface coverage of CO_a increased, the authors suggested a possible migration of these species from the support to the Ru surface. In the presence of H_2, they found that CO_a species were actively consumed and that the cabonates/formates quickly disappeared. Therefore, they suggested that carbonates and formates from the support may be a source of CH_4 via CO_a species in the presence of H_2. They investigated the role of formate species in the

overall mechanism by using a batch reactor where they compared the rate of CH_4 formation from CO_2/H_2 and $HCOOH/H_2$ mixtures, respectively (70). They found that relative initial rates were similar and suggested that CO_2 reduction to formate is not rate-limiting. No adsorbed species were observed when they exposed a blank TiO_2 support to CO or a mixture of CO_2 and H_2; however, formate species formed upon exposure to HCOOH. The formate species did not decompose or desorb in flowing Ar or H_2 stream at 473 K for more than 4h but disappeared in the presence of H_2 from 353 K on the Ru/TiO_2 catalyst. The authors, therefore suggested that formates form more on the catalyst support and that in the presence of CO_2 and H_2, Ru plays a role of catalyzing CO_2 reduction to formates, using dissociated hydrogen, and their subsequent dehydrogenation to form CO_a.

Marwood *et al*. (71 - 73) also observed the formation of CO_a and formate on a Ru/TiO_2 catalyst. Using in-situ IR surface analysis under dynamic cyclic conditions where the concentration of CO_2 was periodically varied in a H_2 reaction feed, they proposed a reaction path where CO_2 chemisorbs on the catalyst surface to form adsorbed bicarbonate species, which is subsequently hydrogenated to a formate species. The latter of which decomposes to adsorbed CO which is subsequently hydrogenated to CH_4 as shown in Fig. 11 (71).

Figure 11: Mechanism of methane formation on Ru/TiO_2.

They found that the formation of CO_a is inhibited by H_2O and enhanced by H_2, while the hydrogenation of CO_a species is not influenced by H_2O partial pressure. They deduced that the rate-limiting step in the overall reaction is the formation of CO_a (72). In a later study (73) , they found that formate species were fixed on the catalyst support, in equilibrium with an active formate species on the metal-support interface. They proposed a mechanism where the

precursor for CO_a is an active formate species that is formed by the reduction of HCO_3^- species at the Ru-support interface.

The formation of methane via adsorbed formate species, which is subsequently transformed into adsorbed CO, was also proposed on Ru/SiO_2 and Ru/ZSM-5 catalysts (74). Upon catalyst exposure to a H_2/CO_2 mixture (H_2:CO_2 ratio of 13:5) at room temperature, the authors detected linearly adsorbed CO on Ru^0 on both Ru/ZSM-5 and Ru/SiO_2 catalysts using FTIR spectroscopy. They suggested that CO and H_2 compete for the same Ru sites forming RuH(CO) species. They also observed formate species and suggested that the adsorbed CO is hydrogenated to methane following the same route as for CO hydrogenation. Using in-situ FTIR technique, Panagiotopoulou *et al*. (75) also detected carbonates and formate species associated with the TiO_2 support when a $5\%Ru/TiO_2$ catalyst was exposed to a mixture containing $1\%CO_2$ and $5\%H_2$ at 298 K. A progressive formation of adsorbed CO on the Ru surface was observed above 373 K and went through a maxiumum at ca. 473K. They found that under CO_2 hydrogenation conditions, the catalyst is able to convert CO_2 into CO species which cannot be dissociated into detectable amount of Ru-C and Ru-O. They also found that the presence of H_2 promotes the conversion of CO_2 to CO_a. Coupling these findings with their H_2-TPD results, they proposed a mechanism where the hydrogen adsorbed on Ru surface migrates to the Ru-TiO_2 interface where it reacts with the CO_2 adsorbed on the TiO_2 support to form formate and Ru-CO species.

3 Kinetics

3.1 Effect of temperature

The work of Cratty, Jr and Russell (76) was one of the earliest studies that systematically investigated the effect of temperature on CO_2 hydrogenation over an unsupported nickel catalyst. The catalyst was prepared by precipitation of nickel as carbonate, reduced by hydrogen and tested from 473 to 773 K. Using a H_2:CO_2 feed ratio of 2:1, they observed that

CH_4 was the predominant product with a small yield of CO. The CH_4 yield increased with the reaction temperature and went through a maximum of ca. 50% between 573 and 673 K.

Similar trends where CO_2 conversion and methane production passed through a maximum between 573 and 673 K were also reported on supported nickel catalysts (18, 55, 77 - 79). Weatherbee and Bartholomew (18) measured maximum CO_2 conversion and methane production at around 635 K in a more diluted system (1% CO_2 and 4% CO_2 in N_2) over a 3%Ni/SiO_2 catalyst. Maximum CO_2 conversion and methane production were measured at 623 K over model Ni (53), 10-25 wt.% Ni /Al_2O_3 (78), Ni/bentonite (79) and Ni/$MgAlO_4$ (55) catalysts, respectively. An increase in CO_2 conversion with temperature up to 773 K has been reported for Ni supported on rice husk ash (RHA) (77); Ce- and Sm- doped Ni/ZrO_2 (80) and 69.1% Ni/Al_2O_3 (14, 81).

High temperatures have also been reported to increase the formation of CH_4 on molecular sieve-supported Ru (1.8% Ru, 400 – 525 K) (32), Ru/Al_2O_3 and molecular-sieve-supported Ru (400 – 600 K) (33), Ru/Al_2O_3 (443 – 553 K) (82) catalysts. Some studies have reported that that the CO_2 conversion and/or the formation of methane increased and went through a maximum over a 0.5% Ru/SiO_2 (max. at 675 K) (83), 0.5%Ru/Al_2O_3 (max. at 623 K) (84), 10%Ru/ɣ-Al_2O_3 (max. at 548 K) (85) and 3% Ru/TiO_2 (max. at 623 K) (86) when the reaction temperature was increased. On the other hand, Panagiotopoulou *et al*. (87) found that CO_2 conversion increased and the methane selectivity decreased with an increasing temperature (423 – 723K) on a 0.5%Ru/Al_2O_3 catalyst.

Increases in catalyst activity with an increasing reaction temperature can be expected as the system gains more heat to overcome the activation energy. The latter is significantly affected by catalyst composition, preparation method and testing conditions. Values for the activation energy required for CO_2 hydrogenation over Ni- and Ru-based catalysts are compiled in Tables 1 and 2, respectively.

Table 1. Activation energy for CO_2 hydrogenation over nickel-based catalysts

---

Table 2. Activation energy for CO_2 hydrogenation over ruthenium-based catalysts

---

The lowest value (13.1 kJ/mole) was obtained with a ceria-promoted nickel catalyst supported on carbon nanotubes (12% Ni/4.5% Ce/CNT) (99) and the highest (138 kJ/mole) on a nickel-phosphide catalyst (90). For Ru-based catalysts, the lowest and highest activation energies of ca. 17.6 and 105 kJ/mole were respectively obtained with molecular-sieve-supported Ru (1.8%) catalyst activated by ɣ-irradiation (33) and 0.6%Ru/ɣ-Al_2O_3 (103).

Decreases in activity measured at high temperatures can be due to catalyst deactivation and/or thermodynamic limitations as CO_2 hydrogenation is an exothermic process where the equilibrium conversion decreases with increasing temperatures.

Generally, the rise in operating temperature during CO_2 hydrogenation has been reported to increase the CO_2 conversion and the selectivity for CO, and decrease the selectivity for methanol on Cu catalysts. This trend has been reported on Cu/Al_2O_3 (453 – 533 K) (41), Cu/TiO_2 (493 – 553 K) (105), Cu/ZrO_2 (493 – 553K) (105), (453 – 553K) (36), $Cu/ZnO/La_2O_3$ (523 – 673 K) (42), Cu/SiO_2 (523 – 623 K) (36, 106), $Cu/ZnO/Al_2O_3/Cr_2O_3$ (463-553 K), $Cu/ZnO/Cr_2O_3$ (453 – 593 K) (107) , Cr-CuB, Zr-CuB, Th-CuB and Cu-Zn (473 – 300 K) (108), $Cu/ZnO/Al_2O_3$ (453 – 513 K) (109), (473 – 533 K) (110), $Cu/ZnO/ZrO_2$ and $Cu/ZnO/CeO_2$ (453 – 513 K) (109), and $Cu/ZnO/Al_2O_3/ZrO_2$ (443-583 K) (111) catalysts. In some cases (42), the selectivity to light hydrocarbons, such as CH_4, also increased with the rising temperature.

Using a $Cu/ZnO/Cr_2O_3$ catalyst that was promoted by Pd and Na, Inui *et al*. (37) found that below 20 bar, the formation of methanol decreased with an increase in temperature (493 – 593

K). At high pressure, for example around 50 bar, the yield for methanol increased with temperature and went through a maximum at around 543 K before decreasing, while approaching equilibrium data. They indicated that in the temperature range considered, the catalyst tends to oxidize at higher pressures.

Activation energies of ca. 67 and 69 kJ/mol have been reported on Cu (110) (50) and Cu (100) (47, 48), respectively.

3.2 Effect of pressure and space velocity

Experimental data showing the effect of pressure on CO_2 hydrogenation over nickel-based catalysts are scarce. As the reaction proceeds with gas contraction, the increase in pressure is expected to increase the equilibrium conversion. Some experimental data have been reported by Weatherbee and Bartholomew (18) and Abelló *et al*. (81) suggesting a positive effect of high pressure on CO_2 hydrogenation on nickel catalysts. Weatherbee and Bartholomew (18) found that the yield for methane during CO_2 hydrogenation on a 35%Ni/SiO_2 catalyst increased with an increase in reaction pressure (1.4 – 26 bar). Abelló *et al*. (81) used 5, 10 and 20 bar for CO_2 hydrogenation over a 69.1% Ni/Al_2O_3 catalyst at different temperatures. They found that CO_2 conversion and CH_4 selectivity were lower and the CO selectivity was higher at 5 bar. Pressure did not have a significant effect above 10 bar.

Understanding the effect that the space velocity has on a catalytic process is very important as more insight on equilibrium and non-equilibrium product composition can be obtained.

Increasing the space velocity decreased the methane yield on a Ni/SiO_2 catalyst (18). Using space velocities of 0.2 – 1 mole $CO_2/g_{Cat}/h$ during CO_2 hydrogenation over a 69.1 %Ni/Al_2O_3 catalyst at different temperatures, Abelló *et al.* (81) measured equilibrium CO_2 conversion and methane selectivity for all space velocities at temperatures above 723 K. No equilibrium was reached below 623 K even at the lowest space velocity.

Rahmani *et al*. (78) found that the CO_2 conversion decreased but the CH_4 selectivity remained unchanged when the space velocity was increased from 6 to 18 L/gCat/h using a 20%Ni/Al_2O_3 catalyst. These results suggest that methane is a primary product for CO_2 hydrogenation.

Systematic studies on the effect of operating pressure on CO_2 hydrogenation using Ru-based catalysts are also limited. In a study by Weatherbee and Bartholomew (83), it was reported that the rates for CO_2 conversion and CH_4 formation over a 0.5%Ru/SiO_2 catalyst increased with the operating pressure. They fitted their data to a power-law and found that the order of pressure dependence was 0.069 for both CO_2 conversion and CH_4 formation rates.

The dependence of CO_2 hydrogenation on space velocity over Ru-based catalysts has been reported by a number of studies (74, 85). Scirè *et al.* (74) observed that the CO selectivity decreased and the CH_4 selectivity increased with an increase in CO_2 conversion (decrease in space velocity) over 2%Ru/SiO_2 and 2%Ru/ZSM-5 catalysts. Janke *et al*. (85) found that increasing the space velocity over a 10%$Ru/ɣ\text{-}Al_2O_3$ catalyst resulted in a decrease of CH_4 formation.

High pressure has been reported to improve the selectivity and yield for methanol over CuO/ZnO (15 – 40 bar) (112), La-promoted $Cu/ZnO/Cr_2O_3/Al_2O_3$ (20 - 80 bar) (113), $Cu/ZnO/Al_2O_3/Cr_2O_3$ (1 - 30 bar) (46), Pd and Na-promoted $Cu/ZnO/Cr_2O_3$ (10 – 50 bar) (37), $Cu/ZnO/Cr_2O_3$ (1 - 50 bar) (107), $Cu/ZnO/Al_2O_3$, $Cu/ZnO/ZrO_2$ and $Cu/ZnO/CeO_2$ (1– 50 bar) (109), and $Cu/ZnO/Al_2O_3/ZrO_2$ (10 – 90 bar) (111) catalysts.

Denise *et al*. (40) found that short contact times (high space velocity) favored methanol formation, while extended times led to the formation of more CO along with H_2 and H_2O through a reaction involving CO_2 and methanol. Similarly, Amenomiya *et al*. (105) also found that methanol selectivity over CuO/ZrO_2, $CuO/Cr_2O_3\text{-}Al_2O_3$, $CuO/ZrO_2/Al_2O_3$ and $CuO/ZrO_2/SiO_2\text{-}Al_2O_3$ catalysts decreased as the space velocity decreased (conversion

increased) as shown in Fig. 12, where the curves for carbon conversion to methanol, deviate to the right as the total CO_2 conversion increases.

Figure 12: Conversion to methanol vs. total conversion.

In other cases involving $Cu/ZnO/Al_2O_3/Cr_2O_3$ (46) and $Cu/ZnO/Cr_2O_3$ (107) catalysts, the selectivity for methanol was reported to decrease and go through a minimum before rising as the contact time was increased. Gao *et al.* (111) have indicated that when the contact time is long enough, methanol formation prevailed on CO formation over a $Cu/ZnO/Al_2O_3/ZrO_2$ catalyst.

3.3 Effect of feed composition

The data for CO_2 hydrogenation reported in the literature to date have been generated using a wide range of feed composition and this has made any comparison of data from different laboratories difficult. However, a limited number of studies have reported on the effect of CO_2 hydrogenation products such as CH_4 and H_2O (88), CO (88, 114, 115) and H_2:CO_2 ratio (81, 116) in the feed for CO_2 hydrogenation over Ni catalysts.

van Herwijnen, *et al*. (88) studied the effect of reaction product on the rate of CO_2 hydrogenation on a Ni/γ-alumina catalyst by adding CH_4 to the feed (CO_2:CH_4 ratio of 0.55 and 0.61). They concluded that CH_4 and H_2O at low concentrations have no effect on the reaction rate. However, CO in concentrations above 200 ppm inhibit CO_2 methanation. The latter was delayed until very high conversions of CO were achieved. This was explained by a fast CO adsorption that occupied most of the active sites on catalyst surface compared to CO_2. Similar behavior was observed by Inui *et al.* (114) who studied the effect of CO on CO_2 methanation over a Ni/La_2O_3-Ru catalyst. They found that CO inhibits CO_2 methanation as the latter only occurred when the temperature corresponded to high CO conversion.

The study by Sheshko and Serov (115) on the hydrogenation of mixed carbon oxides (9 vol.% CO, 15 vol.% CO_2 in He) with hydrogen to carbon oxides ratios of 2:1 and 4:1 over ultra-dispersed Ni powder at 573 - 823 K rather suggested that both CO and CO_2 were hydrogenated through dissociative adsorption on the catalysts surface and led to methane as the main product. The effects of H_2:CO_2 ratio on the hydrogenation of CO_2 over nickel catalysts have been reported by Abbeló *et al*. (81) and Rahmani *et al*. (116) . Increasing the H_2:CO_2 ratio from 3:1 to 4:1 and 5:1 during CO_2 hydrogenation over a high loaded (69.1 wt.%) Ni/Al_2O_3 catalyst increased the CO_2 conversion as the reaction was promoted by a high concentration of dissociated hydrogen on the catalyst surface (81) . A similar trend was observed by Rahmani *et al*. (116) when the H_2:CO_2 ratio was increased from 3:1 to 4:1 but the CH_4 selectivity remained unchanged and close to 100%.

Addition of water vapor (30%) to a H_2/CO_2 feed for CO_2 hydrogenation over a Ru/Al_2O_3 catalyst, decreased the activity of the catalyst (87). This was attributed to the enhancement of the WGS reaction. The presence of water inhibited the hydrogenation of CO as intermediate toward methane formation.

Lange *et al*. (117) have reported that the presence of N_2 in the feed for CO_2 hydrogenation over Ru/ZrO_2 catalysts did not affect the product selectivity when the H_2/CO_2 ratio was kept unchanged.

3.4 Effect of support

Metal oxides such as Al_2O_3, SiO_2, TiO_2, ZrO_2, ZnO and CeO_2 are the most used supports for Ni, Ru and Cu catalysts for CO_2 hydrogenation. Carbon-based and zeolite supports have also been used in a few studies. Comparison of the effects of various metal oxide supports on these catalysts is yet to be entirely conclusive as it is affected by many other factors such as support phase, metal loading, and catalyst preparation, pretreatment and testing conditions. For

example, tetragonal ZrO_2-supported nickel catalysts displayed higher turnover frequency for methanation and greater CO_2 adsorption than monoclinic ZrO_2-supported nickel catalysts (118).

Vance and Bartholomew (91) compared the effect of Al_2O_3, SiO_2 and TiO_2 supports on the adsorption properties and catalytic performance of Ni for CO_2 hydrogenation. They used low-loaded (3 wt.%) catalysts prepared by an impregnation method and found that the CO_2:H adsorption ratio, the catalyst activity for CO_2 hydrogenation and the CH_4 selectivity increased in the order Ni/SiO_2 < Ni/Al_2O_3 < Ni/TiO_2. Spinicci and Tofanari (23) compared SiO_2 and TiO_2 as supports for 10 wt.% Ni catalysts used for temperature programmed CO and CO_2 hydrogenation and measured the highest activity and CH_4 selectivity on Ni/SiO_2 between 543 and 573 K and between 653 and 673 K for Ni/TiO_2 catalysts, respectively.

Chang *et al*. (77, 119, 120) compared CO_2 hydrogenation activity and selectivity for Ni supported on rice husk ash (RHA) and on silica. They measured higher methane yield and selectivity on a RHA-supported catalyst compared to a silica-gel-supported catalyst. The promotion effect of the RHA-supported catalyst was believed to be due to stronger metal-support interactions compared to the silica-supported catalyst (77).

When catalysts containing 5 wt.% of Ni supported on γ-Al_2O_3, SiO_2, protonated Y zeolite (HY), MCM-41 and mesostructured silica nanoparticles (MSN) were compared, the activity for CO_2 methanation increased in the following order: $Ni/\gamma\text{-}Al_2O_3$ < Ni/SiO_2 < Ni/HY < Ni/MCM-41 < Ni/MSN. The methanation activity increased with an increase in concentration of basic sites (98).

In a recent study, Pandey and Deo (121) found that the effect of support for catalysts containing 10% Ni on the yield for methane increased in the following order Nb_2O_5 < SiO_2 < TiO_2 < ZrO_2 < Al_2O_3. The enhancement was related to the ability of the support to adsorb CO_2.

Rare earth oxides also improve CO_2 hydrogenation on Ni catalysts. Under similar reaction conditions, higher activity for CO_2 hydrogenation was measured on 10%Ni/La_2O_3 catalyst compared to 10%Ni/γ-Al_2O_3 (122). 10 wt.% Ni/CeO_2 catalyst had higher CO_2 conversions and methane selectivity compared to α-Al_2O_3, TiO_2 and MgO-supported catalysts (123). This was explained by more CO_2 adsorbed on the Ni/CeO_2 catalyst and the partial reduction of CeO_2 during catalyst activation in hydrogen. At 673 K, the CO_2 conversion and methane selectivity increased in the following order: Ni/MgO < Ni/TiO_2 < Ni / α-Al_2O_3 < Ni/CeO_2. . Supporting Ni on CeO_2-ZrO_2 mixed oxides leads to higher CO_2 hydrogenation activity (15, 16, 124). The mixed oxide provides mild or medium-strength basic sites (15, 16) where monodentate carbonates form and lead to the formation of monodentate formates that are quickly hydrogenated (16).

A few studies on the use of carbon materials as supports for Ni catalysts have also been reported. Guerrero-Ruiz and Rodriguez-Ramos (93) found that supporting Ni (4.5%) on carbon reduces CH_4 selectivity and increases CO selectivity compared to bulk Ni. The authors indicated that further studies are required to explain these findings. A better catalytic performance for Ni supported on multi-walled CNTs was reported by Wang *et al*. (99) compared to Al_2O_3-supported Ni catalysts. The extent of reduction of Ni was higher on CNT-supported catalysts.

Appropriate support pretreatment can also have a significant effect on CO_2 methanation. For example, higher activity was measured on Ni supported on acid–alkali treated bentonite support compared to the untreated materials. Support treatment led to a higher specific surface area and an improvement in the dispersion of Ni particles (79).

At similar Ru loading (1.8 wt.%), the catalyst that was supported on molecular sieve (MS) showed higher methane yield compared to that of an alumina-supported catalyst (33). CO_2 was more strongly adsorbed on Ru/Al_2O_3 compared to Ru/MS. Solymosi *et al*. (67) compared

Al_2O_3, MgO, SiO_2, and TiO_2 supports for Ru and found that the adsorption of CO_2 in the presence of H_2 increased in the following order: 5%Ru/SiO_2 < 5%Ru/Al_2O_3 < 5%Ru/MgO < 5%Ru/TiO_2. The trend was function of the surface area of Ru. Higher methane selectivity (> 99%) was measured at 298 K on a Ru/TiO_2 catalyst while no activity was measured on Ru/Al_2O_3 and Ru/SiO_2 catalysts under similar conditions (pCO_2: 0.05 bar, pH_2: 0.6 bar) (102). In a subsequent study, Prairie *et al.* (70) found that a Ru/TiO_2 catalyst was 15 times more active than a Ru/Al_2O_3 catalyst at similar Ru loading (3.8%). Both had similar activation energy but the coverage of adsorbed CO was higher (0.4) on the TiO_2-supported catalyst and 0.2 on the Al_2O_3-supported catalyst. The high activity for the Ru/TiO_2 catalyst was explained by a high dispersion of Ru on the TiO_2 support. Scirè *et al*. (74) compared zeolite (H-ZSM-5, SA = 410 m^2/g) and silica (25 and 490 m^2/g) as supports for Ru (2%) and measured higher methane selectivity on Ru/ZSM-5. They explained that this was related to a higher positive polarization of Ru on the zeolite, leading to a weaker Ru-CO bond with corresponding increase of hydrogen coverage on the surface.

At similar Ru loading (ca. 3%), Hu *et al.* (125) found that the conversion of CO_2 increased as Ru/TiO_2 (rutile, SA <5 m^2/g) < Ru/α-Al_2O_3 (SA < 5 m^2/g) < Ru/MgO-Al_2O_3 (SA = 168 m^2/g) < Ru/SiO_2 (SA = 46 m^2/g) < Ru/TiO_2 (P-25, SA = 30 m^2/g) < Ru/TiO_2 (R/A = 60:40, SA = 50 m^2/g). The methane selectivity followed a similar trend. They indicated that the hydrogenation of CO_2 was not only affected by the surface area of the support, as in the case for TiO_2-supported catalysts, but also by the interaction between Ru and the support. Kowalczyk *et al.* (126) compared active Al_2O_3 (225 m^2/g), MgO (94 m^2/g), $MgAl_2O_4$ spinel (96 m^2/g) and turbostatic carbons of low (CA: 66 m^2/g) and high (CB: 440 m^2/g and CB_{H2}: 435 m^2/g) surface area supports for Ru and found that the catalyst activity increased in the following order: 9%Ru/CA < 10%Ru/MgO < 10%Ru/$MgAl_2O_4$ < 10%Ru/Al_2O_3.

The use of ZnO in the formulation of Cu-based catalysts for methanol synthesis from CO_2 and H_2 has been vastly reported (37, 42, 47, 49 – 51, 105, 109,113, 127 – 141), although its effects on Cu surface properties still remain controversial. The various ways in which ZnO has been reported to influence Cu catalyst during CO_2 hydrogenation include improving Cu dispersion (47, 135), maintaining metallic Cu in ultrathin islands that behave like Cu (110) surface (50), and the creation of new active sites (49, 51, 131).

Using XRD and EDX, Kanai *et al.* (131) showed that ZnO_x species migrate onto the Cu surface and dissolve into the Cu particle forming a Cu-Zn alloy during catalyst reduction above 600 K. Combining with their CO-TPD and FTIR results, they found that more active Cu^+ sites for methanol production formed in the vicinity of ZnO_x species on the Cu surface. Nakamura *et al.* (49) deposited Zn species with varying coverage on a polycrystalline Cu surface by vapour-deposition method to form a model system and found that the TOF for methanol increased with Zn coverage and reached a maximum (six times more active than the Zn-free Cu surface) at a Zn coverage of 0.17, after which it started to decrease as the Zn coverage was further increased. They suggested that ZnO_x species directly promote methanol formation by forming new active sites, which they proposed to be Cu^+-O-Zn species that are created in the vicinity of ZnO_x species on the Cu surface. These sites were believed to stabilize reaction intermediates such as formate and methoxy species. The authors also found that the ZnO_x/Cu model catalyst behaved similarly to a powder Cu/ZnO catalyst. A further study (51) involving the coverage of Cu (111) surface with Zn species also showed a similar trend where up to a Zn coverage of 0.19, the TOF for methanol linearly increased with Zn coverage. At a Zn coverage of 0.19, they measured a TOF that was 13 times higher than that on Zn-free Cu (111) surface. As indicated in section 2.2, they suggested that the active sites for methanol synthesis are not only metallic Cu but also Cu-Zn sites.

Other supports for Cu catalysts have also been explored. Denise and Sneeden (127) found that supporting Cu on MgO, La_2O_3 and Sm_2O_3 led to much less active catalysts for CO_2 hydrogenation. However, ZnO, Al_2O_3, ZrO_2, ThO_2-K-supported Cu catalysts and $Cu/ZnO/Al_2O_3$ displayed higher activities. Amenomiya (105) found that, at similar Cu loading, the conversion of CO_2 to methanol varies as $CuO/ZrO_2 > CuO/Cr_2O_3$-$Al_2O_3 > CuO/ZnO > CuO/TiO_2 > CuO/Al_2O_3 > CuO/SiO_2$. CuO/SiO_2 did not show any activity. On the other hand, the selectivity to methanol varied as $CuO/ZrO_2 > CuO/ZnO > CuO/TiO_2 > CuO/Cr_2O_3$-$Al_2O_3 > CuO/Al_2O_3 > CuO/SiO_2$. They found that the surface area for the catalyst did not have a significant role on the catalyst performance but rather the nature of the Cu interaction with the support. Fujitani *et al*. (130) found that the specific activity for methanol formation changed as $Cu/Ga_2O_3 > Cu/ZnO > Cu/Cr_2O_3 > Cu/ZrO_2 \approx Cu/Al_2O_3 > Cu/SiO_2$. They related the role of these oxides to the formation of Cu^+ site at the interface of Cu particle and metal oxide moiety, which is located on the surface of Cu or near the perimeter of the Cu particles.

3.5 Effect of promoter or surface modifier

Nickel catalysts have been modified by adding elements in the form of metals or oxides with the aim of affecting their catalytic properties for CO_2 hydrogenation.

Addition of a small amount of copper (< 4%) greatly increased the yield for CO and decreased that of CH_4 (76). High amounts of Cu diluted Ni and formed alloys that decreased the rate of CO_2 hydrogenation (10) .

Potassium, a well-known promoter that is used to increase the selectivity for heavier hydrocarbons in CO hydrogenation (142 - 144), has also been used to promote Ni catalysts for CO_2 hydrogenation. Increased CH_4 and CO production rates were observed upon preadsorption of potassium on a Ni (100) catalyst but with no promotion for higher hydrocarbons (20). Upon promoting supported Ni catalysts by potassium, Campbell and Falconer (94) found that the

effect is dependent on the support used. On Ni/SiO_2-Al_2O_3 catalyst, they found that potassium at low coverage increased the rate for CO_2 hydrogenation and the opposite happened at higher potassium coverage. Only small amounts of C_2 hydrocarbons were observed on unpromoted and K-promoted samples. However, on Ni/SiO_2 catalyst, potassium rapidly decreased the hydrogenation rate. It did not promote the formation of higher hydrocarbons or olefins but changed the CH_4/CO product ratio by increasing the formation of CO. In addition to small amounts of C_2 hydrocarbons detected on catalyst samples having 0 – 0.81% K, small quantities of C_3 hydrocarbons were observed on Ni/SiO_2 samples that contained 0.25 and 0.81%K.

Rare earth elements and noble metals can also significantly modify Ni catalyst properties for CO_2 methanation. Addition of small amounts of La (0.2% of Ni) and Ru (0.1% of Ni) to a supported Ni catalyst leads to an increase in CO_2 methanation rate (89, 145). La_2O_3 improves CO_2 adsorption by its basicity and Ru serves as a porthole for H_2 spillover (145). Lanthanum added to NiO/Al_2O_3 catalysts in small quantities, e.g. 0.04 elementary molar fraction, enhanced CO_2 conversion to methane (146). Small amounts (< 5%) of Ce promotes Ni reducibility (by improving Ni-support interaction) and dispersion on the support (99, 116) and enhances CO_2 methanation (99, 116, 146). It significantly decreased the activation energy for CO_2 hydrogenation on nickel catalyst supported on carbon nanotubes (CNTs) due to its promotion effect on the charge transfer from the metal surface and the support to the CO_2 molecules (99). Addition of Rh to Ni supported on $Ce_{0.72}Zr_{0.28}O_2$ led to higher Ni dispersion, resulting in increases in both activity and catalyst life-time (124) .

The promoting effects of transition metals or their oxides on nickel catalysts have also been reported. ZrO_2 increased the activity and stability for CO_2 hydrogenation over alumina-supported nickel catalysts (97). Sheshko and Serov (115) found a synergy by using bimetallic Ni-Fe ultradispersed powder for the hydrogenation of mixed carbon oxides (CO and CO_2) where the main products were methane and ethylene compared to ultradispersed nickel powder

alone that mainly led to the formation of methane. Hwang, *et al*. (147) studied the effect of a second metal (Fe, Zr, Ni, Y, and Mg) on Ni/alumina xerogel catalysts and found that CO_2 conversion and CH_4 yield decreased with the type of the second metal added to the catalyst in the following order: Fe > Zr > Ni > Y > Mg. Their catalysts contained 35% of mesoporous Ni and 5% of the second metal. The addition of Fe led to a catalyst which retained most of the optimal CO dissociation energy and with the lowest metal-support interaction.

Addition of Fe (around 3 wt.%), by co-impregnation with Ni nitrate on ZrO_2, enhanced the catalytic activity of 30% Ni/ZrO_2 catalyst for CO_2 methanation at low temperatures. This was explained by an enhancement in nickel dispersion and extent of reduction, and the partial reduction of the ZrO_2 support that enhances CO_2 dissociation at low pressure due to a high concentration of oxygen vacancies in the support (27). Addition of Fe to Ni (Fe:Ni ratio of 1:3) supported on Al_2O_3, ZrO_2, TiO_2 and SiO_2 resulted in a higher CH_4 yield compared to the supported Ni catalysts without Fe (121). The enhancement was explained by the formation of suitable Ni-Fe alloy such as Ni_3F. Small amounts of Mo increased Ni metal dispersion in a low Ni loaded (5 wt.%Ni/Al_2O_3) catalyst resulting in an increase in CO_2 conversion (148). Zr addition to $Ni_{100}O_x$ catalysts (10 mol.%) improved the catalyst activity as a result of Zr ions involvement (149). MnO_2 improved the reducibility of 20%Ni/γ-Al_2O_3 catalysts by changing the Ni-Al_2O_3 interaction (116). Addition of an appropriate amount of V_2O_5 (3%) to nickel catalyst (20% NiO) supported on acid-alkali treated bentonite support increased the activity for CO_2 methanation. V_2O_5 enhances H_2 uptakes, increases Ni dispersion and has been proposed to exert an electronic effect that promotes dissociation of CO in the methanation reaction (79). Ni catalysts have also been promoted by modifying the support. For example, doping ZrO_2 support with Ni^{2+}, and Ca^{2+} (150) or Sm^{3+} (151) enhanced the activity of Ni/ZrO_2 catalysts. This was explained by oxygen vacancies produced by the introduction of these ions into the tetragonal phase of ZrO_2 (Fig. 13) (150).

Figure 13: Reaction mechanism proposed on Ni – ZrO_2 with oxygen vacancies for CO_2 methanation.

Ruthenium catalysts are rarely promoted by a second metal. Limited studies that promoted Ru catalysts involve the addition of Rh (125) and Ni (117, 125)**.** Hu *et al*. (125) respectively added Rh (2%) and Ni (5%) to a 3%Ru/TiO_2 catalyst and found that Rh did not affect the CO_2 conversion while Ni had an inhibiting effect. Low loadings (around 1 wt.%) of equimolar Ru and Ni were reported to favor the formation of alloys that lead to similar performance as for monometallic Ru catalysts. Higher loadings (ca. 2 – 4 wt.%) led to the covering of Ru by Ni and the formation of larger Ni agglomerates resulting in decreased activity (117)**.**

Various components are usually added to binary copper catalysts such Cu/ZnO and Cu/ZrO_2 to improve their catalytic performance for CO_2 hydrogenation to methanol.

Ramaroson *et al*. (42) promoted a 50%Cu/ZnO catalyst with 10% of groups III and IV metal oxides (La_2O_3, MgO, ThO_2, Nd_2O_3, Y_2O_3, Al_2O_3, In_2O_3 and SiO_2) and found that the total CO_2 conversion increased in the following order: Cu/ZnO/MgO < Cu/ZnO/SiO_2 < Cu/ZnO/Al_2O_3 < Cu/ZnO/La_2O_3 < Cu/ZnO/ThO_2 < Cu/ZnO/Y_2O_3 < Cu/ZnO < Cu/ZnO/Nd_2O_3 < Cu/ZnO/In_2O_3. They found that SiO_2 significantly promoted methane formation and led to very low methanol selectivity of ca. 1.5%. The selectivity for methanol that was measured on other promoted catalysts, in comparison to the unpromoted catalyst, was above 90% and increased in the following order: CuO/ZnO/In_2O_3 < CuO/ZnO < CuO/ZnO/Al_2O_3 < CuO/ZnO/Y_2O_3 < CuO/ZnO/Nd_2O_3 < CuO/ZnO/ThO_2 < CuO/ZnO/MgO = CuO/ZnO/La_2O_3. The promoting effect of these oxides was explained by their ability to stabilize oxygenates intermediates like formate on the catalyst surface. Addition of Al_2O_3 (34%) and a small amount of Cr_2O_3 (3%) to Cu/ZnO catalyst improved both CO_2 conversion and selectivity to methanol (46). Ag (4.8%)

increased the selectivity for methanol without significantly affecting the activity of a Cu/ZnO catalyst (129). It decreased the catalyst reduction temperature and possibly influenced the distribution of reduced and oxidized surface species during reaction. Saito *et al.* (133) studied the effect of Ga, Cr, Al and Zr oxides addition to Cu/ZnO catalysts and found that Al_2O_3 or ZrO_2 improve the dispersion of Cu in the catalyst while Ga_2O_3 or Cr_2O_3 optimize the ratio of Cu^+ and Cu^0 on the surface of Cu particles, resulting in the increase of the specific activity. Sahibzada (134) reported that Pd promotes the activity of Cu/ZnO catalysts by a possible hydrogen spillover process that plays a role in counteracting the inhibition by water. Toyir *et al.* (136) found that the addition of Al_2O_3 or ZrO_2 to Cu/ZnO increases the total surface area and the dispersion of Cu particles on the surface, while the addition of Ga_2O_3 to the catalyst improved the specific activity and stability of Cu, and the selectivity for methanol. The promoting effect of Ga_2O_3 was due to small particles of Ga_2O_3 that favour the formation of an intermediate state of copper between Cu^0 and Cu^{2+} or Cu^+.

Amenomiya (105) added ca. 10% of Al_2O_3, ZnO, SiO_2, SiO_2-Al_2O_3, Cr_2O_3-Al_2O_3, WO_3-Al_2O_3, SiO_2-MgO, graphite, ThO_2 and CeO_3 to a 40%CuO/ZrO_2 catalyst and found that Al_2O_3, ZnO, SiO_2-Al_2O_3, and Cr_2O_3-Al_2O_3 increased the conversion to methanol, while SiO_2, WO_3-Al_2O_3, SiO_2-MgO and graphite showed no effect. ThO_2 and CeO_3 decreased the catalyst activity. Al_2O_3 was found to be the most effective in increasing the catalyst activity; however it decreased the selectivity for methanol. When compared at similar CO_2 conversion levels, the selectivity to methanol decreased as CuO/ZrO_2 > $CuO/ZrO_2/Al_2O_3$ > $CuO/ZrO_2/SiO_2$-Al_2O_3 > CuO/Cr_2O_3-Al_2O_3.

Cu/ZnO catalyst associated with ZrO_2 has been reported to have a good performance for CO_2 hydrogenation (109, 138, 140), as ZrO_2 possess high thermal stability under reducing and oxidizing environments (138).

Promotion of other binary copper catalysts has also been reported. For example, Liaw and Chen (108) promoted the dispersion and stability of CuB catalysts for methanol synthesis from CO_2/H_2 by doping the catalyst with Cr, Zr and Th respectively. Addition of vanadium to a 12%Cu/ɣ-Al_2O_3 catalyst improved the catalytic performance (152). The conversion of CO_2 went through a maximum level at ca. 3% V loading, while the selectivity for methanol increased and the CO selectivity decreased with increasing V content up to 9%. V was found to enhance the dispersion of supported CuO.

The modification of a well-known ternary Cu/ZnO/Al_2O_3 catalyst system that is used for commercial methanol synthesis from $CO/CO_2/H_2$ has also received significant research interest with an attempt to make it efficient for CO_2 hydrogenation. Sahibzada *et al.* (132) promoted Cu/ZnO/Al_2O_3 catalyst with Pd in two ways: i) physical mixture of Pd/Al_2O_3 and Cu/ZnO/Al_2O_3 catalysts and ii) impregnation of Cu/ZnO/Al_2O_3 catalyst with Pd. They found that Pd increased the conversion of CO_2 to methanol but had no effect on CO_2 conversion to CO. They also attributed the promoting effect of Pd to hydrogen spillover from Pd that counteracts the oxidizing effect of CO_2 and/or water on active Cu. Gao *et al.* (139) promoted a Cu/ZnO/Al_2O_3 catalyst using Ce, La, Mn, Y and Zr, and found that the CO_2 conversion increased as Cu/Zn/Al < Cu/Zn/Al/Mn < Cu/Zn/Al/La < Cu/Zn/Al/Ce < Cu/Zn/Al/Zr < Cu/Zn/Al/Y. On the other hand, they found that methanol selectivity increased as Cu/Zn/Al < Cu/Zn/Al/Mn < Cu/Zn/Al/La < Cu/Zn/Al/Ce < Cu/Zn/Al/Y < Cu/Zn/Al/Zr and had a linear relationship with the increase of the fraction of strong basic sites in the catalyst. They indicated that the introduction of Mn, La, Ce, Zr and Y (ca. 2.5%) favors the production of methanol and that Y- and Zr-modified catalysts showed the highest CO_2 conversion and methanol selectivity, respectively.

Cu/ZnO/ZrO_2 catalysts have also been promoted using various components. Słoczyński *et al.* (137) added small amounts (3%) of B, Ga, In, Gd, Y, Mn and MgO oxides to a Cu/ZnO/ZrO_2

cayalyst (65wt.%CuO, 23% ZnO, 9% ZrO_2 and 3% metal oxide) for methanol synthesis from CO_2. They found that the addition of Ga_2O_3 led to the highest yield of methanol. In_2O_3 drastically decreased the activity of the catalyst. These changes were due to the following: i) control of the dispersion of Cu in the catalyst; ii) increase in the concentration of ZrO_2 on the catalyst surface and iii) the related decrease of the ability of the surface to adsorb water, which inhibits methanol formation.

Natesakhawat *et al.* (138) incorporated Ga_2O_3 and Y_2O_3 into Cu/ZnO/ZrO_2 catalysts to enhance the dispersion and reducibility of Cu, resulting in high activity for methanol synthesis.

Composite catalysts have also been promoted to improve the catalytic performance. Inui *et al.* (113) added some oxides (ca. 4% of Y, La, Ce, Sm) to a 25%CuO/41.5%ZnO/1.2%Cr_2O_3/Al_2O_3 catalyst and found that the addition of La oxide had the most effect in increasing both methanol selectivity and yield (Fig. 14). The promoting effect was due to the strong basicity of La oxide that enhanced CO_2 adsorption and methanol yield compared to the other oxides used. An increase in La content increased the CO_2 conversion and methanol yield up to equilibrium levels.

Figure 14: Effect of combination of lanthanide oxides with MSCg-S on the performance of methanol synthesis.

In another study (37) from the same laboratory, they added Pd and Na to a Cu/ZnO/Cr_2O_3 catalyst and found that Pd alone did not have any significant effect but the combination of Pd and Na increased the conversion of CO_2 and the formation of methanol. They suggested that sodium oxides promote the adsorption of CO_2 on the catalyst. Zhan *et al.* (141) studied the effect of Y, Ce, Mg and Zr addition to La/Cu/ZnO catalysts for CO_2 hydrogenation. They found that Ce, Mg and Zr lead to lower reduction temperature and higher dispersion of Cu. They also

increased the amount of basic sites leading to an improved methanol yield. They suggested that the improvement in methanol selectivity originates from a special copper valance in the catalyst after reduction.

3.6 Effect of catalyst pore structure, metal loading and particle size

Catalyst pore structure and metal particle size play significant roles in the optimization of industrial catalysts formulations, as these parameters directly affect the transfer of reactants and product in the catalyst.

Inui and Takeguchi (145) studied the effect of pore structure on CO and CO_2 methanation activity using SiO_2-supported catalysts containing 4.6 % Ni-2.6 % La_2O_3. They found that the steady state yield of methane increased when the support pore size was increased from 6 to 760 nm and that the highest activity was measured on the support with meso-macro bimodal pores. They concluded that the mesopores are necessary to provide the sites for catalyst particles and the macropores are responsible for the rapid transport of reactants and products.

Kester *et al.* (153) used TPR to study the effect of Ni loading (1.8 – 15%) on Al_2O_3 for CO and CO_2 hydrogenation. The catalysts were prepared by support impregnation with nickel nitrate solution. They found that methanation occurs on two types of sites: i) sites having higher intrinsic activity that are associated with Ni crystallites formed from the reduction of NiO on the alumina surface and ii) sites possessing lower intrinsic activity resulting from the reduction of a form of $NiAl_2O_4$ that leads to Ni species surrounded by oxygens of the alumina lattice. The distribution of these sites is affected by Ni loading. Increasing Ni loading leads to more active sites as the proportion of $NiAl_2O_4$ species, which are difficult to reduce, decreases.

Hwang *et al*. (154) found a correlation between methane yield and metal particle size over a 30% Ni/5% Fe/Al_2O_3 catalyst that was prepared by a co-precipitation method where they varied the precipitation agent, i.e. $(NH_4)_2CO_3$, Na_2CO_3, NH_4OH or NaOH, to control the particle size of Ni. They found that the yield for methane increased with a decrease in Ni particles size. A

similar trend was also reported by Garbarino *et al*. (14) who found that small Ni particles on Al_2O_3 support were very selective for methane. They also found that the larger the Ni particles, the higher the production of CO as an intermediate. In contrast to the findings by Kester *et al*. (153) , they suggested that fast methanation occurs on the corners of nanoparticles interacting with the alumina support.

Hu *et al*. (125) measured an increase in CO_2 conversion with increases in Ru loading, on a TiO_2 support, up to ca. 3% before declining, while the selectivity for CO and CH_4 remained unchanged. Similarly, Kwak *et al*. (104) found that the TOF for CH_4 increased with Ru loading (0.1 – 5%) on Al_2O_3. However, an opposite trend was observed for the TOF and selectivity of CO. They suggested that the reaction mechanism is different on small particles that are atomically dispersed and larger Ru particles. Single Ru atoms or interfacial Ru favour CO formation, while Ru clusters, which are able to supply large amounts of atomic hydrogen to this process, favour the formation of CH_4. Lange *et al*. (117) also found that increasing the loading of Ru on a ZrO_2 support, from 1 to 3%, increased the CO_2 conversion from 93.9 to ca. 97%.

Fig. 15a displays a relationship between the activity that was measured on various catalysts and the size of Ru particles. The data were replotted from the work of Kowalczyk et *al*. (126) and show that the activity decreases as the Ru particle size, on different supports, increases. However, when the activity is plotted against the size of Ru particles on the same support (Fig. 15b), a slight increase in activity can be observed on larger Ru particles. This reflects some differences in the morphology of Ru crystallites on the different supports, as suggested by the authors.

Figure 15: Effect of a) support type and metal particle size on CO_2 hydrogenation activity over □ 10%Ru/Al_2O_3; ● 10%Ru/$MgAl_2O_4$; ○ 10%Ru/MgO and △ 9%Ru/CA and b)

metal particle size on CO_2 hydrogenation activity over □ Ru/Al_2O_3; ● $Ru/MgAl_2O_4$ and ○ 10%Ru/MgO.

Kusmierz et *al.* (103) found that the apparent activation energy for a $Ru/\gamma\text{-}Al_2O_3$ catalyst decreased with an increasing dispersion of Ru on the support and went through a minimum at a dispersion of 0.5. They indicated that a high dispersion of Ru increases the amount of metal/oxide borders that enhance the generation of adsorbed CO. As a result, the surface coverage with CO increases while the hydrogen coverage decreases, and the heat of hydrogen adsorption increases. Słoczynski *et al*. (137) have reported a linear increase of the yield for methanol with a decrease in Cu crystallite sizes in modified $Cu/ZnO/ZrO_2$ catalysts (Fig. 17). A similar trend was reported by Natesakhawat (138) who measured higher TOF on smaller Cu particles on various supports (Fig. 18) and explained this trend by a synergetic interaction of Cu particles with the support, as smaller Cu particles lead to larger interfacial area with the metal oxide support. They ruled out the possibility of Cu^+ species acting as active sites as they did not observe them on the surface of working catalysts. In a recent study, Dong *et al.* (155) also found that the conversion of CO_2 increases with an increase in Cu surface area.

Figure 16: Yield of methanol as a function of the crystal sizes of copper.

Figure 17: Relationship between TOF for methanol synthesis and copper crystallite size.

3.7 Kinetic models

Studies that specifically focused on the development of kinetic models for CO_2 methanation under conditions relevant to industrial applications are still limited. Table 3 summarizes kinetic models for Ni catalysts that have been proposed in the literature.

Table 3. Kinetic models for CO_2 methanation on Ni catalysts

Most studies suggest Langmuir-type models (19, 88, 100, 156, 158 – 160) although some power-law (92, 157, 161) models are also reported.

Dew *et al*. (156) assumed that two adsorbed molecules of hydrogen reacted with a dissociated CO_2 molecule at a pressure of two atmospheres. A different mechanism was assumed above this pressure, where four adsorbed hydrogen molecules react with one adsorbed CO_2 molecule on the catalyst surface. van Herwijnen *et al*. (88) assumed localized Langmuir chemisorption in a system having very small concentration of CO_2 (0.22 – 2.38%) in H_2. A complex Langmuir-Hinshelwood mechanism involving dissociative adsorption of CO_2 to CO and atomic oxygen followed by hydrogenation of CO via a carbon intermediate to methane (Fig. 3) was assumed by Weatherbee and Bartholomew (19). Values of kinetic constants from their proposed model (Equation 6) are reported in Table 4.

Table 4. Values of kinetic constants from Langmuir-Hinshelwood fit of data.

Kai *et al*. (159) assumed equilibrium of dissociative CO_2 and H_2 adsorption on the catalyst surface and that the hydrogenation of surface carbon was the rate determining elementary step. A recent study by Koschany *et al.* (100) has suggested that differential conversions and higher conversions closer to equilibrium have different kinetics. They found that a simple power law with inhibition by adsorbed hydroxyl (Equation 16 with parameter estimation in Table 5) is adequate to reflect kinetics from differential to equilibrium conversions. However, the best fit of experimental data was obtained for the Langmuir Hinshelwood-type model (equation 17) with parameter estimation reported in Table 6.

Table 5. Parameter estimation for the power law with inhibition by adsorbed hydroxyl (Eqt. 2-16, T_{ref} = 555 K).

Table 6. Parameter estimation for Langmuir Hinshelwood rate equation (Eqt. 2-17, T_{ref} =555 K).

The Langmuir Hinshelwood model was derived assuming hydrogen-assisted carbon oxygen bond cleavage where formyl formation was assumed to be the rate determining step as described in Fig. 18.

Figure 18: Proposed elementary steps for CO_2 hydrogenation via hydrogen assisted carbon oxygen cleavage.

Few studies that have developed kinetic models on Ru- and Cu-based catalysts are summarized in Table 7.

Table 7. Kinetic models for CO_2 hydrogenation on Ru and Cu catalysts

---

Table 8. Summarized literature data for CO_2 hydrogenation kinetics over Ni catalysts

---

Table 9. Summarized literature data for CO_2 hydrogenation kinetics over Ru catalysts

---

Table 10. Summarized literature data for CO_2 hydrogenation kinetics over Cu catalysts

---

4 Conclusions

It can generally be accepted that CO and formate species form on Ni, Ru or Cu catalyst during CO_2 hydrogenation. In some cases, CO is suggested to form from formate species and acts as an active intermediate on Ni and Ru catalysts. It forms during a parallel RWGS reaction on Cu catalysts, where formate species are proposed to be the main intermediate for methanol formation. Physicochemical properties of the catalyst support can influence the formation of intermediate species on the surface of the catalyst. Active supports are proposed to participate in the catalyst and may promote the formation of formates species having a different coordination geometry to the catalyst surface which makes them active for further hydrogenation.

A significant amount of CO_2 hydrogenation data has been reported in literature. However, the large difference in testing conditions has made the comparison of data from different laboratories difficult. Tables 8 to 10 summarize the data for CO_2 hydrogenation respectively over Ni, Ru and Cu catalysts for a wide range of temperature, pressure, H_2:CO_2 ratio, space velocities and catalyst preparation methods. Methane is the major reaction product on Ni and Ru catalysts. In some cases CO and C_{2+} hydrocarbons also formed in small amounts. The major products that form over Cu catalysts are methanol and CO.

Long-chain hydrocarbons are not practically formed on these catalysts. Where these products are desired, a different approach should be envisaged. For example, composite catalysts and two-step processes involving the production of methanol with subsequent conversion to hydrocarbons (19, 71, 94) can be explored further.

References

1. Vlasenko, V.M.; Yuzefovich, G.E. Mechanism of the Catalytic Hydrogenation of Oxides of Carbon. Russ. Chem. Rev. 1969, 38 (9), 728 - 739.
2. Darensbourg, D.J.; Bauch, C.G.; Ovalles, C. Mechanistic Aspects of Catalytic Carbon Dioxide Methanation. Rev. Inorg. Chem. 1985, 7 (4), 315 - 340.
3. Wang, W.; Wang, S.; Ma, X.; Gong, J. Recent Advances in Catalytic Hydrogenation of Carbon Dioxide. Chem. Soc. Rev. 2011, 40 (7), 3369 - 4260.
4. Wang, W.; Gong, J. Methanation of Carbon Dioxide: an Overview. Front. Chem. Sci. Eng. 2011, 5 (1), 2 - 10.
5. Aziz, M.A.A.; Jalil, A.A.; Triwahyono, S.; Ahmad, A. CO_2 Methanation over Heterogeneous Catalysts: Recent Progress and Future Prospects. Green Chem. 2015, 17 (5), 2647 - 2663.
6. Saeidi, S.; Amin, N.A.S.; Rahimpour, M.R. Hydrogenation of CO_2 to Value-added Products—A Review and Potential Future Developments. J. CO_2 Util. 2014, 5, 66 - 81.
7. Ganesh, I. Conversion of Carbon Dioxide into Methanol – A potential Liquid Fuel: Fundamental Challenges and Opportunities (a review). Renew. Sust. Energ. Rev. 2014, 31, 221 - 257.
8. Jadhav, S.G.; Vaidya, P.D.; Bhanage, B.M.; Joshi, J.B. Catalytic Carbon Dioxide Hydrogenation to methanol: A Review of Recent Studies. Chem. Eng. Res. Des. 2014, 92 (11), 2557 - 2567.
9. Wang, W.-H.; Himeda, Y.; Muckerman, J.T.; Manbeck, G.F.; Fujita, E. CO_2 Hydrogenation to Formate and Methanol as an Alternative to Photo- and Electrochemical CO_2 Reduction. Chem. Rev. 2015, 115 (23), 12936 - 12973.
10. Araki, M.; Ponec, V. Methanation of Carbon Monoxide on Nickel and Nickel-Copper Alloys. J. Catal. 1976, 44 (3), 439 - 448.

11. Martin, G.A.; Primet, M.; Dalmon, J.A. Reactions of CO and CO_2 on Ni/SiO_2 above 373 K as Studied by Infrared Spectroscopic and Magnetic Methods. J. Catal. 1978, 53 (3), 321 - 330.
12. Dalmon, J.-A.; Martin, G.A. Intermediates in CO and CO_2 Hydrogenation over Ni Catalysts. J. Chem. Soc., Faraday Trans. 1. 1979, 75 (0), 1011 - 1015.
13. Falconer, J.L.; Zagli, A.E. Adsorption and Methanation of Carbon Dioxide on a Nickel/Silica Catalyst. J. Catal. 1980, 62 (2), 280 - 285.
14. Garbarino, G.; Riani, P.; Magistri, L.; Busca, G. A Study of the Methanation of Carbon Dioxide on Ni/Al_2O_3 Catalysts at Atmospheric Pressure. Int. J. Hydrogen Energ. 2014, 39 (22), 11557 - 11565.
15. Ussa Aldana, P.A.; Ocampo, F.; Kobl, K.; Louis, B.; Thibault-Starzyk, F.; Daturi, M.; Bazin, P.; Thomas, S.; Roger, A.C. Catalytic CO_2 Valorization into CH_4 on Ni-based Ceria-Zirconia. Reaction Mechanism by Operando IR Spectroscopy. Catal. Today 2013, 215, 201 - 207.
16. Pan, Q.; Peng, J.;Sun, T.; Wang, S.; Wang, S. Insight into the Reaction Route of CO_2 Methanation: Promotion Effect of Medium Basic Sites. Catal. Commun. 2014, 45, 74 - 78.
17. Osaki, T.; Mori, T. Kinetics Studies on CO_2 Dissociation on Supported Ni Catalysts. React. Kinet. Catal. Lett. 2006, 87 (1), 149 - 156.
18. Weatherbee, G.D.; Bartholomew, C.H. Hydrogenation of CO_2 on Group VIII Metals, I. Specific Activity of Ni/SiO_2. J. Catal. 1981, 68 (1), 67 - 76.
19. Weatherbee, G.D.; Bartholomew, C.H. Hydrogenation of CO_2 on Group VIII Metals, II. Kinetics and Mechanism of CO_2 Hydrogenation on Nickel. J. Catal. 1982, 77 (2), 460 - 472.
20. Peebles, D.E.; Goodman, D.W.; White, J.M. Methanation of Carbon Dioxide on Ni(100) and the Effects of Surface Modifiers. J. Phys. Chem. 1983, 87 (22), 4378 - 4387.

21. Vesselli, E.; De Rogatis, L.; Ding, X.; Baraldi, A.; Savio, L.; Vattuone, L.; Rocca, M.; Fornasiero, P.; Peressi, M.; Baldereschi, A.; Rosei, R.; Comelli, G. Carbon Dioxide Hydrogenation on Ni(110). J. Am. Chem. Soc. 2008, 130 (34), 11417 – 11422.
22. Fujita, S.; Terunuma, H.; Kobayashi, H.; Takezawa, N. Methanation of Carbon Monoxide and Carbon Dioxide over Nickel Catalyst under The Transient State. React. Kinet. Catal. Lett. 1987, 33 (1), 179 - 184.
23. Spinicci, R.; Tofanari, A. Comparative Study of the Activity of Titania- and Silica-Based Catalysts for Carbon Dioxide Methanation. Appl. Catal. 1988, 41, 241 - 252.
24. Fujita, S-i.; Terunuma, H.; Nakamura, M.; Takezawa, N. Mechanisms of Methanation of CO and CO_2 over Ni. Ind. Eng. Chem. Res. 1991, 30 (6), 1146 - 1151.
25. Fujita, S-i.; Nakamura, M.; Doi, T.; Takezawa, N.; Mechanisms of Methanation of Carbon Dioxide and Carbon Monoxide over Nickel/Alumina Catalysts. Appl. Catal. A: Gen. 1993, 104 (1), 87-100.
26. Lapidus, A.L.; Gaidai, N.A.; Nekrasov, N.V.; Tishkova, L.A.; Agafonov, Yu. A.; Myshenkova, T.N. The Mechanism of Carbon Dioxide Hydrogenation on Copper and Nickel Catalysts. Petrol. Chem. 2007, 47 (2), 75 - 82.
27. Ren, J.; Qin, X.; Yang, J.-Z. Qin, Z.-F.; Guo, H.-L.; Lin, J.-Y.; Li, Z. Methanation of Carbon Dioxide over Ni–M/ZrO_2 (M = Fe, Co, Cu) Catalysts: Effect of Addition of a Second Metal. Fuel Process. Technol. 2015, 137, 204 - 211.
28. Bartos, B.; Freund, H.-J.; Kuhlenbeck, H.; Neumann, M.; Lindner, H.; Müller, K. Adsorption and Reaction of CO_2 and CO_2/O_2 Co-adsorption on Ni (110): Angle Resolved Photoemission (ARUPS) and Electron Energy Loss (HREELS) Studies. Surf. Sci. 1987, 179 (1), 59 - 89.
29. Lindner, H.; Rupprecht, D.; Hammer, L.; Müller, K. Reactivity of Carbon Dioxide at Ni (110). J. Electron Spectrosc. 1987, 44 (1), 141 - 148.

30. Illing, G., Heskett, D.; Plummer, E.W.; Freund, H.-J.; Somers, J.; Lindner, Th.; Bradshaw, A.M.; Buskotte, U.; Neumann, M.; Starke, U.; Heinz, K.; De Andres, P.L.; Saldin, D.; Pendry, J.B. Adsorption and Reaction of CO_2 on Ni{110}: X-ray Photoemission, Near-edge X-ray Absorption, Fine-structure and Diffuse Leed Studies. Surf. Sci. 1988, 206 (1-2), 1 - 19.
31. Ding, X.; De Rogatis, L.; Vesselli, E.; Baraldi, A.; Comelli, G.; Rosei, R.; Savio, L.; Vattuone, L.; Rocca, M.; Fornasiero, P.; Ancilotto, F.; Baldereschi, A.; Peressi, M. Interaction of Carbon Dioxide with Ni(110): A Combined Experimental and Theoretical Study. Phys. Rev. B. 2007, 76 (19), 195425: 1 - 12.
32. Gupta, N.M; Kamble, V.S.; Annaji Rao, K.; Iyer, R.M. On the Mechanism of CO and CO_2 Methanation over Ru/Molecular-Sieve Catalyst. J. Catal. 1979, 60 (1), 57 - 67.
33. Gupta, N.M..; Kamble, V.S.; Iyer, R.M. Effect of ɣ-Irradiation on Methanation of Carbon Dioxide over Supported Ru Catalysts. J. Catal. 1980, 66 (1), 101 - 111.
34. Gupta, N.M.; Kamble, V.S.; Kartha, V.B.; Iyer, R.M.; Ravindranathan Thampi, K.; Gratzel, M. FTIR Spectroscopic Study of the Interaction of CO_2 and CO_2 + H_2 over Partially Oxidized Ru/TiO_2 Catalyst. J. Catal. 1994, 146 (1), 173 - 184.
35. Hadden, R.A.; Vandervell, H.D.; Waugh, K.C.; Webb, G. The Adsorption and Decomposition of Carbon Dioxide on Polycrystalline Copper. Catal. Lett. 1988, 1 (1 – 3), 27-34.
36. Gasser, D.; Baiker, A. Hydrogenation of Carbon Dioxide over Copper-Zirconia Catalysts Prepared by In-Situ Activation of Amorphous Copper-Zirconium Alloy. Appl. Catal. 1989, 48 (2), 279-294.
37. Inui, T.; Kitagawa, K.; Takeguchi, T.; Hagiwara, T.; Makino, Y. Hydrogenation of Carbon Dioxide to C_1-C_7 Hydrocarbons via Methanol on Composite Catalysts. Appl. Catal. A: Gen. 1993, 94 (1), 31-44.

38. Schild, C.; Wokaun. A.; Koeppel, R.A.; Baiker, A. CO_2 Hydrogenation over Nickel/Zirconia Catalysts from Amorphous Precursors: On the Mechanism of Methane Formation. J. Phys. Chem. 1991, 95 (16), 6341 - 6346.

39. Kieffer, R.; Ramaroson, E.; Deluzarche, A.; Trambouze, Y. A comparison of Reactivity in the Synthesis of Methanol from $CO_2 + H_2$ and $CO + H_2$ (Catalysts Cu, Zn/Al_2O_3, P = 515×10^4 Pa). React. Kinet. Catal. Lett. 1981, 16 (2), 207–212.

40. Denise, B.; Sneeden, R.P.A.; Hamon, C. Hydrocondensation of Carbon Dioxide: IV. J. Mol. Catal. 1982, 17 (2-3), 359 - 366.

41. Tagawa, T.; Pleizier, G.; Amenomiya, Y. Methanol Synthesis from $CO_2 + H_2$: I. Characterization of Catalysts by TPD. Appl. Catal. 1985, 18 (2), 285 - 293.

42. Ramaroson, E.; Kieffer, R.; Kiennemann, A. Reaction of $CO\text{-}H_2$ and $CO_2 - H_2$ on Copper-Zinc Catalysts Promoted by Metal Oxides of Group III and IV. Appl. Catal. 1982, 4 (3), 281 - 286.

43. Chinchen, G.C.; Spencer, M.S.; Waugh, K.C.; Whan, D.A. Promotion of Methanol Synthesis and the Water-gas Shift Reactions by Adsorbed Oxygen on Supported Copper Catalysts. J. Chem. Soc., Faraday Trans. 1. 1987, 83 (7), 2193-2212.

44. Bowker, M.; Hadden, R.A.; Houghton, H.; Hyland, J.N.K.; Waugh, K.C. The Mechanism of Methanol Synthesis on Copper/Zinc Oxide/Alumina Catalysts. J. Catal. 1988, 109 (2), 263 - 273.

45. Kinnaird, S.; Webb, G.; Chinchen, G.C. Radiotracer Studies of Chemisorption on Copper-based Catalysts. J. Chem. Soc., Faraday Trans. 1. 1988, 84 (6), 2135 - 2145.

46. Arakawa, H.; Dubois, J.-L.; Sayama, K. Selective Conversion of CO_2 to Methanol by Catalytic Hydrogenation over Promoted Copper Catalyst. Energ. Convers. Manage. 1992, 33 (5-8), 521–528.

47. P. B. Rasmussen, P.B.; Holmblad, P.M.; Askgaard, T.; Ovesen, C.V.; Stoltze, P.; Nørskov, J.K.; Chorkendorff, I. Methanol Synthesis on Cu (100) from a Binary Gas Mixture of CO_2 and H_2. Catal. Lett. 1994, 26 (3 – 4), 373 - 381.
48. Rasmussen, P.B.; Kazuta, M.; Chorkendorff, I. Synthesis of Methanol from a Mixture of H_2 and CO_2 on Cu (100)," Surf. Sci. 1994, 318 (3), 267 - 280.
49. Nakamura, J.; Nakamura, I.; Uchijima, T.; Kanai, Y.; Watanabe, T.; Saito, M.; Fujitani, T. A Surface Science Investigation of Methanol Synthesis over a Zn-Deposited Polycrystalline Cu Surface. J. Catal. 1996, 160 (1), 65 - 75.
50. Yoshihara, J.; Campbell, C.T. Methanol Synthesis and Reverse Water–Gas Shift Kinetics over Cu (110) Model Catalysts: Structural Sensitivity. J. Catal. 1996, 161 (2), 776 – 782.
51. Fujitani, T.; Nakamura, I.; Uchijima, T.; Nakamura, J. The Kinetics and Mechanism of Methanol Synthesis by Hydrogenation of CO_2 over a Zn-deposited Cu (111) Surface. Surf. Sci. 1997, 383 (2-3), 285 - 298.
52. Vesselli, E.; Rizzi, M.; De Rogatis, L.; Ding, X.; Baraldi, A.; Comelli, G.; Savio, L.; Vattuone, L.; Rocca, M.; Fornasiero, P.; Baldereschi, A.; Peressi, M. Hydrogen-Assisted Transformation of CO_2 on Nickel: The Role of Formate and Carbon Monoxide. J. Phys. Chem. Lett. 2010, 1 (1), 402 - 406.
53. Vesselli, E.; Schweicher, J.; Bundhoo, A.; Frennet, A.; Kruse, N. Catalytic CO_2 Hydrogenation on Nickel: Novel Insight by Chemical Transient Kinetics. J. Phys. Chem. C. 2011, 115 (4), 1255 - 1260.
54. Westermann, A.; Azambre, B.; Bacariza, M.C.; Graça, I.; Ribeiro, M.F.; Lopes, J.M.; Henriques, C. Insight into CO_2 Methanation Mechanism over NiUSY Zeolites: An Operando IR Study. Appl. Catal. B: Environ. 2015, 174 - 175, 120 - 125.

55. Fan, Z.; Sun, K.; Rui, N.; Zhao, B.; Liu. C.-j. Improved Activity of Ni/$MgAl_2O_4$ for CO_2 Methanation by the Plasma Decomposition. J. Energy Chem. 2015, 24 (5), 655 - 659.
56. Aksoylu, A.E.; Akin, A.N.; Önsan, Z.İ.; Trimm. D.L. Structure/Activity Relationships in Coprecipitated Nickel-Alumina Catalysts using CO_2 Adsorption and Methanation. Appl. Catal. A: Gen. 1996, 145 (1-2), 185 - 193.
57. Lo Jacono, M.; Schiavello, M.; Cimino, A., Structural, Magnetic, and Optical Properties of Nickel Oxide Supported on η- and ɣ- Aluminas. J. Phys. Chem. 1971, 75 (8), 1044 - 1050.
58. Zielinski, J. Morphology of Nickel/Alumina Catalysts. J. Catal. 1982, 76 (1), 157 - 163.
59. Gavalas, G.R.; Phichitkul, C.; Voecks, G.E. Structure and Activity of NiO/a-Al_2O_3 and NiO/ZrO_2 Calcined at High Temperatures. J. Catal. 1984, 88 (1), 54 - 64.
60. Scheffer, B.; Heijeinga, J.J.; Moulijn, J.A. An Electron Spectroscopy and X-ray Dlffraction Study of NiO/AI_2O_3 and NiO-WO_3/AI_2O_3 Catalysts. J. Phys. Chem. 1987, 91 (18), 4752 - 4759.
61. de Bokx, P.K.; Wassenberg, W.B.A.; Geus, J.W. Interaction of Nickel Ions with a ɣ-Al_2O_3 Support during Deposition from Aqueous Solution. J. Catal. 1987, 104 (1), 86 - 98.
62. Kadkhodayan, A.; Brenne, A. Temperature-programmed Reduction and Oxidation of Metals Supported on γ-alumina. J. Catal. 1989, 117 (2) , 311-321.
63. Scheffer, B.; Molhoek, P.; Moulijn, J.A. Temperature-Programmed Reduction of NiO-WO_3/Al_2O_3 Hydrodesulphurization Catalysts. Appl. Catal. 1989, 46 (1), 11 - 30.
64. Rynkowski, J.M.; Paryjczak, T; Lenik, M. On the Nature of Oxidic Nickel Phases in NiO/γ-Al_2O_3 Catalysts. Appl. Catal. A: Gen. 1993, 106 (1), 73 - 82.
65. Chang, F.-W.; Kuo, M.-S.; Tsay, M.-T.; Hsieh, M.-C. Hydrogenation of CO_2 over Nickel Catalysts on Rice Husk Ash-Alumina Prepared by Incipient Wetness Impregnation. Appl. Catal. A: Gen. 2003, 247 (2), 309 - 320.

66. Wambach, J.; Illing, G.; Freund, H.-J. CO_2 Activation and Reaction with Hydrogen on Ni(110): Formate Formation. Chem. Phys. Lett. 1991, 184 (1-3), 239 - 244.

67. Solymosi, F.; Erdöhelyi, A.; Kocsis, M. Methanation of CO_2 on Supported Ru Catalysts. J. Chem. Soc., Faraday Trans. 1. 1981, 77 (5), 1003 - 1012.

68. Highfield, J.G.; Prairie, M.; Renken, A. In-situ DRIFT Spectroscopy in a Continuous Recycle reactor: a Versatile Tool for Catalytic Process Research. Catal. Today 1991, 9 (1-2), 39 - 46.

69. Prairie, M.R.; Highfield, J.G.; Renken, A. Diffuse-Reflectance FTIR Spectroscopy for Kinetic and Mechanistic Studies of CO_2 Hydrogenation in a Continuous Recycle Reactor. Chem. Eng. Sci. 1991, 46 (1), 113 - 121.

70. Prairie, M.R.; Renken, A.; Highfield, J.G.; Ravindranathan Thampi, K.; Grätzel, M. A Fourier Transform Infrared Spectroscopic Study of CO_2 Methanation on Supported Ruthenium. J. Catal. 1991, 129 (1), 130 - 144.

71. Marwood, M.; Van Vyve, F.; Doepper, R.; Renke, A. Periodic Operation Applied to the Kinetic Study of CO_2 methanation. Catal. Today 1994, 20 (3), 437 - 448.

72. Marwood, M.; Doepper, R.; Prairie, M.; Renken, A. Transient Drift Spectroscopy for the Determination of the Surface Reaction Kinetics of CO_2 Methanation. Chem. Eng. Sci. 1994, 49 (24), 4801 – 4809.

73. Marwood, M.; Doepper, R.; Renken, A. In-situ Surface and Gas Phase Analysis for Kinetic Studies under Transient Conditions: The Catalytic Hydrogenation of CO_2. Appl. Catal. A: Gen. 1997, 151 (1), 223 - 246.

74. Scirè, S.; Crisafulli, C.; Maggiore, R.; Minicò, S.; Galvagno, S. Influence of the Support on CO_2 Methanation over Ru Catalysts: an FT-IR Study. Catal. Lett. 1998, 51 (1 – 2), 41 - 45.

75. Panagiotopoulou, P.; Kondarides, D.I.; Verykios, X.E. Mechanistic Study of the Selective Methanation of CO over Ru/TiO_2 Catalyst: Identification of Active Surface Species and Reaction Pathways. J. Phys. Chem. C. 2011 , 115 (4), 1220 - 1230.

76. Cratty, Jr, L.E.; Russell, W.W. Nickel, Copper and Some of their Alloys as Catalysts for the Hydrogenation of Carbon Dioxide. J. Am. Chem. Soc. 1958, 80 (4), 767 - 772.

77. Chang, F.-W.; Hsiao, T.-J.; Chung, S.-W.; Lo, J.-J. Nickel Supported on Rice Husk Ash - Activity and Selectivity in CO_2 Methanation. Appl. Catal. A: Gen. 1997, 164 (1-2), 225 - 236.

78. Rahmani, S.; Rezaei, M.; Meshkani, F. Preparation of Highly Active Nickel Catalysts Supported on Mesoporous Nanocrystalline γ-Al_2O_3 for CO_2 Methanation. J. Ind. Eng. Chem. 2014, 20 (4), 1346 - 1352.

79. Lu, X.; Gu, F.; Liu,Q.; Gao, J.; Liu, Y.; Li, H.; Jia, L.; Xu, G.; Zhong, Z.; Su, F. VO_x Promoted Ni Catalysts Supported on the Modified Bentonite for CO and CO_2 Methanation. Fuel Process. Technol. 2015, 135, 34 - 46.

80. Perkas, N.; Amirian, G.; Zhong, Z.; Teo, J.; Gofer, Y.; Gedanken, A. Methanation of Carbon Dioxide on Ni Catalysts on Mesoporous ZrO_2 Doped with Rare Earth Oxides. Catal. Lett. 2009, 130 (3), 455 - 462.

81. Abelló, S.; Berrueco, C.; Montané, D. High-loaded Nickel–Alumina Catalyst for Direct CO_2 Hydrogenation into Synthetic Natural Gas (SNG). Fuel 2013, 113, 598 - 609.

82. Solymosi, F.; Erdöhelyi, A. Hydrogenation of CO_2 to CH_4 over Alumina-supported Noble Metals. J. Mol. Catal. 1980, 8 (4), 471 - 474, 1980.

83. Weatherbee, G.D.; Bartholomew, C.H. Hydrogenation of CO_2 on Group VIII Metals: IV. Specific Activities and Selectivities of Silica-Supported Co, Fe, and Ru. J. Catal. 1984, 87 (2), 352 - 362.

84. Ohya, H.; Fun, J.; Kawamura, H.; Itoh, K.; Ohashi, H.; Aihara, M.; Tanisho, S.; Negishi, Y. Methanation of Carbon Dioxide by Using Membrane Reactor Integrated with Water Vapor Permselective Membrane and its Analysis. J. Membrane. Sci. 1997 , 131 (1-2), 237 - 247, 1997.

85. Janke, C.; Duyar, M.S.; Hoskins, M.; Farrauto, R. Catalytic and Adsorption Studies for the Hydrogenation of CO_2 to Methane. Appl. Catal. B: Environ. 2014, 152–153 , 184–191.

86. Brooks, K.P.; Hu, J.; Zhu, H.; Kee, R.J. Methanation of Carbon Dioxide by Hydrogen Reduction Using the Sabatier Process in Microchannel Reactors. Chem. Eng. Sci., 62 (4), 1161 – 1170.

87. Panagiotopoulou, P.; Kondarides, D.I.; Verykios, X.E. Selective Methanation of CO over Supported Noble Metal Catalysts: Effects of the Nature of the Metallic Phase on Catalytic Performance. Appl. Catal. A: Gen. 2008 , 344 (1 – 2), 45 – 54.

88. van Herwijnen , T.; van Doesburg, H.; De Jong, W.A. Kinetics of the Methanation of CO and CO_2 on a Nickel Catalyst. J. Catal. 1973, 28 (3), 391 - 402.

89. Inui, T.; Funabiki, M. Methanation of Carbon Dioxide and Carbon Monoxide on Supported Ni–La_2O_3–Ru Catalyst. Chem. Lett. 1978, 7 (3), 251 - 252.

90. Okamoto, Y.; Matsunaga, E.; Imanaka, T.; Teranishi, S. Surface State and Catalytic Activity and Selectivity of Nickel Catalysts in Hydrogenation Reactions, V. Electronic Effects on Methanation of CO and CO_2. J. Catal. 1982, 74 (1), 183 - 187.

91. Vance, C.K; Bartholomew, C.H. Hydrogenation of Carbon Dioxide on Group VIII Metals: III, Effects of Supports on Activity/Selectivty and Adsorption Properties of Nickel. Appl. Catal. 1983, 7 (2), 169 - 177.

92. Chiang, J.H.; Hopper, J.R. Kinetics of the Hydrogenation of Carbon Dioxide over Supported Nickel. Ind. Eng. Chem. Prod. Res. Dev. 1983, 22 (2), 225 - 228.

93. Guerrero-Ruiz, A.; Rodriguez-Ramos, I. Hydogenation of CO_2 on Carbon-Supported Nickel and Cobalt. React. Kinet. Catal. Lett. 1985, 29 (1), 93 - 99.

94. Campbell, T.K.; Falconer, J.L. Carbon Dioxide Hydrogenation on Potassium-Promoted Nickel Catalysts. Appl. Catal. 1989, 50 (1), 189 - 198.

95. Mori, S.; Xu, W.-C.; Ishidzuki, T.; Ogasawara, N.; Imai, J.; Kobayash, K. Mechanochemical Activation of Catalysts for CO_2 Methanation. Appl. Catal. A: Gen. 1996, 137 (2), 255-268.

96. Lee, G.D.; Moon, M.J.; Park, J.H.; Park, S.S.; Hong, S.S. Raney Ni Catalysts Derived from Different Alloy Precursors, Part II: CO and CO_2 Methanation Activity. Korean J. Chem. Eng. 2005, 22 (4), 541 - 546.

97. Cai, M.; Wen, J.; Chu, W.; Cheng, X.; Li, Z. Methanation of Carbon Dioxide on Ni/ZrO_2-Al_2O_3 Catalysts: Effects of ZrO_2 Promoter and Preparation Method of Novel ZrO_2-Al_2O_3 Carrier. J. Nat. Gas Chem. 2011, 20 (3), 318 - 324.

98. Aziz, M.A.A.; Jalil, A.A.; Triwahyono, S.; Mukti, R.R.; Taufiq-Yap, Y.H.; Sazegar, M.R. Highly Active Ni-promoted Mesostructured Silica Nanoparticles for CO_2 Methanation. Appl. Catal. B: Environ. 2014, 147, 359 - 368.

99. Wang, W.; Chu, W.; Wang, N.; Yang, W.; Jiang, C. Mesoporous Nickel Catalyst Supported on Multi-walled Carbon Nanotubes for Carbon Dioxide Methanation. Int. J. Hydrogen Energ. 2016, 41 (2), 967 - 975.

100. Koschany, F.; Schlereth, D.; Hinrichsen, O. On the Kinetics of the Methanation of Carbon Dioxide on Coprecipitated $NiAl(O)_x$. Appl. Catal. B: Environ. 2016, 181, 504 - 516.

101. Lunde, P.J.; Kester, F.L. Rates of Methane Formation from Carbon Dioxide and Hydrogen over a Ruthenium Catalyst. J. Catal. 1973, 30 (3), 423 - 429.

102. Ravindranathan Thampi, K.; John Kiwi, J.; Michael Grätzel, M. Methanation and Photo-methanation of Carbon Dioxide at Room Temperature and Atmospheric pressure. Nature 1987, 327, 506 - 508.

103. Kuśmierz, M. Kinetic Study on Carbon Dioxide Hydrogenation over Ru/ɣ-Al_2O_3 Catalysts. Catal. Today 2008 , 137 (2-4) , 429 – 432.

104. Kwak, J.H.; Kovarik, L.; Szanyi, J. CO_2 Reduction on Supported Ru/Al_2O_3 Catalysts: Cluster Size Dependence of Product Selectivity. ACS Catal. 2013 , 3 (11), 2449−2455.

105. Amenomiya, Y. Methanol Synthesis from CO_2 + H_2: II. Copper-based Binary and Ternary Catalysts. Appl. Catal. 1987, 30 (1), 57 - 68.

106. Nozaki, F.; Sodesawa, T.; Satoh, S.; Kimura, K. Hydrogenation of Carbon Dioxide into Light Hydrocarbons at Atmospheric Pressure over Rh/Nb_2O_5 or Cu/SiO_2-Rh/Nb_2O_5 Catalyst. J. Catal. 1987, 104 (2), 339 - 346.

107. Fujiwara, M.; Ando, H.; Tanaka, M.; Souma, Y. Hydrogenation of Carbon Dioxide over Cu–Zn–Cr Oxide Catalysts. Bull. Chem. Soc. Jpn. 1994 , 67 (2), 546 – 550.

108. Liaw, B.J.; Chen, Y.Z. Liquid-phase Synthesis of Methanol from CO_2/H_2 over Ultrafine CuB Catalysts. Appl. Catal. A: Gen. 2001, 206 (2), 245 - 256.

109. Arena, F.; Mezzatesta, G.; Zafarana, G.; Trunfio, G.; F. Frusteri, F.; Spadaro, L. Effects of Oxide Carriers on Surface Functionality and Process Performance of the Cu–ZnO System in the Synthesis of Methanol via CO_2 Hydrogenation. J. Catal. 2013, 300 (1), 141–151.

110. Bukhtiyarova, M.; Lunkenbein, T.; Kähler, K.; Schlögl, R. Methanol Synthesis from Industrial CO_2 Sources: A Contribution to Chemical Energy Conversion. Catal. Lett. 2017, 147 (2), 416-427.

111. Gao, P.; Xie, R.; Wang, H.; Zhong, L.; Xia, L.; Zhang, Z.; Wei, W.; Sun, Y. Cu/Zn/Al/Zr Catalysts via Phase-pure Hydrotalcite-like Compounds for Methanol Synthesis from Carbon Dioxide. J. CO_2 Util. 2015 , 11, 41-48.

112. Beguin, B.; Denise, B.; Sneeden, R.P.A. Hydrocondensation of CO_2: Reaction of CO_2(CO)/H_2 on CuO/ZnO Contact Masses. React. Kinet. Catal. Lett. 1980, 14 (1), 9 - 14.

113. Inui, T.; Takeguchi, T.; Kohama, A.; Kohama, K. Effective Conversion of Carbon Dioxide to Gasoline. Energ. Convers. and Manage. 1992, 33 (5-8), 513–520.

114. Inui, T.; Funabiki, M.; Takegami, Y. Effect of CO on CO_2 Methanation over a supported Ni-La_2O_3-Ru Catalyst. React. Kinet. Catal. Lett. 1979, 12 (3), 287 - 290.

115. Sheshko, T.F.; Serov, Y.M. Combined Hydrogenation of Carbon Oxides on Catalysts Bearing Iron and Nickel Nanoparticles. Russ. J. Phys. Chem. A. 2011, 85 (1), 51 - 54.

116. Rahmani, S.; Rezaei, M. ; Meshkani, F. Preparation of Promoted Nickel Catalysts Supported on Mesoporous Nanocrystalline Gamma Alumina for Carbon Dioxide Methanation Reaction. J. Ind. Eng. Chem. 2014, 20 (6), 4176 - 4182.

117. Lange, F.; Armbruster, U.; Martin, A. Heterogeneously-Catalyzed Hydrogenation of CarbonDioxide to Methane using RuNi Bimetallic Catalysts. Energ Technol. 2015, 3 (1), 55 – 62.

118. Yamasaki, M.; Habazaki, H.; Asami, K.; Izumiya, K.; Hashimoto, K. Effect of Tetragonal ZrO_2 on the Catalytic Activity of Ni/ZrO_2 Catalyst Prepared from Amorphous Ni–Zr Alloys. Catal. Commun. 2006, 7(1), 24 - 28.

119. Chang, F.-W.; Hsiao, T.-J.; Shih, J.-D. Hydrogenation of CO_2 over a Rice Husk Ash Supported Nickel Catalyst Prepared by Deposition-Precipitation. Ind. Eng. Chem. Res. 1998, 37 (10), 3838 - 3845.

120. Chang, F.-W.; Tsay, M.-T.; Liang, S.-P. Hydrogenation of CO_2 over Nickel Catalysts Supported on Rice Husk Ash Prepared by Ion Exchange. Appl. Catal. A: Gen. 2001, 209 (1-2), 217 – 227.

121. Pandey, D.; Deo, G. Effect of Support on the Catalytic Activity of Supported Ni–Fe Catalysts for the CO_2 Methanation Reaction. J. Ind. Eng. Chem. 2016, 33, 99 - 107.

122. Huanling, S.; Jian, Y.; Jun, Z.; Lingjun , C. Methanation of Carbon Dioxide over a Highly Dispersed Ni/La_2O_3 Catalyst. Chin. J. Catal. 2010, 31 (1), 21 - 23.

123. Tada, S.; Shimizu, T.; Kameyama, H.; Haneda, T.; Kikuchi, R. Ni/CeO_2 Catalysts with High CO_2 Methanation Activity and High CH_4 Selectivity at Low Temperatures. Int. J. Hydrogen Energ. 2012, 37 (7), 5527 - 5531.

124. Ocampo, F.; Louis, B.; Kiwi-Minsker, L.; Roger, A.-C. Effect of Ce/Zr Composition and Noble Metal Promotion on Nickel Based $Ce_xZr_{1-x}O_2$ Catalysts for Carbon Dioxide Methanation. Appl. Catal., A: Gen. 2011, 392 (1-2), 36 - 44.

125. Hu, J.; Brooks, K.P.; Holladay, J.D.; Howe, D.T.; Simon, T.M. Catalyst Development for Microchannel Reactors for Martian in situ Propellant Production. Catal. Today 2007, 125 (1-2), 103 - 110.

126. Kowalczyk, Z.; Stołecki, K.; Raróg-Pilecka, W.; Miśkiewicz, E. Wilczkowska, E.; Karpiński, Z. Supported Ruthenium Catalysts for Selective Methanation of Carbon Oxides at Very Low COx/H2 ratios. Appl. Catal. A: Gen. 2008, 342 (1 - 2), 35 - 39.

127. Denise, B.; Sneeden, R.P.A. Oxide-Supported Copper Catalysts Prepared from Copper Formate: Differences in Behaviour in Methanol Synthesis from CO/H_2 and CO_2/H_2 Mixtures. Appl. Catal. 1986, 28, 235 - 239.

128. Denise, B.; Cherifi, O.; Bettahar, M.M.; Sneeden, R.P.A. Supported Copper Catalysts Prepared from Copper(II) Formate - Hydrogenation of Carbon Dioxide Containing Feedstocks. Appl. Catal. 1989, 48 (2), 365 - 372.

129. Fröhlich, C.; Köppel, R.A.; Baiker, A.; Kilo, M.; Wokaun, A. Hydrogenation of Carbon Dioxide over Silver Promoted Copper/Zirconia Catalysts. Appl. Catal. A: Gen. 1993, 106 (2), 275-293.

130. Fujitani, T.; Saito, M. ; Kanai, Y. ; Kakumoto, T.; Watanabe, T.; Nakamura, J.; Uchijima, T. The Role of Metal Oxides in Promoting a Copper Catalyst for Methanol Synthesis. Catal. Lett. 1994 , 25 (3 – 4), 271 - 276.

131. Kanai, Y.; Watanabe, T.; Fujitani, T.; Saito, M.; Nakamura, J; Uchijima, T. Evidence for the Migration of ZnO_x in a Cu/ZnO Methanol Synthesis Catalyst. Catal. Lett. 1994, 27 (1 – 2), 67-78.

132. Sahibzada, M.; Chadwick, D.; Metcalfe, I.S. Hydrogenation of Carbon Dioxide to Methanol over Palladium-promoted $Cu/ZnO/Al_2O_3$ Catalysts. Catal. Today 1996, 29 (1-4), 367 - 372.

133. Saito, M.; Fujitani, T.; Tekeuchi, M.; Watanabe, T. Development of Copper/Zinc Oxide-based Multicomponent Catalysts for Methanol Synthesis from Carbon Dioxide and Hydrogen. Appl. Catal. A: Gen. 1996, 138 (2), 311 - 318.

134. Sahibzada, M. Pd-Promoted Cu/ZnO Catalysts for Methanol Synthesis from CO_2/H_2. Trans. IChemE. 2000, 78A, 943 - 946.

135. Toyir, J.; de la Piscina, P.R.; Fierro, J.L.G.; Homs, N. Catalytic Performance for CO_2 Conversion to Methanol of Gallium-promoted Copper-based Catalysts: Influence of Metallic Precursors. Appl. Catal. B: Environ. 2001, 34 (4), 255 - 266.

136. Toyir, J.; de la Piscina, P.R.; Fierro, J.L.G.; Homs, N. Highly Effective Conversion of CO_2 to Methanol over Supported and Promoted Copper-based Catalysts: Influence of Support and Promoter. Appl. Catal. B: Environ. 2001, 29 (3) , 207–215.

137. Słoczyński, J.; Grabowski, R.; Olszewski, P.; Kozłowska, A.; Stoch, J.; Lachowska, M.; Skrzypek, J. Effect of Metal Oxide Additives on the Activity and Stability of

Cu/ZnO/ZrO_2 Catalysts in the Synthesis of Methanol from CO_2 and H_2. Appl. Catal. A: Gen. 2006 , 310 , 127–137.

138. Natesakhawat, S.; Lekse, J.W.; Baltrus, J.P.; Ohodnicki Jr., P.R.; Howard, B.H.; Dengand, X.; Matranga, C. Active Sites and Structure-Activity Relationships of Copper-based Catalysts for Carbon Dioxide Hydrogenation to Methanol. ACS Catal. 2012, 2 (8), 1667-1676.

139. Gao, P.; Li, F., Zhao, N.; Xiao, F.; Wei, W.; Zhong, L. Influence of Modifier (Mn, La, Ce, Zr and Y) on the Performance of Cu/Zn/Al Catalysts via Hydrotalcite-like Precursors for CO_2 Hydrogenation to Methanol. Appl. Catal. A: Gen. 2013, 468, 442 - 452.

140. Frei, E.; Schaadt, A.; Ludwig, T.; Hillebrecht, H.; Krossing, I. The Influence of the Precipitation/Ageing Temperature on a Cu/ZnO/ZrO_2 Catalyst for Methanol Synthesis from H_2 and CO_2. ChemCatChem. 2014, 6 (6), 1721-1730.

141. Zhan, H.; Li, F.; Gao, P.; Zhao, N.; Xiao, F.; Wei, W.; Zhong, L.; Sun, Y. Methanol Synthesis from CO_2 Hydrogenation over La-M-Cu-Zn-O (M = Y, Ce, Mg, Zr) Catalysts Derived from Perovskite-type Precursors. J. Power Sources 2014, 251, 113-121.

142. Dry, M.E.; Shingles, T.; Boshoff, L.J.; Oosthuizen, G.J. Heats of Chemisorption on Promoted Iron Surfaces and the Role of Alkali in Fischer-Tropsch Synthesis. J. Catal. 1969, 15 (2), 190 - 199.

143. Bonzel, H.P. ; Krebs, H.J. Ehnanced Rate of Carbon Deposition during Fischer-Tropsch Synthesis on K Promoted Fe. Surf. Sci. 1981, 109 (2), L527 - L531.

144. Campbell, C.T.; Goodman, D.W. A Surface Science Investigation of the Role of Patassium Promoters in Nickel Catalysts for CO Hydrogenation. Surf. Sci. 1982, 123 (2-3), 413 - 426.

145. Inui, T.; Takeguchi, T. Effective Conversion of Carbon Dioxide and Hydrogen to Hydrocarbons. Catalysis Today 1991, 10 (1), 95 - 106.

146. Znak, L.; Stołecki, K.; Zieliński, J. The Effect of Cerium, Lanthanum and Zirconium on Nickel/Alumina Catalysts for the Hydrogenation of Carbon Oxides. Catal. Today 2005, 101 (2), 65 - 71.

147. Hwang, S.; Hong, U.G.; Lee, J.; Baik, J.H.; Koh, D.J.; Lim, H.; Song, I.K. Methanation of Carbon Dioxide Over Mesoporous Nickel–M–Alumina (M = Fe, Zr, Ni, Y, and Mg) Xerogel Catalysts: Effect of Second Metal. Catal. Lett. 2012, 142 (7), 860 - 868.

148. Aksoylu, A.E.; Misirli, Z.; Onsan, Z.I. Interaction Between Nickel and Molybdenum in Ni-Mo/Al_2O_3 catalysts: I: CO_2 methanation and SEM-TEM studies. Appl. Catal. A: Gen. 1998, 168 (2), 385 - 397.

149. Krämer, M.; Stöwe, K.; Duisberg, M.; Müller, F.; Reiser, M.; Sticher, S.; Maier, W.F. The Impact of Dopants on the Activity and Selectivity of a Ni-based Methanation Catalyst. Appl. Catal. A: Gen. 2009, 369 (1-2), 42 - 52.

150. Takano, H.; Shinomiya, H.; Izumiya, K. ; Kumagai, N.; Habazaki, H.; Hashimoto, K. CO_2 Methanation of Ni Catalysts Supported on Tetragonal ZrO_2 Doped with Ca^{2+} and Ni^{2+} ions. Int. J. Hydrogen Energ. 2015, 40 (26), 8347 - 8355.

151. Takano, H.; Izumiya, K.; Kumagai, N.; Hashimoto, K. The Effect of Heat Treatment on the Performance of the Ni/(Zr-Sm oxide) Catalysts for Carbon Dioxide Methanation. Appl. Surf. Sci. 2011, 257 (19), 8171– 8176.

152. Zhang, Y.; Fei, J.; Yu, Y.; Zheng, X. Study of CO_2 Hydrogenation to Methanol over Cu-V/ɣ-Al_2O_3 Catalyst. J. Nat. Gas Chem. 2007 , 16 (1), 12-15.

153. Kester, K.B.; Zagli, E.; Falconer, J.L. Methanation of Carbon Monoxide and Carbon Dioxide on Ni/Al_2O_3 Catalysts: Effects of Nickel Loading. Appl. Catal. 1986, 22 (2), 311 - 319.

154. Hwang, H.; Hong, U.G.; Lee, J.; Seo, J.G.; Baik, J.H.; Koh, D.J.; Lim, H.; Song, I.K. Methanation of Carbon Dioxide over Mesoporous Ni–Fe–Al_2O_3 Catalysts

Prepared by a Coprecipitation Method: Effect of Precipitation Agent. J. Ind. Eng. Chem. 2013, 19 (6), 2016 - 2021.

155. Dong, X.; Li, F.; Zhao, N.; Xiao, F.; Wang, J.; Tan, Y. CO_2 Hydrogenation to Methanol over Cu/ZnO/ZrO_2 Catalysts Prepared by Precipitation-reduction Method. Appl. Catal. B: Environ. 2016, 191, 8-17.

156. Dew, J.N.; White, R.R.; Sliepcevich, C.M. Hydrogenation of Carbon dioxide on Nickel-Kieselguhr Catalyst. Ind. Eng. Chem. 1955, 47 (1), 140 - 146.

157. Muller, J.; Pour, V.; Regner, A. Specific Catalytic Activity of Nickel in Hydrogenation of Carbon Dioxide to Methane. J. Catal. 1968, 11 (4), 326 - 335.

158. Inoue, H.; Funakoshi, M. Kinetics of Methanation of Carbon Monoxide and Carbone Dioxide. J. Chem. Eng. Jpn. 1984, 17 (6), 602 - 610.

159. Kai, T., Takahashi, T.; Farusaki, S. Kinetics of the Methanation of Carbon Dioxide over a Supported Ni-La_2O_3 Catalyst. Can. J. Chem. Eng. 1988, 66 (2), 343 – 347.

160. Xu, G.; Froment, G.F. Methane Steam Reforming, Methanation and Water-Gas Shift: 1. Intrinsic Kinetics. AIChE J. 1989, 35 (1), 88 - 96.

161. Lu, B.; Ju, Y.; Abe, T.; Kawamoto, K. Grafting Ni Particles onto SBA-15, and Their Enhanced Performance for CO_2 Methanation. RSC Adv. 2015, 5 (70), 56444 - 56454.

162. Lunde, P.J.; Kester, F.L. Carbon Dioxide Methanation on a Ruthenium Catalyst. Ind. Eng. Chem. Process Des. Dev. 1974, 13 (1), 27 - 33.

163. Garbarino, G.; Bellotti, D.; Riani, P.; Magistri, L.; Busca, G. Methanation of Carbon Dioxide on Ru/Al_2O_3 and Ni/Al_2O_3 Catalysts at Atmospheric Pressure: Catalysts Activation, Behaviour and Stability. Int. J. Hydrogen Energy 2015 , 40 (30), 9171 - 9182.

164. Du, G.; Lim, S.; Yang, Y.; Wang,C.; Pfefferle, L.; Haller, G.L. Methanation of Carbon Dioxide on Ni-incorporated MCM-41 Catalysts: The Influence of Catalyst Pretreatment and Study of Steady-state Reaction. J. Catal. 2007, 249 (2), 370 - 379.

165. Ocampo, F.; Louis, B.; Roger, A.-C. Methanation of Carbon Dioxide over Nickel-based $Ce_{0.72}Zr_{0.28}O_2$ Mixed Oxide. Appl. Catal. A: Gen. 2009, 369 (1-2), 90 - 96.

166. Mutz, B.; Carvalho, H.W.P.; Mangold, S.; Kleist, W.; Grunwaldt, J-D. Methanation of CO_2: Structural Response of a Ni-based Catalyst under Fluctuating Reaction Conditions Unraveled by Operando Spectroscopy. J. Catal. 2015, 327, 48 - 53.

167. Karn, F.S.; Shultz, J.F.; Anderson, R.B. Hydrogenanation of Carbon Monoxide and Carbon Dioxide on Supported Ruthenium Catalysts at Moderate Pressures. Ind. Eng. Chem. Prod. Res. Dev. 1965, 4 (4), 265 - 269.

168. Fujimoto, K.; Shikada, T. Selective Synthesis of C_2-C_5 Hydrocarbons from Carbon Dioxide Utilizing a Hybrid Catalyst Composed of a Methanol Synthesis Catalyst and Zeolite. Appl. Catal. 1987, 31 (1), 13 - 23.

169. Jingfa, D.; Qi, S.; Yulong, Z.; Songying, C.; Dong, W. A Novel process for Preparation of $Cu/ZnO/Al_2O_3$ Ultrafine catalyst for Methanol Synthesis from CO_2 + H_2: Comparison of various Preparation Methods. Appl. Catal. A: Gen. 1996 , 139 (1 – 2), 75 - 85.

Figures

$$CO_{2gas} \leftrightarrows Ni_4CO_{ads.} + NiO_{ads}$$

$$Ni_4CO_{ads.} \leftrightarrows Ni_3C_{surf.} + NiO_{ads.}$$

$$Ni_3C_{surf.} \text{ hydrogenation to } CH_4$$

where Ni_3C_{surf} is the superficial carbide.

Figure 1: CO_2 hydrogenation via CO and superficial carbide. Redrawn from Journal of Chemical Society, Faraday Transactions 1, Vol. 75, Dalmon and Martin, "Intermediates in CO and CO_2 Hydrogenation over Ni Catalysts", Pages 1011 - 1015, Copyright (1979), with permission from Royal Society of Chemistry.

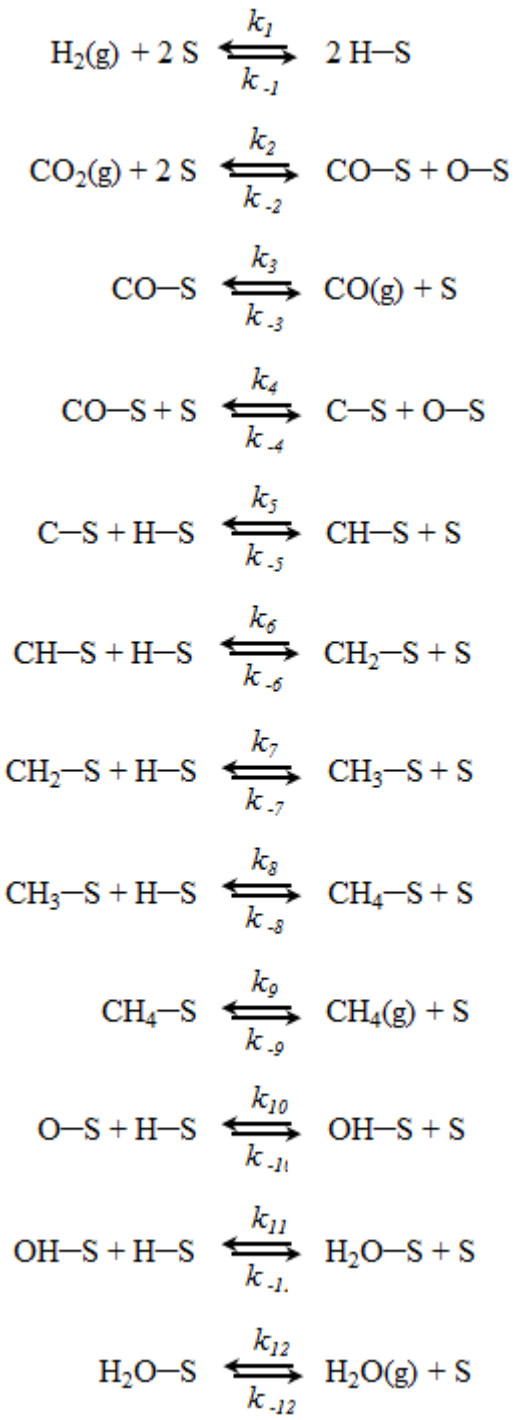

Figure 2: Proposed sequence of elementary steps in CO_2 methanation (S refers to a surface site). Redrawn from Journal of Catalysis, Vol. 77, Weatherbee and Bartholomew, "Hydrogenation of CO_2 on Group VIII Metals. II. Kinetics and Mechanism of CO_2 Hydrogenation on Nickel", Pages 460 - 472, Copyright (1982), with permission from Elsevier.

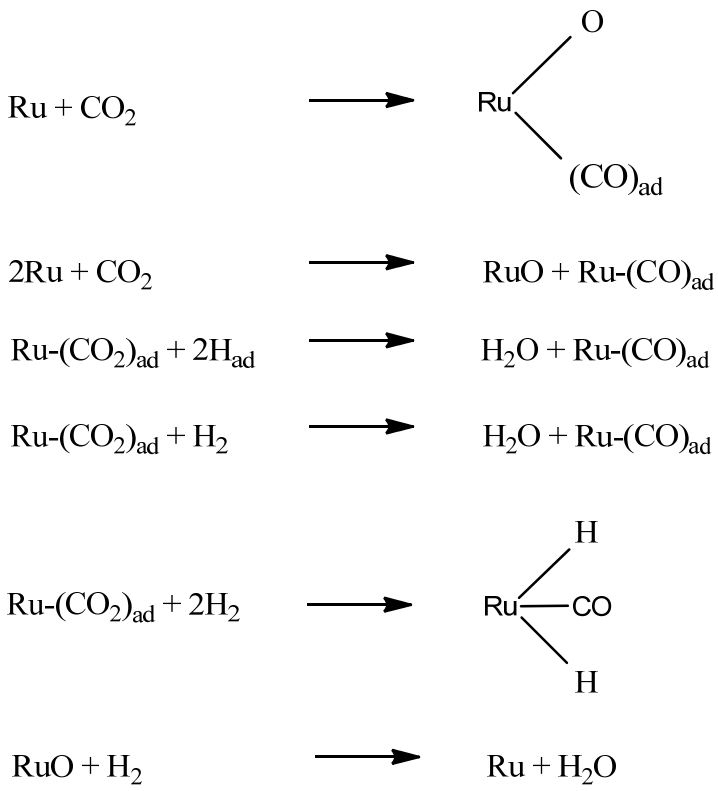

Figure 3: Reactions occurring at catalyst surface during CO_2 or CO_2/H2 interaction with Ru/TiO_2 catalyst. Redrawn from Journal of Catalysis, Vol. 146, Gupta *et al.*, "FTIR Spectroscopic Study of the Interaction of CO_2 and CO_2 + H_2 over Partially Oxidized Ru/TiO_2 Catalyst", Pages 173 - 184, Copyright (1994), with permission from Elsevier.

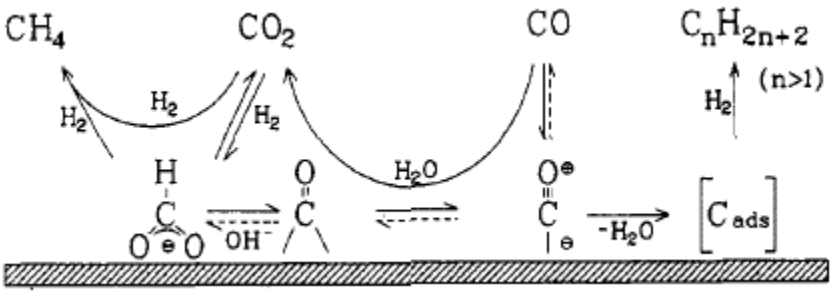

Figure 4: Proposed reaction scheme for the hydrogenation of CO and CO_2 over nickel/zirconia catalysts. Reprinted from The Journal of Physical Chemistry, Vol. 95, Schild *et al*., "CO_2 Hydrogenation over Nickel/Zirconia Catalysts from Amorphous Precursors: On the Mechanism of Methane Formation", Pages 6341 - 6346, Copyright (1991), with permission from American Chemical Society.

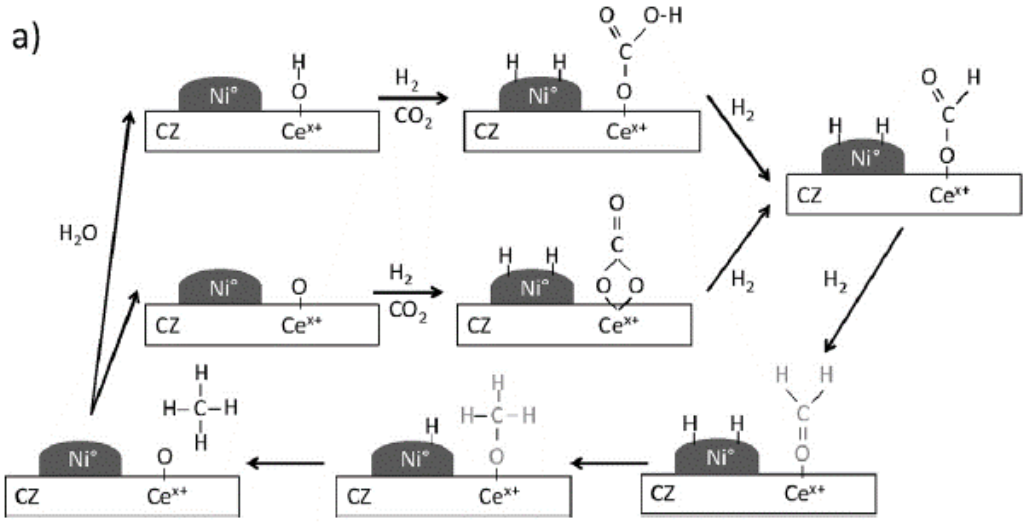

Figure 5: Reaction mechanism proposed on Ni-CZsol-gel sample for CO_2 methanation. Reprinted from Catalysis Today, Vol. 215, Aldana *et al*., "Catalytic CO_2 valorization into CH_4 on Ni-based ceria-zirconia. Reaction mechanism by operando IR spectroscopy", Pages 201 - 207, Copyright (2013), with permission from Elsevier.

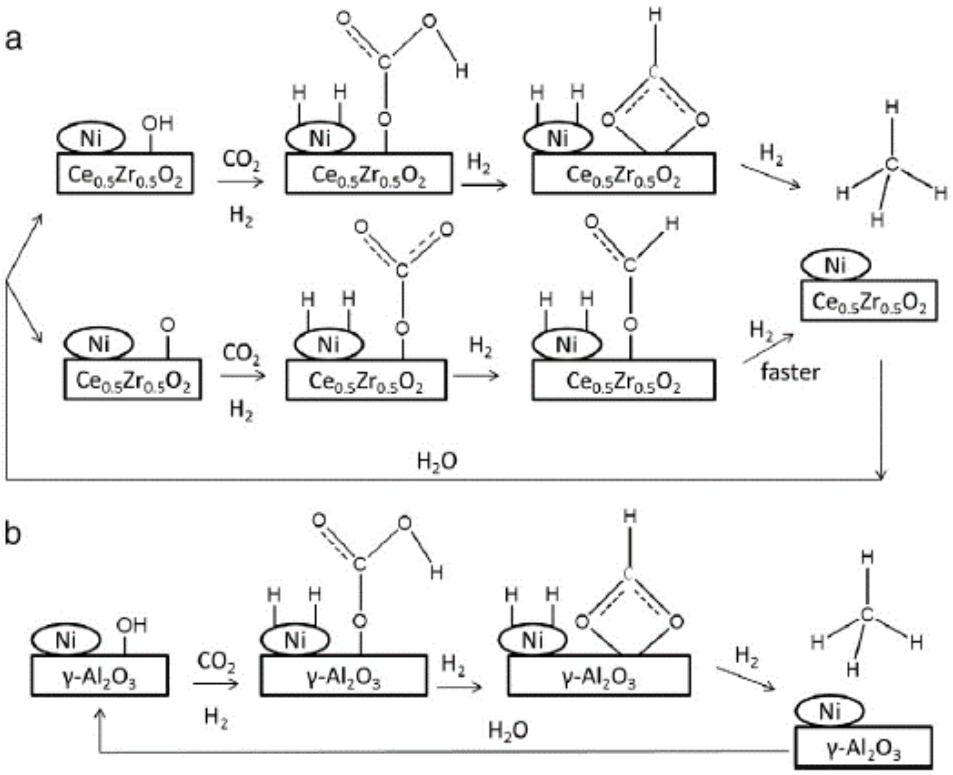

Figure 6: Proposed pathways for CO_2 activation and methanation, a) on Ni/$Ce_{0.5}Zr_{0.5}O_2$, b) on Ni/γ-Al_2O_3. Reprinted from Catalysis Communications, Vol. 45, Pan *et al*., "Insight into the reaction route of CO_2 methanation: Promotion effect of medium basic sites", Pages 74 - 78, Copyright (2014), with permission from Elsevier.

$H_2(g) + 2*$	⇌	$2H*$	(1)
$CO_2(g) + *$	⇌	CO_2*	(2)
$CO_2* + *$	⇌	$CO* + O*$	(3)
$CO(g) + *$	⇌	$CO*$	(4)
$O_2(g) + 2*$	⇌	$2O*$	(5)
$CO_2* + H*$	⇌	$HCOO* + *$	(6)
$HCOO* + H*$	⇌	$H_2CO_2* + *$	(7)
$H_2CO_2* + H*$	⇌	$C_3O* + O*$	(8)
$C_3O* + H*$	⇌	$C_3O* + *$	(9)
$C_3O(g) + *$	⇌	C_3O*	(10)
$H_2CO_2* + *$	⇌	$H_2CO* + O*$	(11)
$H_2CO(g) + *$	⇌	H_2CO*	(12)
$H_2CO* + H*$	⇌	$C_3O* + *$	(13)
$H_2O(g) + *$	⇌	H_2O*	(14)
$H_2O* + *$	⇌	$O* + H*$	(15)
$O* + *$	⇌	$O* + H*$	(16)
$2O* + *$	⇌	$H_2O* + O*$	(17)

Figure 7: The elementary reaction steps relevant for methanol synthesis. Redrawn from Surface Science, Vol. 318, Rasmussen *et al*., "Synthesis of Methanol from a Mixture of H_2 and CO_2 on Cu (100)", Pages 267 - 280, Copyright (1994), with permission from Elsevier.

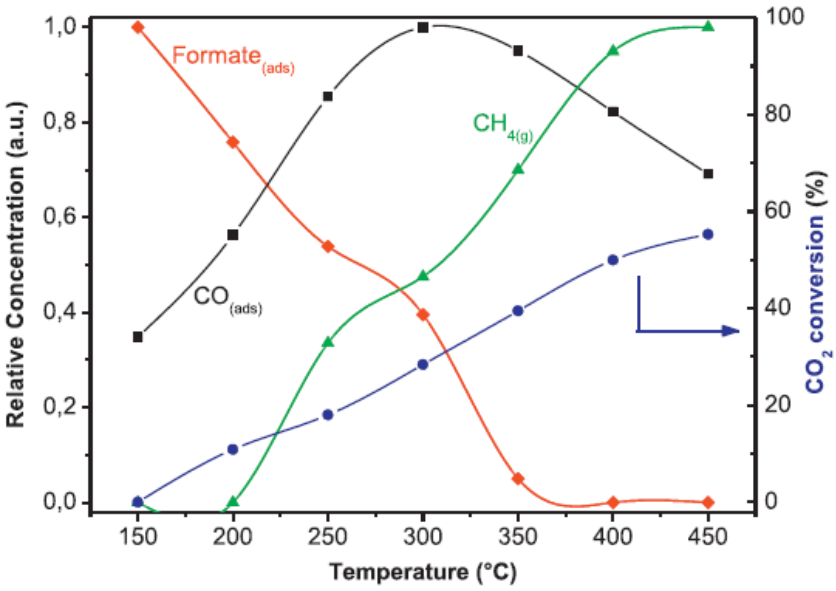

Figure 8. Evolution of the relative concentrations of $CH_{4(g)}$, adsorbed CO (2100-1740 cm $^{-1}$) and formates (1573 cm^{-1}) and CO_2 conversion (%) during TPSR Ar/H_2/CO_2 (75/20/5) over 14% NiUSY zeolite. Reprinted from Applied Catalysis B: Environment, Vol. 174 - 175, Wetermann *et al.*, "Insight into CO_2 methanation mechanism over NiUSY zeolites: An Operando IR Study", Pages 120 - 125, Copyright (2015), with permission from Elsevier.

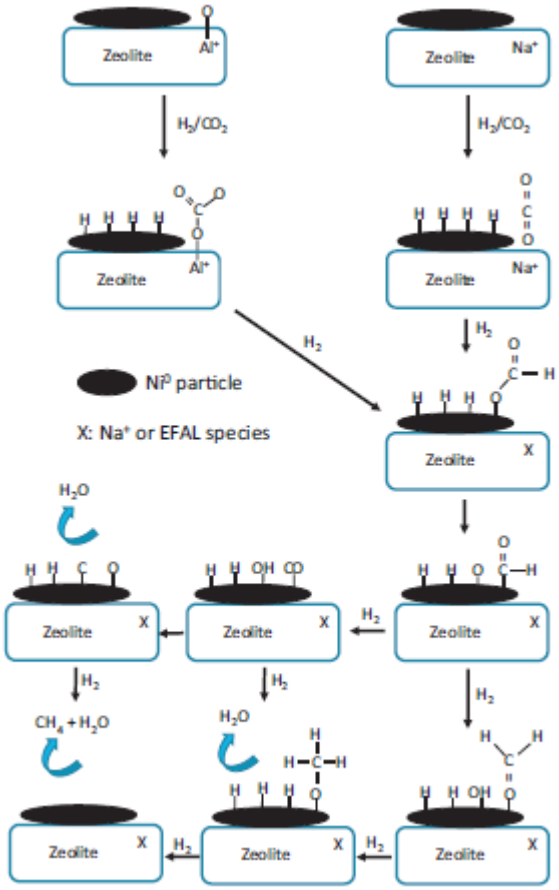

Figure 9: Proposed mechanism for CO_2 hydrogenation on NiUSY zeolites. Reprinted from Applied Catalysis B: Environment, Vol. 174 - 175, Wetermann *et al.*, "Insight into CO_2 methanation mechanism over NiUSY zeolites: An Operando IR Study", Pages 120 - 125, Copyright (2015), with permission from Elsevier.

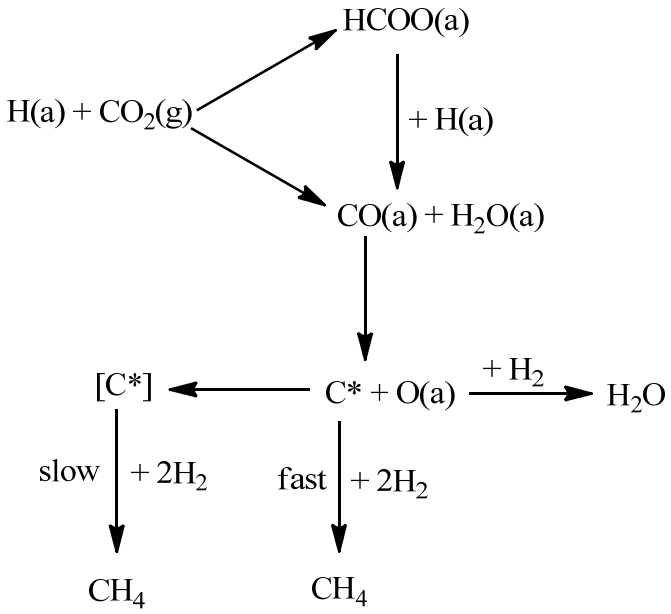

Figure 10: Mechanism for CO_2 methanation on Ru catalyst. [C*] represents less reactive form of surface carbon that requires high activation energy to be hydrogenated. Redrawn from Journal of Chemical Society, Faraday Transactions 1, Vol. 77, Solymosi *et al*., "Methanation of CO_2 on Supported Ru Catalysts", Pages 1003 - 1012, Copyright (1981), with permission from Royal Society of Chemistry.

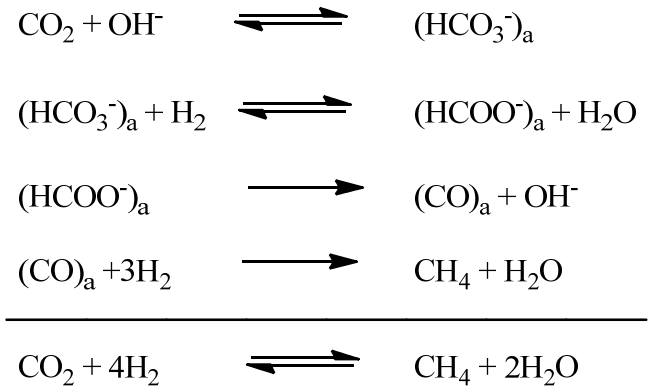

Figure 11: Mechanism of methane formation on Ru/TiO_2. Redrawn from Catalysis Today, Vol. 20, Marwood *et al*., "Periodic Operation Applied to the Kinetic Study of CO_2 Methanation", Pages 437 - 448, Copyright (1994), with permission from Elsevier.

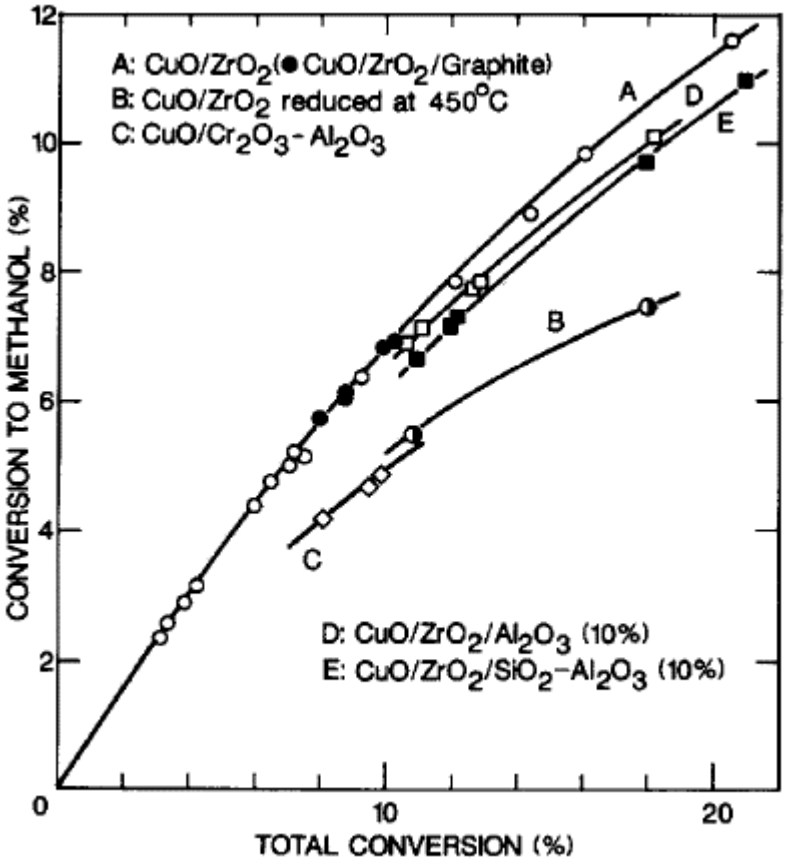

Figure 12: Conversion to methanol vs. total conversion. Reprinted from Applied Catalysis, Vol. 30, Amenomiya, "Methanol Synthesis from CO_2 + H_2: II. Copper-based Binary and Ternary Catalysts", Pages 57 - 68, Copyright (1987), with permission from Elsevier.

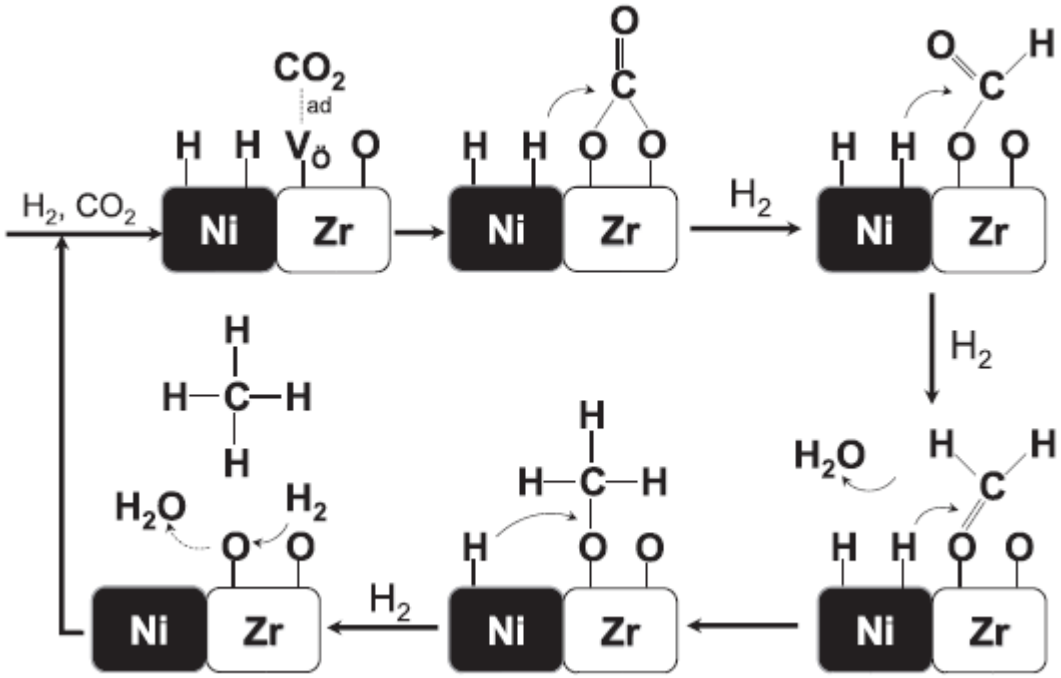

Figure 13: Reaction mechanism proposed on Ni – ZrO_2 with oxygen vacancies for CO_2 methanation. Reprinted from International Journal of Hydrogen Energy, Vol. 40, Takano *et al*., "CO_2 Methanation on Ni Catalysts Supported on Tetragonal ZrO_2 Doped with Ca^{2+} and Ni^{2+} ions", Pages 8347 - 8355, Copyright (2015), with permission from Elsevier.

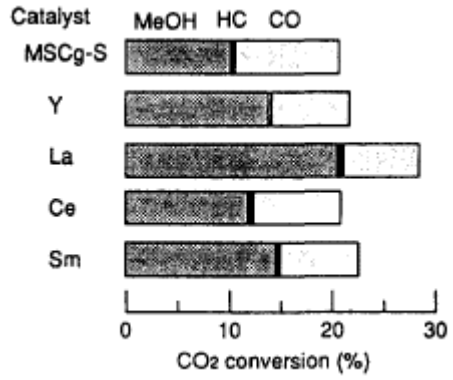

Figure 14: Effect of combination of lanthanide oxides with MSCg-S on the performance of methanol synthesis. 25.0% CO_2 - 75.0% H_2, SV = 4700 h^{-1}, 50 atm., 250 ^oC, Catalyst 1.8 ml. The composition at optimum methanol yield is the same as MSCg-S. Reprinted from Energy Conversion and Management, Vol. 33, Inui *et al*., "Effective Conversion of Carbon Dioxide to Gasoline", Pages 513 - 520, Copyright (1992), with permission from Elsevier.

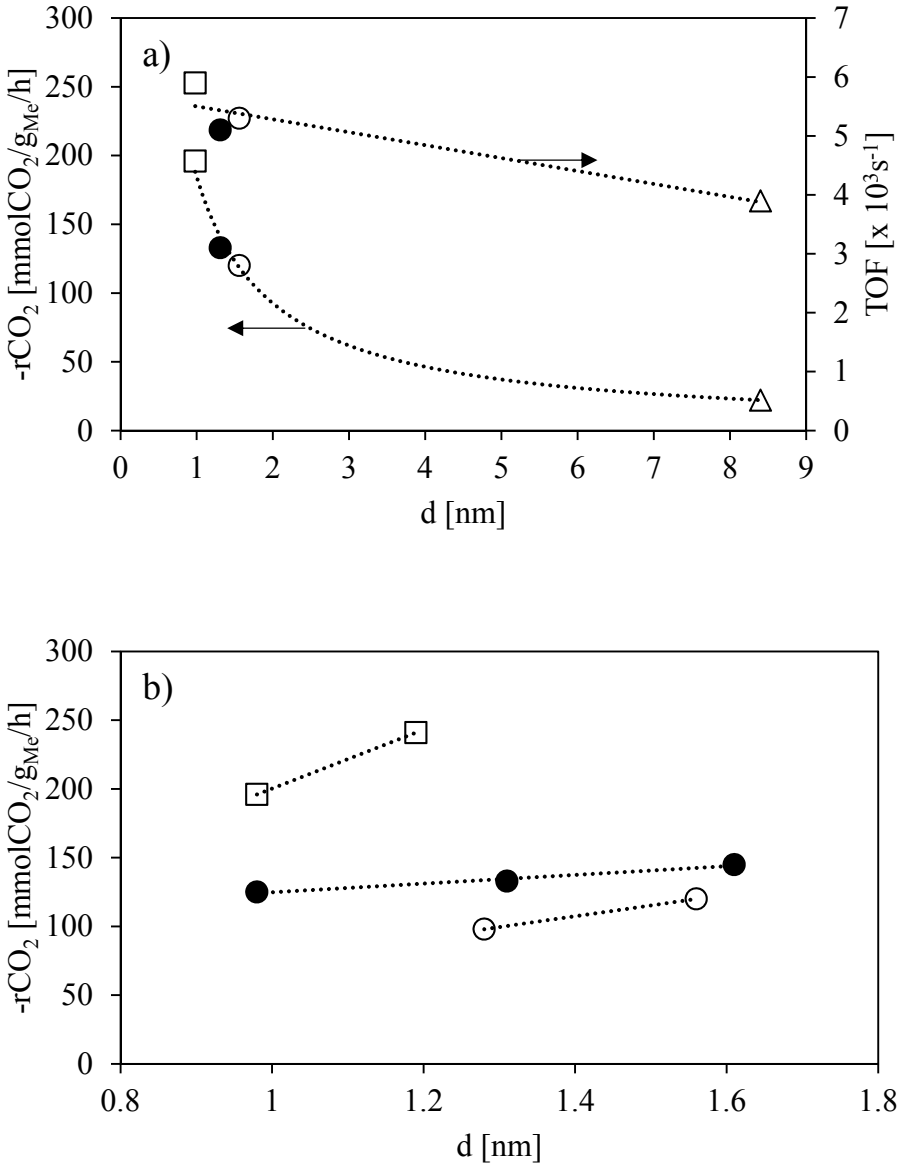

Figure 15: Effect of a) support type and metal particle size on CO_2 hydrogenation activity over □ 10%Ru/Al_2O_3; ● 10%Ru/$MgAl_2O_4$; ○ 10%Ru/MgO and △ 9%Ru/CA and b) metal particle size on CO_2 hydrogenation activity over □ Ru/Al_2O_3; ● Ru/$MgAl_2O_4$ and ○ 10%Ru/MgO. Drawn from data from Kowalczyk *et al.* (126).

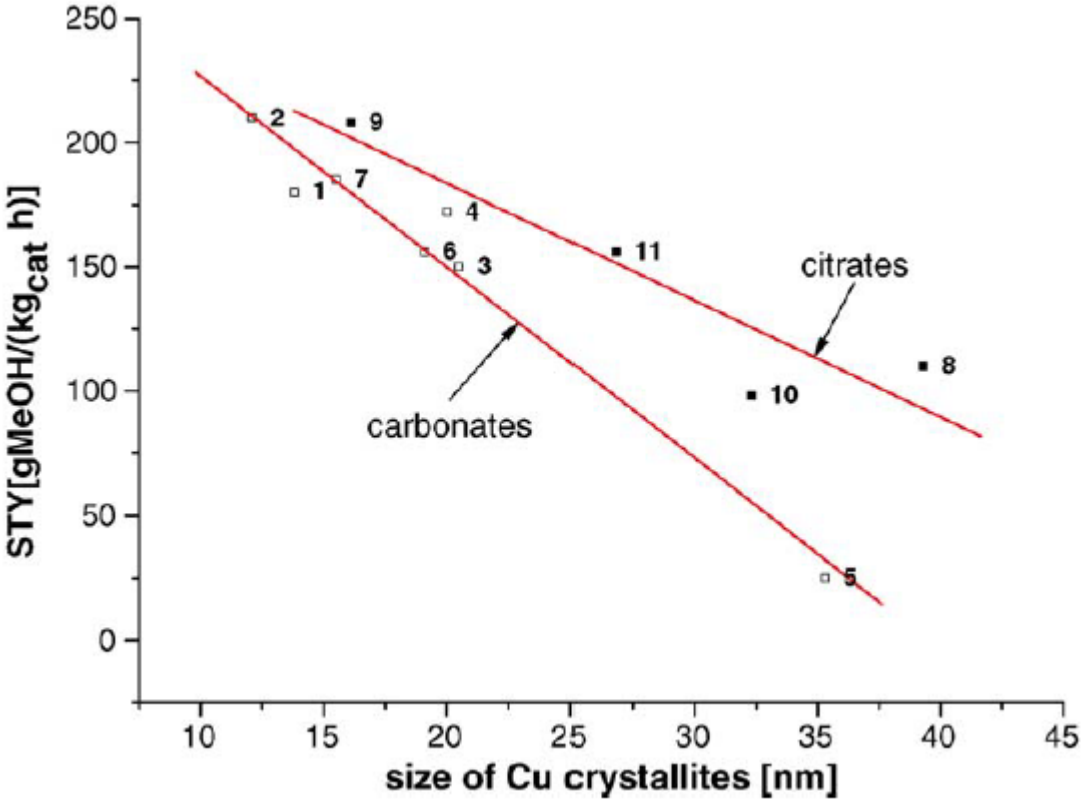

Figure 16: Yield of methanol as a function of the crystal sizes of copper. The numbers 1 and 8 represent Cu/ZnO/ZrO_2 catalysts that were prepared by co-precipitation as carbonates and by complexing with citric acid, respectively. The numbers 2 to 7 represent the co-precipitated catalysts that were respectively modified by the following additives: 2.8% Ga_2O_3, 2% MnO, 2.1% B_2O_3, 4.0% In_2O_3, 4.0%Gd_2O_3, and 4.0%Y_2O_3. The catalysts prepared by complexing with citric acid and modified by 2.8% Ga_2O_3, 3.9 MgO and 2% MnO are represented by numbers 9, 10 and 11 respectively. Reprinted from Applied Catalysis A: General, Vol. 310, Słoczyński *et al*., "Effect of Metal Oxide Additives on the Activity and Stability of Cu/ZnO/ZrO_2 Catalysts in the Synthesis of Methanol from CO_2 and H_2", Pages 127 - 137, Copyright (2006), with permission from Elsevier.

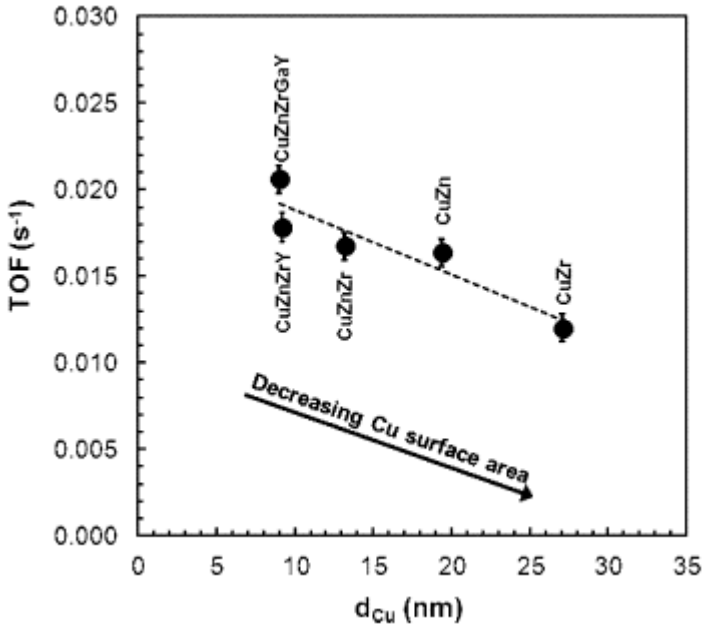

Figure 17: Relationship between TOF for methanol synthesis and copper crystallite size. Reaction conditions: 240 ºC, 20 bar, $CO_2/H_2/N_2$ = 1/3/0.4, CO_2 conversion ≈ 5%. Reprinted from ACS Catalysis, Vol. 2, Natesakhawat *et al*., "Active sites and Structure-Activity relationships of Copper-based Catalysts for Carbon Dioxide Hydrogenation to Methanol", Pages 1667 - 1676, Copyright (2012), with permission from American Chemical Society.

1: $CO_2 + 2^* \leftrightarrows CO^* + O^*$

2: $H_2 + 2^* \leftrightarrows 2H^* +$

3: $CO^* + H^* \leftrightarrows CHO^* + *$

4: $CHO^* + * \leftrightarrows CH^* + O^*$

5: $CH^* + 3H^* \leftrightarrows CH_4^* + 3^*$

6: $CH_4^* \leftrightarrows CH_4 + *$

7: $O^* + H^* \leftrightarrows OH^* + *$

8: $OH^* + H^* \leftrightarrows H_2O^* + *$

9: $H_2O^* \leftrightarrows H_2O + *$

Figure 18: Proposed elementary steps for CO_2 hydrogenation via hydrogen assisted carbon oxygen cleavage. Reprinted from Applied Catalysis B: Environmental, Vol. 181, Koschany *et al*., "On the Kinetics of the Methanation of Carbon Dioxide on Coprecipitated $NiAl(O)_x$", Pages 504 - 516, Copyright (2016), with permission from Elsevier.

Tables

Table 1. Activation energy for CO_2 hydrogenation over nickel-based catalysts

Catalyst	Preparation method	Reduction	H_2:CO_2 ratio	Temp. [K]	Press. [bar]	Ea [kJ/mol]		Ref.
						CO_2	CH_4	
Ni/Al_2O_3	(Commercial)	H_2, 623 K	454/1-41/1	473-503	1	106		(88)
5.5%Ni/0.8%Ru/SiO_2	Spraying	H_2, 623 K	3:1		Atmospheric		82	(89)
4.6%Ni/2.6%La_2O_3/SiO_2	Spraying	H_2, 623 K	3:1		Atmospheric		82	(89)
4.3%Ni/2.5%La_2O_3/0.7%Ru/SiO_2	Spraying	H_2, 623 K	3:1		Atmospheric		82	(89)
3%Ni/SiO_2	Impregnation	H_2, 750 K	4:1 (95% N_2)	500-550	1.4	70	80	(18)
NiB(P-1)	Reduction of Ni acetate with $NaBH_4$	H_2	3:1	413-498			71	(90)
Raney Ni	Activated by NaOH at 70 ºC for 30 min	H_2	3:1	413-498			54	(90)
Ni-P-1	Reacting $NiCl_2$ with NaH_2PO_2	H_2	3:1	573-623			138	(90)
D-Ni	Ni formate decomposition	H_2	3:1	498-563			96	(90)
Ni (100)		H_2, 750 K	4:1	430-710	0.16		89	(20)
Ni (100)		H_2, 750 K	96:1	550-710	0.13		89	(20)
100% Ni		H_2, 553 K		500-550	1.01	97		(91)
3% Ni/SiO_2	Impregnation	H_2, 723 K	4:1 (95% N_2)	500-550	1.01	81		(91)
3% Ni/SiO_2	Impregnation	H_2, 723 K	4:1 (95% N_2)	500-550	1.01	72		(91)
3% Ni/Al_2O_3	Impregnation	H_2, 723 K	4:1 (95% N2)	500-550	1.01	69		(91)
3% Ni/TiO_2	Impregnation	H_2, 723 K	4:1 (95% N2)	500-550	1.01	85		(91)
58%Ni/SiO_2		H_2, 700 K	4:1 - 2:1	530-605	6 - 18	61		(92)
100% Ni	Reduction of NiO	H_2 , 673 K	4:1	523-573	Atmospheric	98		(93)
4.5% Ni/S1	Impregnation	H_2, 673 K	4:1	533-583	Atmospheric	95		(93)
4.5% Ni/S3	Impregnation	H_2, 673 K	4:1	503-553	Atmospheric	100		(93)
9.2%Ni/SiO_2	Impregnation	H_2, 773 K	3.3:1		1.2		89	(94)
0.25%K/9.2%Ni/SiO_2	Co-impregnation	H_2, 773 K	3.3:1		1.2		90	(94)
0.70%K/11.0%Ni/SiO_2	Co-impregnation	H_2, 773 K	3.3:1		1.2		88	(94)
0.81%K/9.2%Ni/SiO_2	Co-impregnation	H_2, 773 K	3.3:1		1.2		90	(94)
4.1%K/11.0%Ni/SiO2	Co-impregnation	H_2, 773 K	3.3:1		1.2		89	(94)
9.5%Ni/SiO_2-Al_2O_3	Impregnation	H_2, 773 K	3.3:1		1.2		86	(94)
0.25%K/11.5%Ni/SiO_2-Al_2O_3	Co-impregnation	H_2, 773 K	3.3:1		1.2		82	(94)
0.81%K/9.7%Ni/SiO_2-Al_2O_3	Co-impregnation	H_2, 773 K	3.3:1		1.2		84	(94)
3.9%K/11.5%Ni/SiO_2-Al_2O_3	Co-impregnation	H_2, 773 K	3.3:1		1.2		89	(94)
Ni(14.7g)-Fe(14.0g)-MgO (2.02g)	Powder mixing	Milling	5:1	363-393	0.8	39		(95)
5%Ni/Al_2O_3	Coprecipiation	H_2, 623 K	9:1	433-533	Atmospheric		68	(56)
11%Ni/Al_2O_3	Coprecipiation	H_2, 623 K	9:1	433-533	Atmospheric		73	(56)
16.5%Ni/Al_2O_3	Coprecipiation	H_2, 623 K	9:1	433-533	Atmospheric		62	(56)
25%Ni/Al_2O_3	Coprecipiation	H_2, 623 K	9:1	433-533	Atmospheric		59	(56)
Raney Ni (77.7%)	Leaching	H_2, 623 K	4:1	433-533		88		(96)

Raney Ni (75.3%)	Leaching	H_2, 623 K	4:1	433-533		91		(96)
Raney Ni (84.6%)	Leaching	H_2, 623 K	4:1	433-533		90		(96)
12%Ni/ZrO_2-Al_2O_3 ^{CP}	Impregnation		3.5:1	453-633	Atmospheric	72		(97)
12%Ni/γ-Al_2O_3	Impregnation		3.5:2	453-633	Atmospheric	77		(97)
12%Ni/ZrO_2-Al_2O_3 ^{Imp}	Impregnation		3.5:3	453-633	Atmospheric	75		(97)
12%Ni/ZrO_2-Al_2O_3 $^{I-P}$	Impregnation		3.5:4	453-633	Atmospheric	55		(97)
5%Ni/MSN	Impregnation	H_2, 773 K	4:1	523–573	Atmospheric	76		(98)
5%Ni/MCM-41	Impregnation	H_2, 773 K	4:1	523–573	Atmospheric	78		(98)
5%Ni/HY	Impregnation	H_2, 773 K	4:1	523–573	Atmospheric	81		(98)
5%Ni/SiO_2	Impregnation	H_2, 773 K	4:1	523–573	Atmospheric	84		(98)
5%Ni/γ-Al_2O_3	Impregnation	H_2, 773 K	4:1	523–573	Atmospheric	103		(98)
20%Ni/Bentonite	Impregnation	H_2, 873 K	4:1	470-515	1	107		(79)
20%Ni/3%V_2O_5/Bentonite	Co-impregnation	H_2, 873 K	4:1	470-515	1	69		(79)
20%Ni/5%V_2O_5/Bentonite	Co-impregnation	H_2, 873 K	4:1	470-515	1	74		(79)
20%Ni/8%V_2O_5/Bentonite	Co-impregnation	H_2, 873 K	4:1	470-515	1	86		(79)
12%Ni/CNT	Impregnation	H_2, 623 K	4:1	560-595	Atmospheric	85		(99)
12%Ni4.5Ce/CNT	Impregnation	H_2, 623 K	4:1	560-595	Atmospheric	13		(99)
NiAl(O)x (N/Al molar ration from 5/1 to 1/5)	Coprecipitation	H_2, 758 K	4:1	510-580	3		85	(100)
					6		82	(100)
					9		83	(100)

^{CP}: support prepared by coprecipitation of aluminium nitrate and zirconyl chloride
^{Imp}: Support prepared by impregnation of γ-Al_2O_3 with an aqueous solution of zirconyl chloride
$^{I-P}$: Support prepared by impregnation-precipitation
D-Ni: decomposed-nickel catalyst
MSN: Mesostructured silica nanoparticles
NiB(P-1): nickel-boride catalyst
Ni-P-1: nickel-phosphide catalyst
S1 & S3: Saran carbon

Table 2. Activation energy for CO_2 hydrogenation over ruthenium-based catalysts

Catalyst	Preparation method	Reduction	H_2:CO_2 ratio	Temp. [K]	Pressure [bar]	Ea [kJ/mol]		Ref.
						CO_2	CH_4	
0.5%Ru/Al_2O_3	(Commercial)		1.9:1 - 3.9:1	478-644	1	70.4		(101)
3.3%Ru/SiO_2	Precipitation-deposition	H_2	3:1	500-523	Atmospheric		81.9	(89)
1.8%/ɣ-Al_2O_3	Impregnation	H_2, 675K	2%CO_2 in H_2	400-600	1.2		57.7	(33)
		H_2, 675K, ɣ*					32.2	(33)
1.8%Ru/Molecular Sieve (13X)	Impregnation	H_2, 625K	2%CO_2 in H_2	400-600	1.2		30.5	(33)
		H_2, 625K, ɣ*					17.6	(33)
5%Ru/Al_2O_3	Impregnation	H_2, 673K	4:1	443-543	1		67.3	(82)
0.5%Ru/SiO_2	Impregnation	H_2, 750K	4:1	502-563	1	72	72	(83)
				485-550	11	103	103	(83)
			4:1 (95% N_2)	500-550	1	73	68	(83)
3.8%Ru/TiO_2	Impregnation	H_2, 493 K	12:1	298-362	1		54	(102)
3.8%Ru/TiO_2	Impregnation	H_2, 483K	4.4 : 1	393-445	0.48		79	(69)
3.8%Ru/TiO_2	Impregnation	H_2, 498K	4:1	393-463			80.7	(69)
3.8%Ru/Al_2O_3	Impregnation	H_2, 498K	5:1	394-463			79.8	(69)
2%Ru/TiO_2	Impregnation	H_2, 498K				80		(71)
Ru/ɣ-Al_2O_3 (0.575% Ru)	Impregnation	H_2, 773K	4.2:1	573-653		96.5		(103)
Ru/ɣ-Al_2O_3 (0.607% Ru)	Impregnation	H_2, 773K	4.2:1	573-653		105.2		(103)
Ru/ɣ-Al_2O_3 (0.699% Ru)	Impregnation	H_2, 773K	4.2:1	573-653		87.7		(103)
Ru/ɣ-Al_2O_3 (0.766% Ru)	Impregnation	H_2, 773K	4.2:1	573-653		82.6		(103)
Ru/ɣ-Al_2O_3 (0.815% Ru)	Impregnation	H_2, 773K	4.2:1	573-653		102.3		(103)
0.5%Ru/Al_2O_3	Impregnation	H_2, 573K	3.3:1	450-600	Atmospheric	75.2		(87)
0.5-5%Ru/Al_2O_3	Impregnation	H_2, 773K	3:1 (80% He)	543-623			62	(104)

. ɣ* : ɣ-irradiation

Table 3. Kinetic models for CO_2 methanation on Ni catalysts

Catalyst details	Testing conditions	Kinetic model	Equation number	Ref.
Ni/Kieselguhr (ca. 59.4% Ni) from Harshaw Chemical Co., reduced by H_2	555 - 672 K, 2 - 30 bar, 5 - 90% CO_2	$r_0 = \frac{k p_{CO_2} p_{H_2}^4}{\left(1 + K_1 p_{H_2} + K_2 p_{CO_2}\right)^5}$ Where r_0 = initial rate of methane formation; k = reaction rate constant; K_1 and K_2 = adsorption equilibrium constants; pCO_2 and pH_2: partial pressures of H_2 and CO_2 respectively.	1	(156)
	555 - 672 K, 2 bar, 5 - 90% CO_2	$r_0 = \frac{k p_{CO_2}^{\frac{1}{2}} p_{H_2}^{\ 2}}{\left(1 + K_1 p_{H_2}\right)^3}$	2	
	555 - 672 K, 2 bar, 5 - 90% CO_2	$r_0 = \frac{k p_{CO_2}^{\frac{1}{2}} p_{H_2}}{\left(1 + K_1 p_{H_2} + K_2 p_{CO_2}\right)^2}$ r_0 = initial rate of carbon monoxide formation	3	
Ni/gamma-Al_2O_3 (33.6% of NiO) obtained from Girdler-Sudchemie, reduced by H_2	473 - 503 K, atmospheric pressure, 0.22 - 2.38% CO_2 in H_2	$r_{CO_2} = \frac{1.36 \times 10^{12} \cdot \exp\left(-{}^{25300}/_{RT}\right) \cdot p_{CO_2}}{\left(1 + 1270 \cdot p_{CO_2}\right)}$	4	(88)
Ni/Cr_2O_3 (100% Ni to 1:4 Ni/Cr_2O_3 ratio) prepared by co-precipitation and reduced by H_2	423 - 493 K, 5 - 25 x 10^{-5} moles/liter of CO_2 with large excess of H_2	$r = k C_{CO_2}^{\frac{1}{2}}$	5	(157)

Ni/SiO_2 (3% Ni) prepared by impregnation method and reduced by H_2	500 - 600 K, 1.40 - 1.75 kPa, differential conditions (CO_2 conv. < 10%)	$$r_{CH_4} = \frac{\left(\frac{K_1 K_2 K_{10} k_4 k_{11}}{2}\right)^{\frac{1}{2}} L^2 P_{CO_2}{}^{\frac{1}{2}} P_{H_2}{}^{\frac{1}{2}}}{\left(1+\left(\frac{2K_2 k_4}{K_1 K_{10} k_{11}}\right)^{\frac{1}{2}} \frac{P_{CO_2}{}^{\frac{1}{2}}}{P_{H_2}{}^{\frac{1}{2}}} + \left(\frac{K_1 K_2 K_{10} k_{11}}{2k_4}\right)^{\frac{1}{2}} P_{CO_2}{}^{\frac{1}{2}} P_{H_2}{}^{\frac{1}{2}} + \frac{P_{CO}}{K_3}\right)^2}$$ Where r_{CH4} = rate of methane formation expressed as molecules of methane produced per site per second and L = the total number of available surface sites.	6	(19)
Ni/SiO_2 (58% Ni) reduced by H_2	550 to 591 K, 6.9 - 17.2 bar, 20 - 30% CO_2; 67 - 70% H_2, CO_2 conversion: 10 - 45%	$$r_{CH_4} = 1.19 \times 10^6 \exp\left(\frac{-14600}{RT}\right) P_{H_2}{}^{0.21} P_{CO_2}{}^{0.66}$$	7	(92)
Electrodeposited Ni on the inner wall of aluminium tube.	573 K, P_{CO2}: changed up to 0.72 x 10^{-2} bar, P_{H2} changed up to 1 bar.	$$-r_{CO_2} = \frac{k_2 P_{H_2}^{\frac{1}{2}} P_{CO_2}^{\frac{1}{2}}}{\left(1 + K_{H_2} P_{H_2}^{\frac{1}{2}} + K_{CO_2} P_{CO_2}^{\frac{1}{2}}\right)^2}$$	8	(158)
Ni-La_2O_3/Al_2O_3 (20% Ni, Ni/La = 5/1) prepared by impregnation and reduced by H_2	513 - 593 K, 1 bar, differential and integral conditions	$$r_{CH_4} = \frac{k P_{H_2}^{\frac{1}{2}} P_{CO_2}^{\frac{1}{3}}}{\left(1 + K_{H_2} P_{H_2}^{\frac{1}{2}} + K_{CO_2} P_{CO_2}^{\frac{1}{2}} + K_{H_2O} P_{H_2O}\right)^2}$$	9	(159)

$Ni/MgAl_2O_4$-spinel (15.2 % Ni) reduced by H_2	573 - 673K, 10 bar	$r_1 = \frac{\frac{k_1}{p_{H_2}^{2.5}}\left(p_{CH_4}p_{H_2O} - \frac{p_{H_2}^3 p_{CO}}{K_1}\right)}{\left(1 + K_{CO}P_{CO} + K_{H_2}P_{H_2} + K_{CH_4}P_{CH_4} + \frac{K_{H_2O}P_{H_2O}}{P_{H_2}}\right)^2}$	10	(160)
		$r_2 = \frac{\frac{k_2}{p_{H_2}}\left(p_{CO}p_{H_2O} - \frac{p_{H_2}p_{CO_2}}{K_2}\right)}{\left(1 + K_{CO}P_{CO} + K_{H_2}P_{H_2} + K_{CH_4}P_{CH_4} + \frac{K_{H_2O}P_{H_2O}}{P_{H_2}}\right)^2}$	11	
		$r_3 = \frac{\frac{k_3}{p_{H_2}^{3.5}}\left(p_{CH_4}p_{H_2O}^2 - \frac{p_{H_2}^4 p_{CO_2}}{K_3}\right)}{\left(1 + K_{CO}P_{CO} + K_{H_2}P_{H_2} + K_{CH_4}P_{CH_4} + \frac{K_{H_2O}P_{H_2O}}{P_{H_2}}\right)^2}$	12	
		$r_{CO_2} = r_2 + r_3$	13	
		$r_{CH_4} = r_1 + r_3$	14	

Ni-grafted SBA-15 reduced by H_2	733 K, atmospheric pressure	$r = kC_{CO_2}{}^{0.64} C_{H_2}{}^{4.05}$	15	(161)
$NiAl(O)_x$ (N/Al molar ratio from 5/1 to 1/5) reduced by H_2	453 - 613 K, 1 - 15 bar, H_2/CO_2 ratio: 0.25 - 8	$r = k \cdot \frac{p_{H_2}^{n_{H2}} p_{CO2}^{n_{CO_2}}}{1 + K_{OH} \frac{p_{H_2O}}{P_{H_2}^{\frac{1}{2}}}} \left(1 - \frac{p_{CH_4} p_{H_2O}{}^2}{p_{H_2}{}^4 p_{CO_2} Keq} \right)$	16	(100)
		$r = \frac{k p_{H_2}^{0.5} p_{CO_2}^{0.5} \left(1 - \frac{p_{CH_4} p_{H_2O}^2}{p_{H_2}^4 p_{CO_2} Keq} \right)}{\left(1 + K_{OH} \frac{p_{H_2O}}{p_{H_2}^{0.5}} + K_{H_2} p_{H_2}^{0.5} + K_{mix} p_{CO_2}^{0.5} \right)^2}$	17	

Table 4. Values of kinetic constants from Langmuir-Hinshelwood fit of data. Redrawn from Journal of Catalysis, Vol. 77, Weatherbee and Bartholomew, "Hydrogenation of CO_2 on Group VIII Metals, II. Kinetics and Mechanism of CO_2 Hydrogenation on Nickel", Pages pp. 460 - 472, Copyright (1982), with permission from Elsevier.

Temperature [K]	$\left(\frac{K_1K_2K_{10}k_4K_{11}}{2}\right)^{1}$	$\left(\frac{2K_2k_4}{K_1K_{10}k_{11}}\right)^{1/2}$	$\left(\frac{K_1K_2K_{10}k_{11}}{2k_4}\right)^{1/2}$	$\left(\frac{1}{K_3}\right)$	K_2	k_4	$\frac{\sum err^2}{(ft)^2}$
500	0.535	0.156	0.0997	22.8	0.016	5.37	0.0136
525	1.86	0.289	0.14	8.24	0.04	13.3	0.00732
550	4.73	0.419	0.143	1.99	0.06	33.1	0.0074
575	8.05	0.704	0.0936	1.38	0.066	86	0.00125
600	15.9	0.998	0.0678	0.909	0.068	235	0.00429

Table 5. Parameter estimation for the power law with inhibition by adsorbed hydroxyl (Eqt. 2-16, T_{ref} = 555 K). Redrawn from Applied Catalysis B: Environmental, Vol. 181, Koschany *et al*., "On the Kinetics of the Methanation of Carbon Dioxide on Coprecipitated $NiAl(O)_x$", Pages 504 - 516, Copyright (2016), with permission from Elsevier.

$k_{0,\ 555\ K}$	6.41e-05 ± 3.0e-6	mol $bar^{-0.54}s^{-1}g_{Cat}^{-1}$
EA	93.6 ± 2.5	$kJmol^{-1}$
n_{H2}	0.31 ± 0.02	-
n_{CO2}	0.16 ± 0.02	-
$A_{OH,\ 555\ K}$	0.62 ± 0.09	$bar^{-0.5}$
ΔH_{OH}	64.3 ± 6.3	$kJmol^{-1}$

Table 6. Parameter estimation for Langmuir Hinshelwood rate equation (Eqt. 2-17, T_{ref} =555 K). Redrawn from Applied Catalysis B: Environmental, Vol. 181, Koschany *et al*., "On the Kinetics of the Methanation of Carbon Dioxide on Coprecipitated $NiAl(O)_x$", Pages 504 - 516, Copyright (2016), with permission from Elsevier.

$k_{0,\ 555\ K}$	3.46e-4 ± 4.1e-5	mol $bar^{-1}s^{-1}g_{Cat}^{-1}$
E_A	77.5 ± 6.9	$kJmol^{-1}$
$A_{OH,\ 555\ K}$	0.50 ± 0.05	$bar^{-0.5}$
ΔH_{OH}	22.4 ± 6.4	$kJmol^{-1}$
$A_{H2,\ 555\ K}$	0.44 ± 0.08	$bar^{-0.5}$
ΔH_{H2}	-6.2 ± 10.0	$kJmol^{-1}$
$A_{mix,\ 555\ K}$	0.88 ± 0.10	$bar^{-0.5}$
ΔH_{mix}	-10.0 ± 5.7	$kJmol^{-1}$

Table 7. Kinetic models for CO_2 hydrogenation on Ru and Cu catalysts

Catalyst details	Testing conditions	Kinetic model	Equation number	Ref.
0.5%Ru/Al_2O_3, Commercial	478 – 644K, 1 bar, H_2:CO_2 = 1.9:1 – 3.9:1	$-\frac{dP_{CO_2}}{dt} = k\exp\left(\frac{-E_a}{RT}\right)\left\{\left[P_{CO_2}\right]^n\left[P_{H_2}\right]^{4n} - \frac{\left[P_{CH_4}\right]^n\left[P_{H_2O}\right]^{2n}}{\left[K_e(T)\right]^n}\right\}$	18	(101, 162)
		Where , $K_e(T) = \exp\left[(1.0/1.987)\left(\frac{56000}{T_k^{\,2}} + \frac{34633}{T_k} - 16.4\ln T_k + 0.00557T_k\right) + 33.165\right]$ Tk = gas temperature in K, P = pressure in atm.		
Ru/Al_2O_3		$N_{CH_4} = 2.7\times10^6\exp\left(\frac{-16.1}{RT}\right)\times P_{H_2}\times P_{CO_2}^{\,0.47}$	19	(67)
		Where, N_{CH4} = the turnover number.		
		$R_{CH_4} = k_r\theta_{CO}\,p_{H_2}^n = \frac{k_r k_1\left[CO_2\right]p_2^{m+n}}{k_2\,p_{H_2O} + k_r\,p_{H_2}^m}$	20	(69)
		Where, k_1 and k_2 are respectively the forward and reverse rate constants for CO_2 reduction to adsorbed CO, through the RWGS reaction. k_r is the rate constant for CO hydrogenation		
		$R_{CH_4} = 0.0167\times\left(P_{CO_2}\right)^{0.22}\left(P_{H_2}\right)^{0.57}\left(P_{H_2O}\right)^{-0.28}$	21	(72)
		Where R_{CH4} is the rate of CO_2 methanation in μmol/gRu/s under steady-steate conditions at 383K.		

Ru/CA, $Ru/MgAl_2O_4$ and Ru/Al_2O_3	2000–5000 ppm COx in the gas mixture	$r = kp_{COx}^{n}$ Where, n = reaction order which depends on the temperature and, to a lower extent, on the kind of support material. The values of n for Ru/CA at 493, 513 and 543 K are respectively 0.05, 0.15 and 0.55. The corresponding value for Ru/Al_2O_3 are 0.4, 07 and 0.8.	22	(126)
3% Ru/Al_2O_3 commercial catalyst (Acta S.p.A, Crespina, Pista, Italy)	573 K, 15 000/h in excess of H_2	$r_{CH_4} = -r_{CO_2} = \left(\frac{-dP_{CO_2}}{dt}\right) = \frac{dp_{CH_4}}{dt} = ke^{(-E_A/RT)} P_{CO_2}{}^{0} P_{H_2}{}^{0.39} n_{SA}$ Where n_{SA} is the number of the active sites for the reaction	23	(163)
Cu(100)		$r_{CH_3OH} = k_{11}K_{10}\frac{\theta_{HCOO*}\theta_{H*}^2}{\theta_*} - \frac{k_{11}}{K_{11}}\theta_{H_3CO*}\theta_{O*}$	24	(47)
		$r_{H_2O} = k_{11}K_{10}\frac{\theta_{HCOO*}\theta_{H*}^2}{\theta_*} - \frac{k_{11}}{K_{11}}\theta_{H_3CO*}\theta_{O*} - k_7 CO_*\theta_{O*} + \frac{k_7}{K_7}\theta_{CO_2*}\theta_*$ Where: K_i are the equilibrium constants calculated from the partition functions of the intermediates; k_i are the rate constants assumed to be of the Arrhenius form and θx* represents the coverage of the intermediates.	25	
10%Cu/ANM (activated nonwoven carbon material)		$r = k_1 \frac{p_{CO_2} P_{H_2} \gamma}{p_{H_2}^{0.5} + k_2 p_{CO_2} + k_3 p_{H_2O}}$ $k_1 = 2.46 \times 10^{10} e^{-15200/T}$ (mol. g^{-1}. h^{-1}. $Atm^{-1.5}$), $k_2 = 7.81 \times 10^{-3} e^{5500/T}$ ($atm^{-0.5}$) and $k_3 = 2.28 \times 10^{-5} e^{8520/T}$.	26	(26)

Table 8. Summarized literature data for CO_2 hydrogenation kinetics over Ni catalysts

Catalyst	Prep. method / reduction details	H_2:CO_2	T [K]	P [bar]	SV	Conv. [%]	TOF or specific rate		%Selectivity			Ref.
							CO_2	CH_4	CH_4	CO	C_{2+}	
5.5%Ni/0.8%Ru/SiO_2	Spraying method / H_2 at 673 K	3:1	500	Atm.	10 000/h			1.4 mol CH_4 / h/LCat	99.8			(89)
			523					3.17 mol CH4 / h/LCat	100			
4.6%Ni/2.6%La_2O_3/SiO_2	Spraying method / H_2 at 673 K	3:1	500	Atm.	10 000/h			4.57 mol CH4 / h/LCat	99.3			(89)
			523					8.13 mol CH4 / h/Lcat	99.7			
4.3%Ni/2.5%La_2O_3/0.7%Ru/SiO_2	Spraying method / H_2 at 673 K	3:1	500	Atm.	10 000/h			9.55 mol CH4 / h/Lcat	98.6			(89)
			523					12.6 mol CH4 / h/Lcat	99.6			
3%Ni/SiO_2	Impregnation / H_2 at 750 K	4:1, 95%N_2	500	1.4	16 350/h	3.9		0.00085/s	70	9	0.07	(18)
			525		16 350/h	8.6		0.0021/s	77	15	0.05	
			550		32 900/h	11.2		0.005/s	70	25	0.02	
Ni (100)	Single crystal disk / H_2 at 750 K	96:1	552	0.13		5			17	83		(20)
			600			13			16	84		
			650			43			21	79		
			710			78			32	68		
100% Ni	/H_2 at 553 K		525	1.01		< 10	10/s		70	30		(91)
3% Ni/SiO_2	Impregnation / H_2 at 723 K	4:1, 95%N_2	525	1.01		< 10	3.6/s		58	34		(91)
3% Ni/SiO_2	Impregnation / H_2 at 723 K	4:1, 95%N_2	525	1.01		< 10	5.9/s		56	44		(91)
3% Ni/Al_2O_3	Impregnation / H_2 at 723 K	4:1, 95%N_2	525	1.01		< 10	13/s		86	11		(91)
3% Ni/TiO_2	Impregnation / H_2 at 723 K	4:1, 95%N_2	525	1.01		< 10	19/s		98	1		(91)
100% Ni	Reduction of NiO / H_2 at 723 K	4:1	543	Atm.		2.4	0.00239/s		61	39		(93)
4.5% Ni/S1	Impregnation / H_2 at 673 K	4:1	543	Atm.		1.7	0.0029/s		22	78		(93)
4.5% Ni/S3	Impregnation / H_2 at 673 K	4:1	543	Atm.		6.9	0.0014/s		36	64		(93)
9.2%Ni/SiO_2	Impregnation / H_2 at 773 K	3.3:1	553	1.2		< 8		0.097/s				(94)
0.25%K/9.2%Ni/SiO_2	Co-impregnation / H_2 at 773 K	3.3:1	553	1.2		< 8		0.051/s				(94)
0.70%K/11.0%Ni/SiO_2	Co-impregnation / H_2 at 773 K	3.3:1	553	1.2		< 8		0.0054/s				(94)
0.81%K/9.2%Ni/SiO_2	Co-impregnation / H_2 at 773 K	3.3:1	553	1.2		< 8		0.016/s				(94)
4.1%K/11.0%Ni/SiO_2	Co-impregnation / H_2 at 773 K	3.3:1	553	1.2		< 8		0.00003/s				(94)
9.5%Ni/SiO_2-Al_2O_3	Impregnation / H_2 at 773 K	3.3:1	553	1.2		< 8		0.032/s				(94)
0.25%K/11.5%Ni/SiO_2-Al_2O_3	Co-impregnation / H_2 at 773 K	3.3:1	553	1.2		< 8		0.035/s				(94)
0.81%K/9.7%Ni/SiO_2-Al_2O_3	Co-impregnation / H_2 at 773 K	3.3:1	553	1.2		< 8		0.043/s				(94)
3.9%K/11.5%Ni/SiO_2-Al_2O_3	Co-impregnation / H_2 at 773 K	3.3:1	553	1.2		< 8		0.041/s				(94)
5%Ni/Al_2O_3*	Coprecipiation / H_2 at 623 K	9:1	493	Atm.	2 400/h	21			>99.7			(56)
			513			35			>99.7			

			533			54		>99.7		
11%Ni/Al_2O_3*	Coprecipiation / H_2 at 623 K	9:1	473	Atm.	2 400/h	23		>99.7		(56)
			493			38		>99.7		
			513			68		>99.7		
			533			98		>99.7		
16.5%Ni/Al_2O_3*	Coprecipiation / H_2 at 623 K	9:1	453	Atm.	2 400/h	21		>99.7		(56)
			493			60		>99.7		
			513			100		>99.7		
			533			100		>99.7		
25%Ni/Al_2O_3*	Coprecipiation / H_2 at 623 K	9:1	433	Atm.	2 400/h	15		>99.7		(56)
			473			43		>99.7		
			493			88		>99.7		
			513			100		>99.7		
			533			100		>99.7		
5%Ni/SiO_2-RHA*	Impregnation / H_2	4:1	623	Atm.		12.5		90		(77)
			673			36		89		
			773			59		94		
			873			54		71		
			973			44		18		
5%Ni/SiO_2-gel*	Impregnation / H_2	4:1	623	Atm.		37		16		(77)
			673			49		37		
			773			67		49		
			873			63		31		
			973			61		17		
5%Ni/Al_2O_3	Impregnation / H_2 at 623 K	2:1	523	1	22.3 L/gCat/h	3.72	0.63 mmol/gCat/s		0.62	(148)
5%Ni/5%Mo/Al_2O_3	Co-impregnation / H_2 at 623 K	2:1	523	1	22.3 L/gCat/h	6.71	1.33 mmol/gCat/s		0.38	(148)
5%Ni/10%Mo/Al_2O_3	Co-impregnation / H_2 at 623 K	2:1	523	1	22.3 L/gCat/h	6.78	1.34 mmol/gCat/s		0.34	(148)
5%Ni/15%Mo/Al_2O_3	Co-impregnation / H_2 at 623 K	2:1	523	1	22.3 L/gCat/h	5.89	1.18 mmol/gCat/s		0.35	(148)
10%Ni/Al_2O_3	Impregnation / H_2 at 623 K	2:1	523	1	22.3 L/gCat/h	7.2	1.67 mmol/gCat/s		0.19	(148)
10%Ni/5%Mo/Al_2O_3	Co-impregnation / H_2 at 623 K	2:1	523	1	22.3 L/gCat/h	11.7	2.86 mmol/gCat/s		0.1	(148)
10%Ni/10%Mo/Al_2O_3	Co-impregnation / H_2 at 623 K	2:1	523	1	22.3 L/gCat/h	11.86	2.97 mmol/gCat/s		0.07	(148)
10%Ni/15%Mo/Al_2O_3	Co-impregnation / H_2 at 623 K	2:1	523	1	22.3 L/gCat/h	11.04	2.77 mmol/gCat/s		0.07	(148)
15%Ni/Al_2O_3	Impregnation / H_2 at 623 K	2:1	523	1	22.3 L/gCat/h	14.55	3.88 mmol/gCat/s		0.06	(148)
15%Ni/5%Mo/Al_2O_3	Co-impregnation / H_2 at 623 K	2:1	523	1	22.3 L/gCat/h	17.19	4.64 mmol/gCat/s		0.03	(148)
15%Ni/10%Mo/Al_2O_3	Co-impregnation / H_2 at 623 K	2:1	523	1	22.3 L/gCat/h	15.6	4.05 mmol/gCat/s		0.04	(148)
15%Ni/15%Mo/Al_2O_3	Co-impregnation / H_2 at 623 K	2:1	523	1	22.3 L/gCat/h	12.95	3.26 mmol/gCat/s		0.05	(148)
2.5%Ni/RHA-Al_2O_3*	Impregnation / H_2 at 1073 K	4:1	773	Atm	30 L/gCat/h	47		9		(65)
5%Ni/RHA-Al_2O_3*	Impregnation / H_2 at 1073 K	4:1	773	Atm	30 L/gCat/h	55		24		(65)
10%Ni/RHA-Al_2O_3*	Impregnation / H_2 at 1073 K	4:1	773	Atm	30 L/gCat/h	59		43		(65)
15%Ni/RHA-Al_2O_3*	Impregnation / H_2 at 1073 K	4:1	773	Atm	30 L/gCat/h	64		58		(65)
20%Ni/RHA-Al_2O_3*	Impregnation / H_2 at 1073 K	4:1	773	Atm	30 L/gCat/h	65		64		(65)
25%Ni/RHA-Al_2O_3*	Impregnation / H_2 at 1073 K	4:1	773	Atm	30 L/gCat/h	67		60		(65)
1%Ni/MCM-41	Ni ions incorporation / H_2 at 923 K	2.6:1	573	0.069	11.5 L/gCat/h	1.2	0.018 g/gCat/h	55.6	44.4	(164)
	Ni ions incorporation / H_2 at 973 K	2.6:1	573	0.069	11.5 L/gCat/h	2.1	0.0395 g/gCat/h	73.7	26.3	
	Ni ions incorporation / H_2 at 673 K	2.6:1	573	0.069	5 760/h	1.3	0.0018 g/gCat/h	31.1	68.9	

	Ni ions incorporation / H_2 at 773 K	2.6:1	573	0.069	5 760/h	1.9		0.0023 g/gCat/h	26.4	73.6		
	Ni ions incorporation / H_2 at 923 K	2.6:1	573	0.069	5 760/h	4.7		0.0356 g/gCat/h	85.1	14.9		
3%Ni/MCM-41	Ni ions incorporation / H_2 at 973 K	2.6:1	573	0.069	5 760/h	5.6		0.0914 g/gCat/h	96	4		(164)
	Ni ions incorporation / H_2 at 973 K	2.6:1	673	0.069	5 760/h	16.8		0.633 g/gCat/h	96.1	3.9		
5%Ni/$Ce_{0.72}Zr_{0.28}O_2$	pseudo sol-gel / H_2 at 673 K	4:1	623	Atm.		71.5	2.07 mol CO_2/gNi/s]		98.5	0.9	0.6	(165)
10%Ni/$Ce_{0.72}Zr_{0.28}O_2$	pseudo sol-gel / H_2 at 673 K	4:1	623	Atm.		85.2	2.07 mol CO_2/gNi/s]		99.7	0.3		(165)
15%Ni/$Ce_{0.72}Zr_{0.28}O_2$	pseudo sol-gel / H_2 at 673 K	4:1	623	Atm.		82.3	2.07 mol CO_2/gNi/s]		99.5	0.5		(165)
10%Ni/La_2O_3	Impregnation / H2 at 673 K	4:1	481	15		4.5		0.0141 g/gCat/h	100			(122)
			503	15		13.4		0.0419 g/gCat/h	100			
			525	15		33		0.1034 g/gCat/h	100			
			553	15		76.6		0.240 g/gCat/h	100			
			573	15		90		0.2817 g/gCat/h	100			
			593	15		97.1		0.3042 g/gCat/h	100			
			653	15		100		1.180 g/gCat/h	100			
10%Ni/γ-Al_2O_3	Impregnation / H_2 at 673 K	4:1	653	15		6.9		0.130 g/gCat/h	88.9			
5%Ni/$Ce_{0.72}Zr_{0.28}O_2$	Pseudo sol–gel / H_2 at 673 K	4:1	623	Atm.	43 000/h	71.5	2.2 mol CO_2 / gNi/s		98.5	0.9	0.6	(124)
5%Ni/$Ce_{0.5}Zr_{0.5}O_2$	Pseudo sol–gel / H_2 at 673 K	4:1	623	Atm.	43 000/h	79.7	2.41 mol CO_2 / gNi/s		99.3	0.6	0.1	(124)
5%Ni/$Ce_{0.14}Zr_{0.86}O_2$	Pseudo sol–gel / H_2 at 673 K	4:1	623	Atm.	43 000/h	73	2.16 mol CO_2 / gNi/s		99	0.9	0.1	(124)
5%Ni–0.5%Rh/$Ce_{0.72}Zr_{0.28}O_2$	Pseudo sol–gel / H_2 at 673 K	4:1	623	Atm.	43 000/h	77.8	2.37 mol CO_2 / gNi/s		99.2	0.8		(124)
69.1%Ni/Al_2O_3	Coprecipitation / H_2 at 773 K	4:1	673	10	2 mol CO_2/gCat/h	92.4			>99			(81)
5%Ni/SiO_2	Impregnation / H_2 at 673 K	4:1	623	Atm.	11 000/h	35	0.076 / s		88.3	11.6	0.1	(15)
5%Ni/CeO_2-ZrO_2	Pseudo sol–gel / H_2 at 673 K	4:1	623	Atm.	43 000/h	79.7	0.429 /s		99.3	0.6	0.1	(15)
	Impregnation / H_2 at 673 K	4:1	623	Atm.	43 000/h	59.8	0.313 /s		97.3	2.6	0.1	(15)
30%Ni/5%Fe/Al_2O_3	Coprecip using $(NH_4)_2CO_3$ / H_2 at 973 K	4:1	493	10	9.6 L/gCat/h	58.5			99.5		0.5	(154)
	Coprecipitation using Na_2CO_3 / H_2 at 973 K	4:1	493	10	9.6 L/gCat/h	55.7			99.5		0.5	
	Coprecipitation using NH_4OH / H_2 at 973 K	4:1	493	10	9.6 L/gCat/h	54.5			99.4		0.4	
	Coprecipitation using NaOH / H_2 at 973 K	4:1	493	10	9.6 L/gCat/h	49.1			99.6		0.6	
16%Ni/Al_2O_3	Impregnation / H_2 at 973 K	5:1	523	Atm.	52 300/h	1			100			(14)
			573			6			100			
			673			50			100			
			773			75			100			
5%Ni/MSN	Impregnation / H_2 at 773 K	4:1	573	Atm.	50 L/gCat/h	64.1	1.61 /s	19.16 mol CH_4/mol Ni/ s	99.9	0.1		(98)

5%Ni/MCM-41	Impregnation / H_2 at 773 K	4:1	573	Atm.	50 L/gCat/h	56.5	1.41 /s	15.12 mol CH4/mol Ni/ s	98.3	1.7	(98)
5%Ni/HY	Impregnation / H_2 at 773 K	4:1	573	Atm.	50 L/gCat/h	48.5	1.21 /s	9.9 mol CH4/mol Ni/ s	96.4	3.6	(98)
5%Ni/SiO_2	Impregnation / H_2 at 773 K	4:1	573	Atm.	50 L/gCat/h	42.4	1.06 /s	7.51 mol CH4/mol Ni/ s	96.6	3.4	(98)
5%Ni/γ-Al_2O_3	Impregnation / H_2 at 773 K	4:1	573	Atm.	50 L/gCat/h	27.6	0.69 /s	4.36 mol CH4/mol Ni/ s	95.2	4.8	(98)
20%Ni/Al_2O_3	Commercial / Unreduced		523	Atm.		4			4	0	(166)
23 wt.% Ni/CaO–Al_2O_3*	Commercial / H2 at 723 K	4:1	473	Atm.	15 000/h	2			100	0	(166)
			523			9.5			100	0	(166)
			573			40			96	4	
			623			68			97	3	
			673			81			98	2	
			723			81			97	3	
			773			79			92	8	
10%Ni/Al_2O_3	Impregnation / H_2 at 773 K	24:1	523	Atm.	31.98 L/gCat/h	11.4	0.0036/s		99.1		(121)
7.5%Ni/2.5%Fe/Al_2O_3	Impregnation / H_2 at 773 K	24:1	523	Atm.	31.98 L/gCat/h	22.1	0.0059/s		98.6		(121)
5%Ni/5%Fe/Al_2O_3	Impregnation / H_2 at 773 K	24:1	523	Atm.	31.98 L/gCat/h	8	0.0019/s		96.3		(121)
12Ni/CNT	Impregnation / H_2 at 623 K	4:1	623	Atm.	30 L/gCat/h	61.1			96.6		(99)
12Ni4.5Ce/CNT	Impregnation / H_2 at 623 K	4:1	623	Atm.	30 L/gCat/h	83.8			99.8		(99)
12Ni/Al_2O_3	Impregnation / H_2 at 623 K	4:1	623	Atm.	30 L/gCat/h	30.2			86.4		(99)
12Ni4.5Ce/Al_2O_3	Impregnation / H_2 at 623 K	4:1	623	Atm.	30 L/gCat/h	64.5			97.5		(99)

Atm. = atmospheric pressure

Table 9. Summarized literature data for CO_2 hydrogenation kinetics over Ru catalysts

Catalyst	Prep. method / reduction details	H_2:CO_2	T [K]	P [bar]	SV	Conv. [%]	TOF or specific rate		% Selectivity			Ref.
							CO_2	CH_4	CH_4	CO	C_{2+}	
5%Ru/Al_2O_3	Commercial/	4:1	497	21.68	300/h	82			>95		<5	(167)
3.3%Ru/SiO_2	Precip.-dep./	3:1	500	Atmospheric	10 000/h			0.199/s	100			(89)
			523					0.390/s	100			
5%Ru/Al_2O_3	Impregn./	4:1	548	1	3 000 – 6 000/h	< 6-10	0.194/s	0.194/s	100			(82)
0.5%Ru/SiO_2	Impregn./	4:1	502	1	1 720/h	5.7	0.0078/s		99.8	0	0.2	(83)
		4:1, 95% N_2	525	1	5 700-49 000/h	6	0.011/s		82	9.8	-	
3.8%Ru/TiO_2 (P25)	Impregn./H_2 at 493K	12:1	298	Atmospheric				2.5 x 10^{-6}/s	>99			(102)
			333					1.6 x 10^{-4}/s				
0.5%Ru/Al_2O_3	Impregn./H_2 at 673K	4:1	523	Atmospheric	6 L/gCat/h	22			100			(106)
			573			70			100			
			623			87			100			
3.8%Ru/TiO_2(P25)	Impregn./H_2 at 498K	4:1	423					0.0012/s				(69)
3.8%Ru/TiO_2 (Anatase)			423					0.00024				(69)
3.8%Ru/TiO_2(Rutile)			423					0.0007				(69)
3.8%Ru/TiO_2(A/R)			423					0.0009				(69)
3.8%Ru/Al_2O_3			423					0.00001				(69)
9%Ru/CA*	Impregn./H_2 at 703K	4000 ppm CO_2 in H_2	493	Atmospheric	6 L/gCat/h			0.0039/s	100			(126)
			513					0.0112	100			
3%Ru/CB	Impregn./H_2 at 703K	4000 ppm CO_2 in H_2	493	Atmospheric	6 L/gCat/h			0.00075	100			(126)
			513					0.0021	100			
3%Ru/CB_{H2}	Impregn./H_2 at 703K	4000 ppm CO_2 in H_2	493	Atmospheric	6 L/gCat/h			0.00094	100			(126)
			513					0.0025	100			
5%Ru/MgO	Impregn./H_2 at 793K	4000 ppm CO_2 in H_2	493	Atmospheric	6 L/gCat/h			0.0037	100			(126)
			513					0.0079	100			
10%Ru/MgO	Impregn./H_2 at 793K	4000 ppm CO_2 in H_2	493	Atmospheric	6 L/gCat/h			0.0053	100			(126)
			513					0.0143	100			
5%Ru/$MgAl_2O_4$	Impregn./H_2 at 793K	4000 ppm CO_2 in H_2	493	Atmospheric	6 L/gCat/h			0.0038	100			(126)
			513					0.00855	100			
10%Ru/$MgAl_2O_4$	Impregn./H_2 at 793K	4000 ppm CO_2 in H_2	493	Atmospheric	6 L/gCat/h			0.0051	100			(126)
			513					0.0088	100			
15%Ru/$MgAl_2O_4$	Impregn./H_2 at 793K	4000 ppm CO_2 in H_2	493	Atmospheric	6 L/gCat/h			0.0065	100			(126)
			513					0.013	100			
10%Ru/Al_2O_3	Impregn./H_2 at 793K	4000 ppm CO_2 in H_2	493	Atmospheric	6 L/gCat/h			0.0059	100			(126)
			513					0.0105	100			
15%Ru/Al_2O_3	Impregn./H_2 at 793K	4000 ppm CO_2 in H_2	493	Atmospheric	6 L/gCat/h			0.0085	100			(126)
Ru/ɣ-Al_2O_3 (0.575% Ru)	Impregn./H_2 at 773K	4.2:1	608			5	2.36/s		ca. 100	trace		(103)
Ru/ɣ-Al_2O_3 (0.607% Ru)	Impregn./H_2 at 773K	4.2:1	608			5	2.48		ca. 100	trace		(103)
Ru/ɣ-Al_2O_3 (0.699% Ru)	Impregn./H_2 at 773K	4.2:1	608			5	1.73		ca. 100	trace		(103)
Ru/ɣ-Al_2O_3 (0.766% Ru)	Impregn./H_2 at 773K	4.2:1	608			5	1.38		ca. 100	trace		(103)
Ru/ɣ-Al_2O_3 (0.815% Ru)	Impregn./H_2 at 773K	4.2:1	608			5	1.23		ca. 100	trace		(103)
3%Ru/Al_2O_3	Commercial/Unreduced	5:1	523	1	5 5000/h	3			100	0		(163)
			573			4			100	0		
			623			39			100	0		

			673			79	97	4	
			723			76	91	9	
			773			69	80	22	
	Commercial/H_2 at 673K	5:1	523	1	55 000/h	2	100	0	
			573			10	100	0	
			623			43	100	0	
			648			74	95	4	
			673			83	94	6	
			723			77	86	14	
			773			71	75	25	
1%Ru/ZrO_2	Impregn./H_2 at 673K	4:1	573	10	6 000/h	93.9	99.5	0.5	(117)
2%Ru/ZrO_2	Impregn./H_2 at 673K	4:1	573	10	6 000/h	97.2	> 99.9	<0.1	(117)
3%Ru/ZrO_2	Impregn./H_2 at 673K	4:1	573	10	6 000/h	96.9	100	-	(117)
3%Ru/TiO_2 (R/A)	Impregn., H_2 at 653K	4:1	623	1	45 000/h	81.5	99.4	0.6	(125)
						78	99.6	0.4	
3%Ru/TiO_2 (P-25)		4:1	623	1	45 000/h	64.1	99	1	(125)
3%Ru/TiO_2 (rutile)		4:1	623	1	45 000/h	9.3	28		(125)
3%Ru/α-Al_2O_3		4:1	623	1	45 000/h	16.4	63.7		(125)
3%Ru/SiO_2		4:1	623	1	45 000/h	46	99.9		(125)
3%Ru/MgO-Al_2O_3		4:1	623	1	45 000/h	40	96.6		(125)

R/A: Mechanical mixture of anatase and rutile

CA*: Carbon support with SA of 66 m2/g

CB: Carbon support with SA of 440 m2/g

CB_{H2}: Carbon support with SA of 435 m2/g

Table 10. Summarized literature data for CO_2 hydrogenation kinetics over Cu catalysts

Catalyst	Prep. method / reduction details	H_2:CO_2	T [K]	P [bar]	SV	Conv. [%]	TOF or specific rate		%Selectivity			Ref.
							CO_2	CH_3OH	CH_3OH	CO	HC	
50%CuO/40%ZnO	Coprecip./ H_2 at 573K	3:1	573	110	6.7 L/gCat/h	31.7			92.1		7.8	(42)
50%CuO/40%ZnO/La_2O_3						29.5			99.9		tr	
50%CuO/40%ZnO/MgO						23.1			99.9		tr	
50%CuO/40%ZnO/ThO_2						29.6			99.7		0.2	
50%CuO/40%ZnO/Nd_2O_3						32.5			99		0.9	
50%CuO/40%ZnO/Y_2O_3						31.5			98.5		1.4	
50%CuO/40%ZnO/Al_2O_3						27.9			93.9		6.1	
50%CuO/40%ZnO/In_2O_3						39			91		7.3	
50%CuO/40%ZnO/SiO_2						27.4			1.5		98.5	
1.27%Cu/ZrO_2	Impregn./H_2 at 573K	3:1	523	10	6.4 L/gCat/h			1824000 g/gCu/h				(127)
3.41%Cu/Al_2O_3	Impregn./ H_2 at 573K		533	26				401200				
9.58%Cu/MgO	Impregn./H_2 at 573K		503	10				38000				
45-50%Cu/ZnO/Al_2O_3	Coprecip./H_2 at 573K		523	10				244000				
40%CuO/ZrO_2	Precip.-dep./CO_2+H_2 at 513K	4:1	513	50	17.1 L/gCat/h	9.7			68[a]			(105)
40%CuO/Al_2O_3						3.6			47[a]			
40%CuO/TiO_2						6.9			59[a]			
49%CuO/ZnO						7.0			63[a]			
40%CuO/Cr_2O_3-Al_2O_3						9.6			49[a]			
36%CuO/54%ZrO_2/Al_2O_3	Coprecip.-dep./CO_2+H_2 at 513K					13.0			62[a]			
36%CuO/54%ZrO_2/ZnO						13.3			58[a]			
36%CuO/54%ZrO_2/SiO_2-Al_2O_3						12.0			61[a]			
36%CuO/54%ZrO_2/Cr_2O_3-Al_2O_3						11.7			63[a]			
36%CuO/54%ZrO_2/WO_3-Al_2O_3						10.2			65[a]			
36%CuO/54%ZrO_2/SiO_2-MgO						11.0			62[a]			
36%CuO/54%ZrO_2/graphite						8.9			69[a]			
Cu-Zn	Commercial/ H_2 at 573K	2:1	553	21	0.2 mol/gCat/h	15.1			19.3	80	0.7	(168)
Cu-Zn + DAY	Commercial/ H_2 at 573K		593		0.05 mol/gCat/h	17			1.1	69.4	23	
12%CuO/Al_2O_3	Impregn./H_2 at 673K	4:1	523	Atm.	6 L/gCat/h	10.0				100		(106)
			573			17.0				100		
			623			28				100		
Cu_7Zr_3	In-situ activation/CO_2+H_2 at 493K	3:1	453	15	0.13 mol/gCat/h	1.2	0.0007		87.4	12.6		(36)
			463			1.7	0.001		86.8	13.2		
			473			2.4	0.0014		83	17.1		
			483			3.3	0.002		71.5	28.5		
			493			4.8	0.0029		63.7	36.3		
	In-situ activation/CO_2+H_2 at 553K		473			1.5	0.0012		89.5	10.5		
			483			2.1	0.0017		80.2	19.8		
			493			3	0.0024		73.3	26.7		
			503			4.1	0.0033		65.9	34.1		
			513			5.2	0.0042		57.7	42.3		

			523			7	0.0057		50.2	49.8		
			533			9.1	0.0073		41.6	58.4		
			553			14.8	0.0119		23.4	76.6		
	In-situ activation/CO+H_2 at 553K		463			1.2	0.0005		79.7	20.3		
			473			1.8	0.0007		74.6	25.4		
			483			2.5	0.001		66.2	33.8		
			493			3.6	0.0015		56.9	43.1		
			503			5	0.002		52	48		
			513			7.1	0.0028		43.7	56.3		
			523			8.9	0.0036		36.8	63.2		
			533			12.5	0.005		29.6	70.4		
			553			17.5	0.0071		15.7	84.3		
Cu/ZrO_2	Coprecip.		483			1.7	0.0016		98	2		
			493			2.5	0.0024		87.8	12.2		
			503			3.4	0.0032		80.7	19.3		
			513			4.4	0.0041		72.7	27.3		
			523			6.3	0.006		62.4	37.6		
			533			8.1	0.0077		50.7	49.3		
			553			13.5	0.0127		26	73.4		
30%CuO/ZnO	Coprecip./H_2 at 523K	3:1	463	30	12 L/gCat/h	3.4			81.6	18.3	0.1	(46)
34%CuO/65%ZnO/Al_2O_3						3.9			82.5	17.4	0.1	
32%CuO/66%ZnO/Al_2O_3						4.6			83.3	16.7	0	
39%CuO/20%ZnO/Al_2O_3						4.2			82	17.9	0.1	
43%CuO/20%ZnO/34%Al_2O_3/Cr_2O_3						4.8			84.3	15.6	0.1	
34.7%Cu/44.5%ZnO/20.8%Cr_2O_3	Precip./diluted syngas at 623K	2.7:1	538	20	6000/h	18.1			8.9	91	0.1	(37)
2.8%Pd/33.7%Cu/ZnO/Cr_2O_3	Precip.+Impreg./diluted syngas 623K					17			7.8	92.1	0.1	
0.1%Na/2.8%Pd/Cu/ZnO/Cr_2O_3						18.4			12.2	87.3	0.5	
Cu(100)		1:1	543	2			0.00027/s					(47, 48)
30%Cu/SiO_2	Coprecip./H_2 at 523K	3:1	523	50	18 L/gCat/h		3.5 mg/m^2					(130)
50%Cu/ZnO							14.1					
50%Cu/45%ZnO/Al_2O_3							15.6					
50%Cu/10%ZnO/Al_2O_3							11.9					
50%Cu/Al_2O_3							9.5					
50%Cu/25%ZnO/Ga_2O_3							19.6					
50%Cu/Ga_2O_3							19.6					
50%Cu/40%ZnO/Cr_2O_3							18					
50%Cu/10%ZnO/Cr_2O_3							11.5					
50%Cu/Cr_2O_3							12.4					
50%Cu/25%ZnO/ZrO_2							14.2					
50%Cu/ZrO_2							9.6					
50%Cu/ZnO	Coprecip./H_2 at 523 K	3:1	523	50	18 L/gCat/h		516 g-CH_3OH/kg-cat h					(133)
50%Cu/25%ZnO/Ga_2O_3							738					
50%Cu/45%ZnO/Al_2O_3							721					
50%Cu/40%ZnO/ZrO_2							665					
50%Cu/45%ZnO/Cr_2O_3							602					
45%Cu/45%ZnO/Al_2O_3	Oxalate coprecip./H_2 at 513K	3:1	513	20	3600/h	19.3			22.3	77.7		(169)
					10000/h	16.8			23.4	76.6		
45%Cu/45%ZnO/Al_2O_3	Oxalate gel-coprecip./H_2 at 513K				3600/h	19.3			36.3	63.7		

					10000/h	17.6		37.9	62.1		
45%Cu/45%ZnO/Al_2O_3	Carbonate coprecip./H_2 at 513K				3600/h	15.8		22.8	77.2		
					10000/h	15.1		21.9	78.1		
Cu(110)		11:1	530	5.1	Batch mode		0.008/s				(50)
CuB	$NaBH_4$ reduction	3:1	523	30	20 ml/min		0.14 mol/kgCu/h	4.2	95.8		(108)
10%Cr-CuB							1.45	46.5	53.5		
20%Cr-CuB							1.66	51.4	48.6		
30%Cr-CuB							1.15	42.9	57.1		
10%Zr-CuB							0.76	47.2	52.8		
20%Zr-CuB							1.49	55.2	44.8		
30%Zr-CuB							1.22	53.4	46.6		
10%Th-CuB							1.12	48.1	51.9		
20%Th-CuB							1.13	43.5	56.5		
30%Th-CuB							0.48	40.4	59.6		
Cu-Zn	Coprecip.						1.2	51.9	48.1		
6%Cu/1.9%Ga/ZnO	Impregn./H_2 at 573K	3:1	523	20	18 L/gCat/h		948 mmol/kgCat/h	47.8	44.3	0.8	(136)
			533				1767	52.1	50.8	0.4	
			543				2392	50.4	48.8	0.6	
6.8%Cu/2.5%Ga/ZnO			523				1177	46	45.4	0.2	
			533				1398	52.6	41.2	0.3	
			543				3539	67	44.4	<0.1	
4.7%Cu/2.6%Zn/1.7%Ga/SiO_2			523				1056	13.3	-	<0.1	
			533				3112	74.5	-	<0.2	
			543				3488	29.6	-	0.3	
4.7%Cu/2.3%Zn/1.5%Ga/SiO_2			523				6126	99.8	-	0.2	
			533				8525	99.3	-	0.3	
			543				10293	99.1	-	0.4	
5%Cu/5%Zn/SiO_2			523				2048	35.7	44.4	-	
			533				2594	60.7	49.3	0.2	
			543				2132	58.8	51.8	0.2	
65%Cu/23%ZnO/9%ZrO_2/Ga_2O_3	Impregn./H_2 at 473 K	3:1	523	80	3300/h		324 MeOH/kgCat/h	75			(137)
	Citric complexing/H_2 at 473K						382	70			
50%Cu/25%ZnO/Al_2O_3	Coprecip./H_2 at 573K	3:1	523	50	12 L/gCat/h	19.7	0.34 g/gcat/h	39.7	59.7		(139)
50%Cu/25%ZnO/22.5Al_2O_3/Mn						22.3	0.42	43	56.5		
50%Cu/25%ZnO/22.5Al_2O_3/La						23.3	0.44	43.8	55.7		
50%Cu/25%ZnO/22.5Al_2O_3/Ce						23.6	0.45	45.9	53.6		
50%Cu/25%ZnO/22.5Al_2O_3/Zr						24.7	0.49	48	51.5		
50%Cu/25%ZnO/22.5Al_2O_3/Y						26.9	0.52	47.1	52.4		
$LaCu_{0.7}Zn_{0.3}O_x$	Sol-gel/H_2 at 623K	3:1	523	50	3600/h	6.4	0.05 g/gcat/h	57.9	39.5	2.5	(141)
$La_{0.8}Ce_{0.2}Cu_{0.7}Zn_{0.3}O_x$						8.1	0.08	63.3	34.9	1.7	
$La_{0.8}Mg_{0.2}Cu_{0.7}Zn_{0.3}O_x$						9.1	0.09	65.2	33	1.8	
$La_{0.8}Zr_{0.2}Cu_{0.7}Zn_{0.3}O_x$						12.6	0.1	52.5	46	1.4	
$La_{0.8}Y_{0.2}Cu_{0.7}Zn_{0.3}O_x$						5	0.04	59.6	37	3.5	
$Cu_2Zn_1Al_{0.6}Zr_{0.1}$	Coprecip./H_2 at 623K	3:1	523	50	4000/h	23	0.14 g/gcat/h	47.6	52.4		(111)
$Cu_2Zn_1Al_{0.9}Zr_{0.1}$						24.1	0.19	55.7	44.3		
$Cu_2Zn_1Al_{1.2}Zr_{0.1}$						25.6	0.28	61.3	38.2		
$Cu_2Zn_1Al_{1.5}Zr_{0.1}$						23.8	0.19	56.9	43.1		

CH_3OH selectivity[a]: calculated from available data in the provided reference
Atm. : Atmospheric pressure